

Bifurcations in Nonsmooth Dynamical Systems*

Mario di Bernardo[†]
Chris J. Budd[‡]
Alan R. Champneys[§]
Piotr Kowalczyk[¶]
Arne B. Nordmark^{||}
Gerard Olivar Tost^{**}
Petri T. Piironen^{††}

Abstract. A review is presented of the one-parameter, nonsmooth bifurcations that occur in a variety of continuous-time piecewise-smooth dynamical systems. Motivated by applications, a pragmatic approach is taken to defining a *discontinuity-induced bifurcation* (DIB) as a nontrivial interaction of a limit set with respect to a codimension-one discontinuity boundary in phase space. Only DIBs that are local are considered, that is, bifurcations involving equilibria or a single point of boundary interaction along a limit cycle for flows. Three classes of systems are considered, involving either state jumps, jumps in the vector field, or jumps in some derivative of the vector field. A rich array of dynamics are revealed, involving the sudden creation or disappearance of attractors, jumps to chaos, bifurcation diagrams with sharp corners, and cascades of period adding. For each kind of bifurcation identified, where possible, a kind of “normal form” or *discontinuity mapping* (DM) is given, together with a canonical example and an application. The goal is always to explain dynamics that may be observed in simulations of systems which include friction oscillators, impact oscillators, DC-DC converters, and problems in control theory.

Key words. nonsmooth, dynamical system, bifurcation, discontinuity, piecewise, equilibria, limit cycles

AMS subject classifications. 34A36, 34D08, 37D45, 37G15, 37G15, 37N05, 37N20

DOI. 10.1137/050625060

1. Introduction. Bifurcation analysis has shown considerable success in explaining, classifying, and drawing analogies among the behaviors of dynamical systems

*Received by the editors February 22, 2005; accepted for publication (in revised form) April 29, 2007; published electronically November 5, 2008. This work was supported by the European Union (FP5 Project SICONOS, grant IST-201-37172).

<http://www.siam.org/journals/sirev/50-4/62506.html>

[†]Department of Systems and Computer Science, University of Naples Federico II, Via Claudio 21, 80125 Napoli, Italy (m.dibernardo@unina.it).

[‡]Department of Mathematical Sciences, University of Bath, Bath BA2 7AY, United Kingdom (cjb@maths.bath.ac.uk).

[§]Department of Engineering Mathematics, University of Bristol, Bristol BS8 1TR, United Kingdom (a.r.champneys@bris.ac.uk).

[¶]School of Engineering, Computer Science and Mathematics, University of Exeter, Exeter EX5 4QF, United Kingdom (P.S.Kowalczyk@exeter.ac.uk).

^{||}Department of Mechanics, Royal Institute of Technology, S-10044 Stockholm, Sweden (nordmark@mech.kth.se).

^{**}Departments of Electrical and Electronic Engineering and Computer Science, Universidad Nacional de Colombia, Sede Manizales Campus La Nubia, Manizales, Colombia (golivart@unal.edu.co).

^{††}Department of Mathematical Physics, National University of Ireland, Galway, University Road, Galway, Ireland (petri.piironen@nuigalway.ie).

arising from a myriad of different application areas. A more or less complete set of mathematical tools exists (e.g., [71, 4]) to describe bifurcations if the system is sufficiently smooth. However, many dynamical systems arising in applications are nonsmooth; examples include the occurrence of impacting motion in mechanical systems [12, 13, 68], stick-slip motion in oscillators with friction [99], switchings in electronic circuits [41, 9], and hybrid dynamics in control systems [43, 112]. In all of these cases the assumptions behind most of the results in bifurcation theory [71] for smooth systems are violated and many new phenomena are observed.

As nonsmooth behavior is so important in applications there is a mature literature describing many different approaches to the study of nonsmooth dynamics such as complementarity systems [60], differential inclusions [32, 5], and Filippov systems [50]. However, this literature does not usually address the nature of the bifurcations that arise specifically from those systems with nonsmooth behavior. Early results were given by Peterka [93, 94], with more recent references by Leine and Nijmeijer [75], Kunze [68], and Banerjee [10]. The purpose of this review paper is to present an account of some of this theory. This subject is so huge that we cannot classify everything, nor do we attempt to.

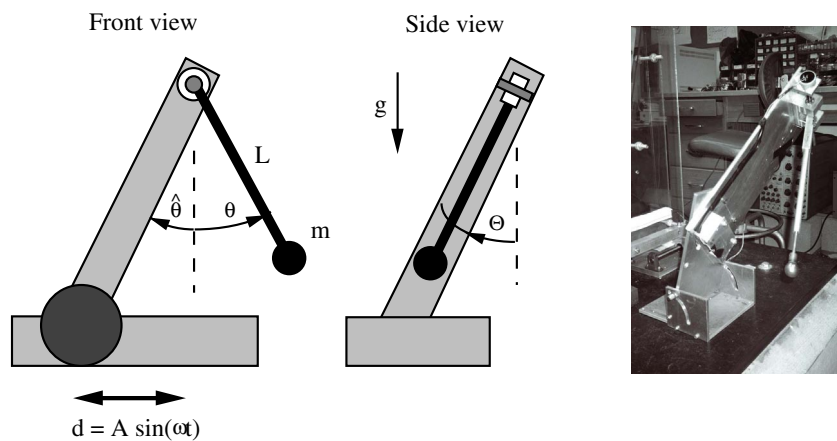


Fig. 1 A schematic and a photo of the pendulum/impact barrier assembly.

Let us start with a motivating example. Figure 1 depicts an experimental system where a free swinging pendulum is allowed to impact with a rigid stop (see [97] and Example 4.4 for more details). This is a canonical example of an impact oscillator, which has received a good deal of attention over the last 30 years since the pioneering work of Peterka [93]. In this particular study, the table on which the pendulum rests is subjected to harmonic forcing and the corresponding motion is recorded under variation of the angular position $\hat{\theta}$ of the stop. Furthermore, $d(t) = A \sin(\omega t)$ is the motion of the support, L is the effective length of the pendulum arm, g is the gravity, m is the mass, θ is the angle of the pendulum, and Θ is the out-of-plane angle. Dissipation is included via a simple linear term $\kappa \dot{\theta}$ and a restitution at impact. Figure 2(a) shows experimental results giving the position of the pendulum at a fixed phase of the forcing, under gradual, quasi-static variation of the dimensionless frequency η . Note several interesting features of the dynamics. The most striking feature is the sudden transition around $\eta = 0.44$. This is where stable periodic motion is first

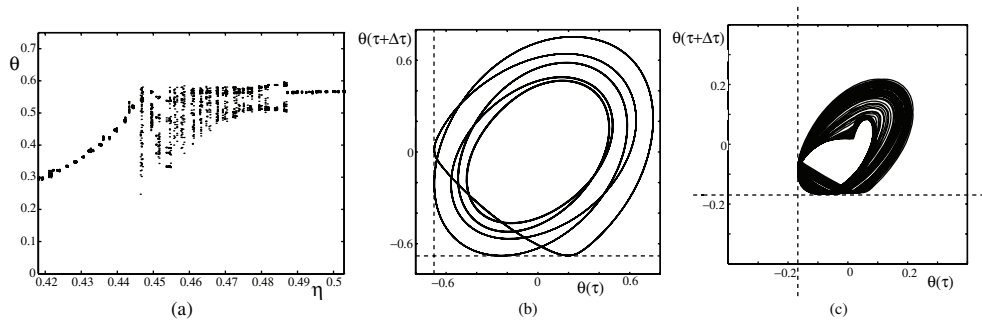


Fig. 2 Experimental results for the impacting pendulum in Figure 1, where (a) depicts a bifurcation diagram of θ , which is plotted once per forcing period under frequency variation, and (b) and (c) depict delay plots of a period-five orbit and chaotic motion, respectively. The parameter values are (a) $\hat{\theta} = 40^\circ$, (b) $\hat{\theta} = 10^\circ$ and $\eta = 0.45$, and (c) $\hat{\theta} = 40^\circ$ and $\eta = 0.35$.

observed to impact with the stop in a so-called *grazing bifurcation*. This creates a band of chaotic motion (Figure 2(c)), where the amplitude range grows rapidly (seemingly discontinuously) with increasing η . The analysis in this review will seek to explain why we should expect to see such a transition and other similar phenomena when a nonsmooth event occurs, such as a grazing of a periodic orbit. Moreover, further details of the dynamics can be explained using the theory we shall review such as the observed “windows” (intervals of η -values) in which there is stable periodic motion embedded within the chaos (Figure 2(b)). Here, there is a “period-adding” sequence where the underlying multiple of the forcing period of the attracting limit cycle increases by one as η is reduced toward the grazing bifurcation value.

Finally, we remark that the dynamics created by such nonsmooth transitions can lead to the coexistence of different attractors for the same parameter values, with highly complex basins of attraction. Figure 3 shows just such a case for a simplified model of the impacting pendulum, where again motion is depicted for a fixed value of the forcing phase. This picture shows the angle and angular velocity of the pendulum at times $t = 2k\pi/\omega$ for $k = 1, 2, \dots$, where ω is the forcing frequency. The black

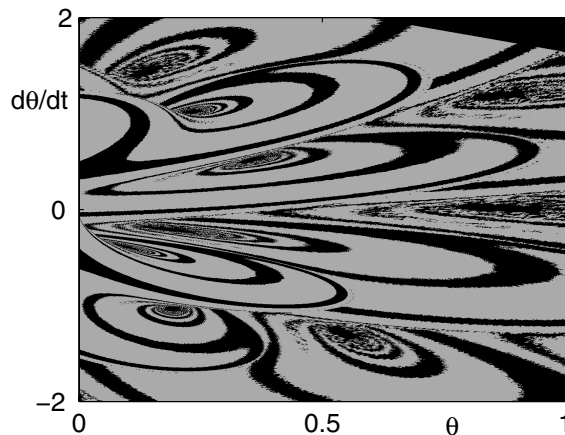


Fig. 3 The domains of attraction of two stable periodic states (period-one and period-six) for a simple forced impact oscillator.

regions correspond to initial conditions that are attracted to a stable period-one orbit and the gray regions to initial conditions attracted to a stable period-six orbit. See [83] for more details on domain of attraction calculations of impacting systems.

Returning to the general theme of this review, we note that in recent years there has been significant progress in identifying, classifying, unfolding, and applying novel kinds of bifurcations that are unique to nonsmooth systems. Three problems emerge when trying to summarize this work and put it in context: What do we mean by a piecewise-smooth system? What do we mean by a bifurcation? What do we mean by “codimension” for a nonsmooth system? Each of these questions warrants significant investigation in its own right. This review shall therefore take a pragmatic approach, motivated by what is known to occur in applications. Let’s take each of these questions in turn.

1.1. Piecewise Smooth Systems. First, what do we mean by a *piecewise smooth (PWS) system*? There are several different formalisms for dealing with continuous-time nonsmooth systems, including hybrid systems, variational inequalities, complementarity problems, and set valued ordinary differential equations (ODEs); see, e.g., [14, 60] for reviews. The key notion is that of a *differential inclusion* [32, 5]. Here we allow the right-hand side of an ODE $\dot{x} = f(x)$ to be not strictly a function, but to be set-valued. For example, such set-valued functions arise in Coulomb dry friction laws encountered in mechanics which model objects in contact that slide with velocity v only if their tangential contact force f_t exceeds some critical value. There are critical issues surrounding the well-posedness of such systems, and often the smooth existence and uniqueness results for smooth ODEs (see, e.g., [23]) do not apply. For example, consider the simple system

$$\dot{x}(t) = \alpha \text{sign}(x(t)),$$

where $\alpha \in \mathbb{R}$ is a parameter that can vary and the sign function is multivalued at $x = 0$ with $\text{sign}(0) = [-1, 1]$. When $\alpha < 0$ for any value $x(0)$, there is a unique solution to this problem and a unique attractor, a stable equilibrium at $x = 0$. For $\alpha = 0$, however, all points $x \in \mathbb{R}$ are equilibria, and when $\alpha > 0$, $x = 0$ is still an equilibrium, but is no longer stable. In the latter case, the equation has three different solutions with initial condition $x(0) = 0$, showing that uniqueness of solution no longer holds. However, from a different point of view, namely, that of bifurcation theory, this example presents no challenge. Instead of focusing on the ill-posedness of the problem in state space, we think instead of the asymptotic behavior as we vary the parameter. This is a simple example of a nonsmooth bifurcation. For $\alpha < 0$ there is a unique attractor, and for $\alpha > 0$ almost all trajectories diverge to infinity. The case $\alpha = 0$ is a pathology; therefore we single this out as a *bifurcation point*.

Because of the intricacy of these well-posedness issues, we shall avoid here the technicalities associated with formulating existence and uniqueness results for the classes of system we study. That material would require a whole separate review paper in its own right. Nevertheless, when introducing various classes of PWS systems below we shall give references to the appropriate research literature dealing with well-posedness and give some indication of the smoothness of the solutions one should expect.

Many interesting examples of PWS systems that contain intricate dynamics of the kind we describe here are contained in the recent books [122, 75]. The purpose of this paper is to review the emerging literature on a new *nonsmooth* bifurcation theory that can help explain the observations.

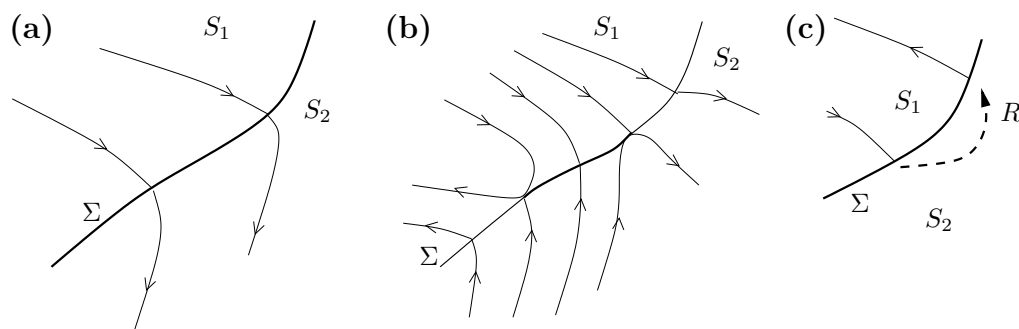


Fig. 4 Sketches of the phase space of the three classes of system under consideration: (a) non-sliding PWS, (b) Filippov, and (c) impacting systems.

There is also a large body of literature on the dynamics of nonsmooth discrete-time maps, in which fixed points of cycles can experience so-called border-collision bifurcations [48, 89, 10, 8]. Here we shall focus on the continuous-time case, although, as we shall see, such nonsmooth mappings can arise as Poincaré maps when we study bifurcations of limit cycles. We will primarily consider the simple paradigm of a PWS system. That is, a set of ODEs in \mathbb{R}^n , where the phase space is partitioned into finitely many open sets S_i in each of which the system is smooth,¹ so that

$$(1.1) \quad \dot{x} = f(x, \mu), \quad x \in \mathbb{R}^n, \quad \mu \in \mathbb{R}^p,$$

where

$$f(x, \mu) = F_i(x, \mu) \quad \forall x \in S_i \subset \mathbb{R}^n, \quad i = 1, \dots, n,$$

and each function F_i is a smooth function of its argument. We shall also assume each boundary Σ_{ij} between regions S_i and S_j to be a smooth $(n-1)$ -dimensional manifold, although we shall also be interested in corners formed by the intersections of two smooth Σ_{ij} (of course, three surfaces may intersect, typically along $(n-3)$ -dimensional manifolds, etc.). Evolution of the dynamics of such a system over time T from initial condition x_0 defines a *flow map* $\phi(x_0, \mu)$, which can also be decomposed into flows ϕ_i defined in each region S_i . Broadly speaking, different classes of PWS systems can be classified according to what is allowed to happen when the overall flow ϕ intersects the boundary Σ_{ij} . Here we shall distinguish three classes of system and give references to where standard well-posedness results may be found:

1. *PWS systems.* The simplest assumption is that the boundary Σ_{ij} is never simultaneously attracting (or repelling) from both sides under the dynamics, hence all trajectories either cross Σ_{ij} transversally (see Figure 4(a)) or both vector fields are simultaneously tangent to it. Hence no *sliding* motion constrained to Σ_{ij} can take place. Such systems arise naturally as models of second-order bilinear oscillators (see Example 2.1 below). This includes the case where the overall vector field f is continuous and has a discontinuity across Σ_{ij} in its first or higher derivative (PWS continuous). In this case, since the vector field is continuous and the jump in derivative across Σ_{ij} is assumed always to be bounded, then the overall function f must be Lipschitz, which is the minimum required for the standard ODE existence and uniqueness theory [23] to apply.

¹We take “smooth” to mean C^r for r sufficiently large.

2. *Filippov PWS systems.* In this case, f is discontinuous across Σ and we allow the possibility that both flows in regions S_i and S_j have their components normal to Σ_{ij} and of opposite sign. This implies the possible existence of a sliding flow inside the discontinuity surface Σ_{ij} (along the bold portion of the boundary illustrated in Figure 4(b)). For many physical systems, this flow can be described by the Filippov convex method

$$(1.2) \quad f = \lambda F_i + (1 - \lambda)F_j, \quad 0 \leq \lambda = \frac{(H_{ij})_x F_j}{(H_{ij})_x (F_j - F_i)} \leq 1,$$

where H_{ij} is a function whose zero set is Σ_{ij} [50]; see section 3. Note that the flow corresponds with that in regions S_i and S_j when $\lambda = 0$ and $\lambda = 1$, respectively; see Figure 4(b). Such flows arise, for example, in models of dry friction oscillators and relay control systems (see Example 3.1). Filippov systems can always be posed using the formalism of differential inclusions. Provided certain so-called cone conditions are satisfied, one has existence and uniqueness of absolutely continuous (but not necessarily differentiable) solutions; see, e.g., [5, 12].

3. *Impacting systems.* Finally, we consider the case where Σ_{ij} is a hard boundary and the region S_j is a forbidden region of the phase space (see Figure 4(c)) so that the dynamics in S_i is governed by a smooth flow. On the boundary Σ_{ij} , the continuous dynamics is replaced by an instantaneous reset (or impact) map R , i.e.,

$$(1.3) \quad x \rightarrow R(x), \quad x \in \Sigma_{ij}.$$

Depending on the properties allowed for the map R , many different dynamics may be seen. Much work in this area has been motivated by the types of mechanical systems where the phase space is composed of velocity and position variables and the reset map acts to reverse the sign of a velocity variable at impact; see, e.g., [93, 52], the introductory example presented above, and section 4. Hence we assume that the boundary Σ_{ij} is divided into regions Σ_{ij}^- , where it is attracting, and Σ_{ij}^+ , where it is repelling. The reset is then assumed to be a map $R : \Sigma_{ij}^- \rightarrow \Sigma_{ij}^+$. More complex situations can arise in three or more dimensions when motion under the dynamics can slide along the $(n - 2)$ -dimensional boundary between Σ_{ij}^- and Σ_{ij}^+ . A convenient theoretical framework for studying well-posedness of impacting systems is that of *complementarity* systems, which model mechanical and electrical devices with unilateral constraints; see, e.g., [12, 13]. Proving well-posedness is more of a challenge in this context, as one has to avoid situations like the so-called Painlevé paradox [80, 74, 106], which can arise when studying impacts with friction. Motivated by mechanical systems that impact without friction we shall restrict attention in this review to the simplest forms of reset maps that avoid this extra complexity [95, 58].

It is also possible to distinguish among the above three cases using the following concept.

DEFINITION 1.1. *Consider the derivative*

$$F_i^{(k)} - F_j^{(k)} = \frac{d^k}{dx^k} F_i - \frac{d^k}{dx^k} F_j,$$

where the vector fields F_i and F_j are sufficiently smooth. Consider also an integer

$d \geq 0$, such that $\forall k, 0 \leq k < d$, one has that $F_i^{(k)} - F_j^{(k)}$ is a continuous function on Σ_{ij} , while $F_i^{(d)} - F_j^{(d)}$ is discontinuous on Σ_{ij} . Then d is the degree of smoothness of the system on Σ_{ij} .

Two examples highlight the meaning of the definition:

- (a) Let $\dot{x}(t) = -\text{sgn}(x(t))$, $x \in \mathbb{R}$; then $\Sigma_{ij} = \{x = 0\}$, $F_i(x) = 1, F_j(x) = -1$, and $d = 0$.
- (b) Let $\dot{x}(t) = |x(t)|$, $x \in \mathbb{R}$; then $\Sigma_{ij} = \{x = 0\}$, $F_i(x) = -x, F_j(x) = x$, and $d = 1$.

One can extend this definition to deal with impacting systems by introducing a δ -function discontinuity in a hypothetical vector field F_2 that exists on the “far” side of the rigid boundary (region S_2 in Figure 4). The effect of this δ -function is to map points back to Σ_{ij} via the reset map (1.3) in zero time.

Thus, the degree is zero since the jump is on the system state itself so that the zeroth partial derivative of the flow is discontinuous. By contrast, Filippov systems have degree 1, since the jump is on the vector field which is the time derivative of the solution state. For PWS continuous systems, where the jump is on the k th derivative of the vector field, the degree is $k + 1$, since this is the number of times one has to differentiate the jump to obtain a discontinuity in the state. Of course, many systems may have the property that in different parts of their phase space, or at different parameter values, they may exhibit more than one kind of dynamics from the above list.

1.2. Bifurcations in PWS Systems. The second problem we face is to define what we mean by a *bifurcation*. There are in essence two approaches to defining bifurcations in smooth systems: analytical or topological. In the *analytical approach*, one defines bifurcation as a parameter value α at which the implicit function theorem fails for a parametrized system of equations, say, $\mathcal{F}(x, \alpha) = 0$. At such points, folding or creation of additional paths of solutions occurs; see, e.g., [61, 22]. The *topological approach*, in contrast, deals with vector fields and the topology of their associated phase portraits. In this case a bifurcation is said to occur when, as a parameter is varied, a phase portrait becomes structurally unstable in the *topological sense* (see, e.g., [59, 71]). A universal unfolding (or topological normal form) of the bifurcation includes a minimal number of terms and parameters to allow all possible structurally stable bifurcation diagrams to be seen at small values of the unfolding parameters. The number of parameters necessary defines the codimension of the bifurcation.

For nonsmooth systems, these concepts are problematical. In the analytical approach, a small change in parameter can cause the instantaneous creation of a chaotic attractor together with infinitely many unstable periodic orbits (see, e.g., [10]). For the topological approach, we need a priori to define a system topology. For example, does the topology allow a change in the number or relative position of discontinuity boundaries Σ_{ij} as a parameter varies, or a change in the degree of smoothness of the flow at those boundaries? For each class of nonsmooth system, there are likely to be several different possible notions of bifurcation.

Rather than deal with these technical issues, we suggest a pragmatic approach. We are interested in describing situations that are unique to nonsmooth systems, specifically, when the system dynamics does something degenerate with respect to a discontinuity boundary. For example, this might involve an invariant set gaining a first contact with a certain Σ_{ij} , or the onset of sliding along the orbits of that invariant set. We shall refer to these events as *discontinuity-induced bifurcations* (DIBs) because, as we shall see, depending on the circumstances this may or may not lead to a bifurcation in either of the classical senses as a parameter is varied. Such

events have in the past been given the name *nonsmooth* bifurcations [75], *discontinuous* bifurcations [76, 77], *discontinuity-driven* bifurcations [30, 109], and, in the Russian literature [49], *C*-bifurcations.²

We shall concentrate on DIBs that involve the simplest kinds of invariant set only: equilibria or periodic orbits. In what follows, the term “bifurcation” shall be used to mean such a discontinuity-induced transition. Of course, nonsmooth systems can also undergo regular bifurcations just like smooth systems, but the focus of this review is on those bifurcations that are unique to nonsmooth systems. We should also contrast the *C*-bifurcations with so-called *border-collision bifurcations* [90, 8], which occur when fixed points of discrete-time maps cross a discontinuity. Here we shall be concerned exclusively with continuous-time systems. There are also notions of bifurcation that only single out events that occur when a change of stability is involved (in which eigenvalues “jump” across the imaginary axis); see [75].

For simplicity, we shall consider each DIB in its simplest possible setting, so we will not allow systems which change their type between the three classes outlined above as parameters vary. Also, we shall deal only with local bifurcations in the sense that the dynamics are governed by the point of interaction with the boundary and do not involve possible heteroclinic connections to other invariant sets (but see [70] for a catalogue of possible bifurcations, both local and global, in two-dimensional Filippov systems with a single discontinuity boundary). A few remarks concerning bifurcations involving other invariant sets are given in section 5.

This brings us to the issue of *codimension*. Broadly speaking, we shall only treat codimension-one situations, that is, DIBs that one should expect to see as a single parameter is varied. However, the classification by codimension relies heavily on what is assumed about the system topology. For example, in a system with four discontinuity boundaries that meet at a point, it may be possible for a bifurcation to occur upon varying one parameter whereby a periodic orbit passes through this point [73, 75]. Hence we shall need to assume that the boundaries themselves are in a general position; that is, any intersection between Σ_{ij} and Σ_{jk} occurs along a smooth $(n - 2)$ -dimensional manifold. For this reason, and since we only consider local neighborhoods of the DIB, we shall only consider cases where there are at most two discontinuity boundaries. The DIBs we consider shall then involve either an equilibrium approaching a single boundary Σ (or leaving the sliding region) or a periodic orbit either grazing a boundary or approaching the intersection point between two boundaries Σ_1 and Σ_2 . As we shall see, even considering this finite set of transitions leads to many possible dynamical consequences. Finally, we should reiterate that we are motivated by examples, and quite often the purely topological definition of codimension can then be unhelpful. For example, in smooth dynamics, we know that conservative or symmetric systems can undergo bifurcations that would be of significantly higher codimension in the generic case. We have already mentioned the case of degenerate piecewise discontinuous systems, where sliding is impossible. Also, motivated by examples with dry friction, there can be Filippov systems where there can exist nonisolated equilibria in the sliding region [111].

1.3. Overview. The next three sections of this review treat each of the three classes of systems in turn, in each case dealing first with DIBs involving equilibria, then periodic orbits. In addition to reviewing the existing literature we include many

²The *C* stands for the Russian word for “sewing,” so that different trajectory segments are being sewn together at the bifurcation point.

new results, especially in sections 2.1, 2.3, 3.1, and much of section 4. For each DIB we give a mathematical example and, where possible, a *physical application*. We shall also give simple maps—sometimes described as “*normal forms*”—that describe all dynamics in the neighborhood of the DIB point, where they are known to exist, and if not, we highlight a method for analyzing what occurs.

In section 2.2 a schematic procedure for deriving such maps for limit-cycle bifurcations is given, by developing the idea of the *discontinuity mapping*. It might also be the case that the simple mathematical examples can serve as *canonical models* that contain all the essential features that can occur in realistic applications. Where possible, we shall also indicate what is known about the dynamics of the unfolding of the transition, indicating which different subcases may occur. In some cases, where complete theory is available we give it with a motivation of the method rather than the complete proof. In other cases, complete results remain unknown and we merely sketch possible DIB scenarios. We shall also introduce techniques of analysis and notation as we go along; thus later sections rely on concepts that are introduced in earlier ones. In this way, we shall also highlight connections between the bifurcations that occur in the three different classes of systems. Many of the examples rely on the presentation of numerical results, most of which were obtained using simple *event-driven* numerical schemes; see [96, 15] for discussion on numerical simulation (and continuation) of nonsmooth systems. Finally, section 5 indicates some of the many problems that are not treated by this review, including open questions and future directions for research.

2. Nonsliding Systems. This section describes the possible DIBs of equilibria and limit cycles of systems with degree of smoothness 2 and also degree 1 systems which are degenerate in that no sliding can occur. We will develop a general theory for these systems and then apply it to various examples, including models of a friction oscillator and a DC-DC converter.

Example 2.1 (the bilinear oscillator, a motivating example). Consider the bilinear oscillator defined by the equation (e.g., see [103])

$$(2.1) \quad \ddot{u} + 2\zeta_i \dot{u} + k_i^2 u = \beta_i \cos(\omega t) + \Theta_i,$$

where $i = 1$ if $u > 0$ and $i = 2$ if $u < 0$. This models a simple one-degree-of-freedom linear oscillator with sinusoidal forcing, where the value of the damping ζ , spring constant k , forcing amplitude β , or offset Θ might change when the displacement u crosses a threshold value, which, without loss of generality, we take to be $u = 0$. We seek to understand the nature of the singularity in the Poincaré maps related to the flow if a trajectory becomes tangent to, i.e., *grazes*, the threshold $u = 0$ at some time $t = t^*$ at a grazing event for which $\dot{u}(t^*) = 0$.

We introduce a state variable

$$x := (x_1, x_2, x_3)^T = (u, \dot{u}, \omega(t - t^*))^T,$$

in which the system becomes autonomous. A grazing event happens automatically at the origin of this coordinate system. For such a coordinate system the regions of phase space over which the system is smooth and the boundary between them are given by

$$S_1 = \{x : x_1 > 0\}, \quad S_2 = \{x : x_1 < 0\}, \quad \Sigma_{12} \equiv \Sigma = \{x : x_1 = 0\}.$$

In terms of this new variable, (2.1) becomes

$$(2.2) \quad \dot{x} = \begin{cases} A_1 x + B_1 & \text{if } H(x) = Cx > 0, \\ A_2 x + B_2 & \text{if } H(x) = Cx < 0, \end{cases}$$

where

$$(2.3) \quad \begin{aligned} A_1 &= \begin{pmatrix} 0 & 1 & 0 \\ -k_1^2 & -2\zeta_1 & 0 \\ 0 & 0 & 0 \end{pmatrix}, & B_1 &= \begin{pmatrix} 0 \\ \beta_1 \cos(x_3 + \omega t^*) + \Theta_1 \\ \omega \end{pmatrix}, \\ A_2 &= \begin{pmatrix} 0 & 1 & 0 \\ -k_2^2 & -2\zeta_2 & 0 \\ 0 & 0 & 0 \end{pmatrix}, & B_2 &= \begin{pmatrix} 0 \\ \beta_2 \cos(x_3 + \omega t^*) + \Theta_2 \\ \omega \end{pmatrix}, \\ C &= (1 \quad 0 \quad 0). \end{aligned}$$

In what follows, let

$$(2.4) \quad \hat{\beta}_i = \beta_i(\cos \omega t^*) + \Theta_i.$$

Consider first the case where $\hat{\beta}_1 \neq \hat{\beta}_2$. Then the vector field itself is discontinuous at the grazing point since $F_i|_{x=0} = (0, \hat{\beta}_i, \omega)^T$. So, we have a jump in the value of the vector field anywhere along the set of potential grazing points. Moreover, at any point in the switching plane Σ , the vector field undergoes a finite jump since

$$(2.5) \quad F_i|_{x_1=0} = (x_2, \beta_i \cos \omega(c + x_3) + \Theta_i - 2\zeta_i x_2, \omega)^T.$$

This situation, where the degree of smoothness of the vector field at all points of Σ is the same, we refer to as representing a *uniform discontinuity* of degree 1.

DEFINITION 2.1. *A discontinuity boundary Σ is said to be uniformly discontinuous in some domain \mathcal{D} if the degree of smoothness of the vector field across Σ is the same throughout \mathcal{D} . Furthermore, we say that the discontinuity is uniform with degree $m + 1$ if the first $m - 1$ derivatives of $F_1 - F_2$, evaluated on Σ , are zero.*

Given (2.7) below and the fact that the accelerations from F_1 and F_2 have the same nonzero sign, then there is no sliding close to the grazing point (but at other places on the boundary there may be sliding).

Now suppose instead that $\Theta_1 = \Theta_2 := \Theta$ and $\beta_1 = \beta_2 := \beta$, so that at the grazing point the vector field is continuous. Then at the grazing point we have $\frac{\partial F_i}{\partial x}|_{x=0} = A_i$, $F_i|_{x=0} = (0, \beta, \omega)^T$, which, if $\zeta_1 \neq \zeta_2$ or $k_1 \neq k_2$, implies that there is a jump in the first derivative of the vector field. Consider separately the cases where the damping coefficient ζ_i or the stiffness term k_i varies across the discontinuity boundary. If $\zeta_1 \neq \zeta_2$ but $k_1 = k_2$, then, at a general point in the switching plane Σ , we have (taking $t^* = 0$), $F_i|_{x_1=0} = (x_2, \beta \cos \omega x_3 + \Theta - 2\zeta_i x_2, \omega)^T$. Hence if $x_2 \neq 0$, we find that the vector field itself is discontinuous, since $F_1 \neq F_2$. Only on the grazing line defined by $x_2 = 0$ is the lowest-order discontinuity in the derivative of the vector field. This is an example of *nonuniform discontinuity*. As mentioned above, it is easy to see that there can be no sliding here, though, since both vector fields graze along the same line. In contrast, if $k_1 \neq k_2$ but $\zeta_1 = \zeta_2 := \zeta$, then at a general point in Σ we have $F_i|_{x_1=0} = (x_2, \beta \cos \omega x_3 + \Theta - 2\zeta x_2, \omega)^T$, so that $F_1 = F_2$ and we have uniform discontinuity of degree 2.

In what follows, we shall be interested in two special forms of allowed jump across Σ . Uniform discontinuity of smoothness degree $m \geq 2$ is ensured by assuming

$$(2.6) \quad F_2(x) = F_1(x) + J(x)H(x)^{m-1},$$

where the boundary Σ is defined by the zero set of the smooth function $H(x)$, and J , F_1 , and F_2 are all sufficiently smooth in a neighborhood of the grazing point $x = 0$. In the case of smoothness of degree 1, that is, where the vector fields are discontinuous across Σ , the generic situation is described by Filippov flows with sliding. However, we saw earlier that the special structure of the bilinear oscillator in the case of jumps in β_i or ζ_i caused a smoothness degree 1 discontinuity that did not lead to sliding. This special structure can be formalized by the assumption that

$$(2.7) \quad H_x(x)F_2(x) = N(x)H(x) + M(x)H_x(x)F_1(x)$$

for functions $M > 0$, N , F_1 , and F_2 that are sufficiently smooth at the grazing point.

2.1. DIBs of Equilibria. DIBs of limit cycles of flows [27, 36, 42] and the associated border collisions of fixed points of related (Poincaré) maps [7, 39] have been studied quite extensively in recent years. Comparatively less is known about the possible DIBs of equilibria in PWS systems. However, [75] studies equilibria of PWS flows that interact with a discontinuity manifold as parameters are varied, and there are also treatments of some cases in the Russian literature [2, 3]. In particular, we focus on nonsmooth continuous systems, i.e., systems with a degree of smoothness equal to 2. For ease of exposition, we restrict our attention to a neighborhood, say, \mathcal{D} , of a single discontinuity surface in phase space, where the system under investigation can be described as follows:

$$(2.8) \quad \dot{x} = \begin{cases} F_1(x, \mu) & \text{if } H(x, \mu) \geq 0, \\ F_2(x, \mu) & \text{if } H(x, \mu) < 0, \end{cases}$$

where $x \in \mathbb{R}^n$, $F_1, F_2 : \mathbb{R}^{n+1} \mapsto \mathbb{R}^n$ are supposed to be sufficiently smooth, and $H : \mathbb{R}^{n+1} \mapsto \mathbb{R}$ is a sufficiently smooth scalar function of the system states. Because of the continuity assumption we must have, for some smooth function $x \mapsto G(x, \mu)$,

$$(2.9) \quad F_2(x, \mu) = F_1(x, \mu) + G(x, \mu)H(x, \mu),$$

so that when $H(x, \mu) = 0$, then $F_1 = F_2$ as required.

According to (2.8), H defines the switching manifold Σ by

$$\Sigma := \{x \in \mathbb{R}^n : H(x) = 0\}.$$

Locally, as in the previous example, Σ divides \mathcal{D} into regions S_1 and S_2 where the system is smooth and defined by the vector fields F_1 and F_2 , respectively:

$$\begin{aligned} S_1 &= \{x \in \mathcal{D} : H(x, \mu) > 0\}, \\ S_2 &= \{x \in \mathcal{D} : H(x, \mu) < 0\}. \end{aligned}$$

We assume that both the vector fields F_1 and F_2 are defined over the entire local region of phase space under consideration, i.e., on both sides of Σ .

We can identify different types of equilibria of system (2.8), giving the following definitions.

DEFINITION 2.2. We term a point $x \in \mathcal{D}$ as a regular equilibrium of (2.8) if x is such that either

$$F_1(x, \mu) = 0 \text{ and } H(x, \mu) > 0$$

or

$$F_2(x, \mu) = 0 \text{ and } H(x, \mu) < 0.$$

Alternatively, we say that a point $y \in \mathcal{D}$ is a virtual equilibrium of (2.8) if either

$$F_1(y, \mu) = 0 \text{ but } H(y, \mu) < 0$$

or

$$F_2(y, \mu) = 0 \text{ but } H(y, \mu) > 0.$$

For some value of the system parameters, it is possible for an equilibrium to lie on the discontinuity boundary.

DEFINITION 2.3. We say that a point $z \in \mathcal{D}$ is a boundary equilibrium of (2.8) if

$$F_1(z, \mu) = F_2(z, \mu) = 0 \text{ and } H(z, \mu) = 0.$$

Note that under parameter variation the system might exhibit a boundary equilibrium for some value of its parameters μ . We shall seek to unfold the bifurcation scenarios that can occur when μ is perturbed away from the origin, i.e., the possible branches of solutions originating from a boundary equilibrium. In order to do this let us introduce the following definitions.

DEFINITION 2.4. A boundary equilibrium bifurcation occurs at $\mu = \mu^*$ if

- $F_1(x^*, \mu^*) = 0$,
- $H(x^*, \mu^*) = 0$, and
- $F_{i,x}(x^*, \mu^*)$ is invertible (or equivalently $\det(F_{i,x}) \neq 0$) for $i = 1, 2$.

While the first two conditions state that x^* is a boundary equilibrium when $\mu = \mu^*$, the third condition ensures nondegeneracy. Obviously, an equivalent definition can be given by considering flow F_2 rather than F_1 . It is worth mentioning here that Definition 2.4 is weaker than that in [75], where nonsmooth bifurcation of an equilibrium is defined as the point at which the eigenvalues of the system are set-valued and contain a value on the imaginary axis. The definition given here is rather more general.

2.1.1. An Overview of Possible Cases. The existence of different types of bifurcation scenarios following a boundary equilibrium bifurcation was discussed in [53, 73, 75] and illustrated there through some one- and two-dimensional examples. It was shown, for example, that such DIBs of equilibria can be associated, in the simplest cases, with the *persistence* of the bifurcating equilibrium or its disappearance through a *fold-like* scenario. Namely, it was conjectured that a boundary equilibrium bifurcation can lead to the following simplest scenarios:

1. *Persistence*: At the bifurcation point, a regular equilibrium lying in region S_1 is turned into a regular equilibrium lying in region S_2 (or vice versa).
2. *Nonsmooth fold*: At the bifurcation point, the collision of a stable and unstable equilibrium is observed on the boundary followed by their disappearance.

An extension of Feigin's classification strategy for border collisions of fixed points of maps to the case of equilibria in flows was given in [42]. In the next section, we will present an alternative derivation of the conditions needed to distinguish between the two scenarios highlighted above.

In addition to the persistence and the nonsmooth fold scenarios, there might be other invariant sets involved in the bifurcation, for example, scenarios where one or more families of limit cycles are either created or destroyed at the nonsmooth bifurcation point. As shown later in Example 2.2, this includes the scenario where an equilibrium undergoes a boundary equilibrium bifurcation, giving rise to a family of limit cycles. Such a DIB is the closest nonsmooth equivalent to a Hopf bifurcation for a smooth system.

More complex, nongeneric scenarios are also possible in systems with symmetry, such as, for example, the *multiple crossing bifurcation* described in [75]. Note that all of these scenarios are due to the interaction between the bifurcating equilibrium and the discontinuity boundary in phase space. Thus, they are not necessarily associated with the eigenvalues of an associated linear operator crossing the unit circle. We discuss now how some of them can be classified.

2.1.2. Persistence and Nonsmooth Fold. Despite their similarity to border collisions, no general classification strategy has been proposed for nonsmooth bifurcations of equilibria in n -dimensional continuous-time systems. Our aim is to classify the simplest possible scenarios associated with a boundary equilibrium bifurcation in n -dimensional nonsmooth continuous flows. We start by giving more precise definitions of the persistence and nonsmooth fold scenarios introduced above. We assume that a boundary equilibrium bifurcation occurs at $x = 0$ when $\mu = 0$, i.e., $F_1(0, 0) = F_2(0, 0) = 0, H(0, 0) = 0$.

DEFINITION 2.5. *We say that (2.8) exhibits a border-crossing bifurcation (persistence) for $\mu = 0$ if, when μ is varied in a neighborhood of the origin, one branch of regular equilibria and a branch of virtual equilibria cross at the boundary equilibrium point $x = 0$ when $\mu = 0$, exchanging their properties. Namely, we assume there exist smooth branches $x^+(\mu)$ and $x^-(\mu)$ such that $x^+(0) = x^-(0)$ and, without loss of generality (reversing the sign of μ if necessary),*

1. $F_1(x^+, \mu) = 0, H(x^+, \mu) > 0$ and $F_2(x^-, \mu) = 0, H(x^-, \mu) > 0$ for $\mu < 0$,
2. $F_1(x^+, \mu) = 0, H(x^+, \mu) < 0$ and $F_2(x^-, \mu) = 0, H(x^-, \mu) < 0$ for $\mu > 0$.

In terms of collision of equilibria with the boundary, this scenario describes how the only regular equilibrium point x^+ for $\mu < 0$ hits the boundary when $\mu = 0$ and turns continuously into the regular equilibrium x^- for $\mu > 0$.

DEFINITION 2.6. *We say that the boundary equilibrium bifurcation is associated with a nonsmooth fold for $\mu = 0$ if two branches of regular equilibria collide at the boundary equilibrium point $x = 0$ when $\mu = 0$ and are both turned into two branches of virtual equilibria past the bifurcation point. Namely, there exist smooth branches $x^-(\mu)$ and $x^+(\mu)$ such that $x^-(0) = x^+(0)$ and*

1. $F_1(x^+, \mu) = 0, H(x^+, \mu) > 0$ and $F_2(x^-, \mu) = 0, H(x^-, \mu) < 0$ for $\mu < 0$,
2. $F_1(x^+, \mu) = 0, H(x^+, \mu) < 0$ and $F_2(x^-, \mu) = 0, H(x^-, \mu) > 0$ for $\mu > 0$.

Here the two equilibria are both regular for $\mu < 0$, turning into two virtual equilibria past the border-collision point (leaving the system with no regular equilibrium either in region S_1 or region S_2). As will be shown later, one of the two equilibria has to be unstable.

We will now give conditions to distinguish between these two fundamental cases in the case of n -dimensional locally linearizable continuous nonsmooth flows. Namely,

in order for x^+ and x^- to be two regular equilibria of the system, we must have

$$(2.10) \quad \begin{aligned} F_1(x^+, \mu) &= 0, \\ \lambda^+ &:= H(x^+, \mu) > 0, \end{aligned}$$

and, using (2.9),

$$(2.11) \quad \begin{aligned} F_2(x^-, \mu) &= F_1(x^-, \mu) + G(x^-, \mu)\lambda^-, \\ \lambda^- &:= H(x^-, \mu) < 0. \end{aligned}$$

Now, linearizing about the boundary equilibrium bifurcation point $x = 0, \mu = 0$, we have

$$(2.12) \quad Ax^+ + B\mu = 0,$$

$$(2.13) \quad Cx^+ + D\mu = \lambda^+,$$

and

$$(2.14) \quad Ax^- + B\mu + E\lambda^- = 0,$$

$$(2.15) \quad Cx^- + D\mu = \lambda^-,$$

where $A = F_{1,x}, B = F_{1,\mu}, C = H_x, D = H_\mu$, and $E = G$, all evaluated at the point $x = 0, \mu = 0$.

Hence, from Definition 2.4 and (2.12) we have

$$x^+ = -A^{-1}B\mu,$$

and substituting into (2.13) we get

$$(2.16) \quad \lambda^+ = (D - CA^{-1}B)\mu.$$

Similarly, using (2.14) and (2.15), we have

$$(2.17) \quad \lambda^- = \frac{(D - CA^{-1}B)\mu}{(1 + CA^{-1}E)} = \frac{\lambda^+}{(1 + CA^{-1}E)}.$$

Therefore we can state the following theorem.

THEOREM 2.7 (equilibrium points branching from a boundary equilibrium). *For the systems of interest, assuming the nondegeneracy conditions*

$$(2.18) \quad \det(A) \neq 0,$$

$$(2.19) \quad D - CA^{-1}B \neq 0,$$

$$(2.20) \quad 1 + CA^{-1}E \neq 0,$$

- a persistence scenario is observed at the boundary equilibrium bifurcation point if

$$(2.21) \quad 1 + CA^{-1}E > 0;$$

- a nonsmooth fold is instead observed if

$$(2.22) \quad 1 + CA^{-1}E < 0.$$

This can be easily proved by considering that, from (2.16) and (2.17), λ^+ and λ^- have the same signs for the same value of μ (persistence) if condition (2.21) is satisfied, whereas they have opposite signs (nonsmooth fold) if condition (2.22) is satisfied.

The strategy presented here is valid for n -dimensional systems. Much work is still needed to account for the other scenarios conjectured in [75]. Particularly interesting is the case where a family of nonsmooth periodic oscillations is involved in the boundary equilibrium bifurcation scenario. There are some results available for this type of bifurcation in planar nonsmooth dynamical systems, but we know of no general result valid in n dimensions.

Example 2.2 (Hopf-like bifurcations in planar systems). Assume that $x^* = 0$ is a boundary equilibrium of a planar system of type (2.8) posed in the plane when $\mu = 0$. Linearizing the system about the origin, we get

$$(2.23) \quad \dot{x} = \begin{cases} A_1x + B\mu & \text{if } Cx + D\mu < 0, \\ A_2x + B\mu & \text{if } Cx + D\mu > 0, \end{cases}$$

where $x^T = (x_1, x_2) \in \mathbb{R}^2$, $A_1 = F_{1x}, A_2 = F_{2x}, B = F_{1\mu} = F_{2\mu}$, and $C = H_x, D = H_\mu$. As discussed earlier, continuity of the vector field implies that $A_2 = A_1 + EC$ for some nonzero vector E of appropriate dimension. It is typically often possible to find a similarity transformation that puts the system in general *observer canonical form* [33, 18], where the matrices A_1 and A_2 have their last columns equal to the vector $(0 \ 1)^T$, and where $C = (1 \ 0)$.

We seek to explain the possible birth of a family of stable limit cycles originating from a boundary equilibrium bifurcation. We present sufficient conditions for such a Hopf-like event to occur:

1. First, the boundary equilibrium bifurcation at $\mu = 0$ must represent a persistence scenario with a regular stable focus equilibrium becoming unstable.
2. Second, when $\mu = 0$ the origin should be an asymptotically stable equilibrium of the piecewise linear system formed by linearizing F_1 and F_2 about their values at the origin.

Using a continuity argument, it is easy to show that a stable attractor must exist in a neighborhood of the bifurcation point when the stable focus turns into an unstable one. The only other possible attractor that remains in a neighborhood of the origin in a two-dimensional system is a periodic orbit.

The first condition can be easily verified by using Theorem 2.7, i.e., assuming $(1 + CA^{-1}E) > 0$. Moreover, we require the eigenvalues of A_1 and A_2 to be complex with real parts characterized by opposite sign. To fulfill the second condition, and hence ensure the existence of a limit cycle for $\mu > 0$, we need to find conditions to ensure that the origin is asymptotically stable when $\mu = 0$. Since the system is in canonical form, we can assume $C = [1 \ 0]$, and the solutions for $\mu = 0$ are

$$\begin{cases} x_1(t) = e^{\alpha_i t}(x_{10} \cos(\omega_i t) + x_{20} \sin(\omega_i t)), \\ x_2(t) = e^{\alpha_i t}(x_{20} \cos(\omega_i t) - x_{10} \sin(\omega_i t)), \end{cases}$$

where $\alpha_i + j\omega_i, i = 1, 2$, are the eigenvalues of A_1 and A_2 , respectively.

Now, without loss of generality, let x_{20} be positive and start from initial conditions on the x_2 axis given by $x_{10} = x_1(0) = 0, x_{20} = x_2(0)$. Then, we have

$$\begin{cases} x_1(t) = e^{\alpha_1 t}x_{20} \sin(\omega_1 t), \\ x_2(t) = e^{\alpha_1 t}x_{20} \cos(\omega_1 t), \end{cases}$$

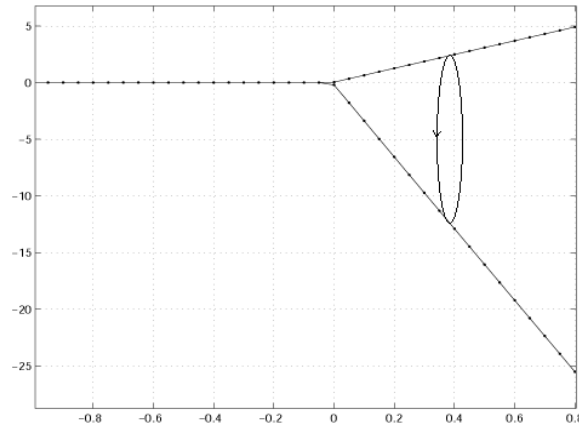


Fig. 5 Bifurcation diagram for (2.23) and (2.24) showing the creation of a limit cycle at a Hopf-like boundary equilibrium bifurcation at $\mu = 0$.

and the orbit will again cross the vertical axis at some time $t = t_1$ such that $x_1(t_1) = 0$, i.e.,

$$e^{\alpha_1 t_1} x_{20} \sin(\omega_1 t_1) = 0.$$

Thus, we must have $\sin(\omega_1 t_1) = 0$ and therefore we find

$$t_1 = \frac{\pi}{\omega_1}.$$

Moreover, we have

$$x_2(t_1) = e^{\alpha_1 \frac{\pi}{\omega_1}} x_{20} \cos(\pi) = -x_{20} e^{\alpha_1 \frac{\pi}{\omega_1}} < 0.$$

Now, the vector field characterized by A_2 drives the system trajectory, and it can be shown similarly that the next time the orbit hits the vertical axis is $t_2 = \frac{\pi}{\omega_2}$, at which time

$$x_2(t_2) = x_{20} e^{\alpha_1 \frac{\pi}{\omega_1} + \alpha_2 \frac{\pi}{\omega_2}}.$$

The origin will be stable, as required, if $x_2(t_2) < x_{20}$; thus we get the condition

$$\frac{\alpha_1}{\omega_1} + \frac{\alpha_2}{\omega_2} < 0.$$

Hence, the origin is stable for $\mu = 0$ and for continuity for further variations of μ , past the bifurcation point an attractor must exist. As the system is planar and no other equilibria can exist, such an attractor must be a stable limit cycle.

Figure 5 shows the bifurcation diagram of a planar system with

$$(2.24) \quad A_1 = \begin{pmatrix} -1 & 1 \\ -1 & 0 \end{pmatrix}, \quad A_2 = \begin{pmatrix} 2 & 1 \\ -5 & 0 \end{pmatrix}, \quad B = \begin{pmatrix} 0 \\ 1 \end{pmatrix}.$$

Here a stable focus hits the boundary and becomes unstable. We observe that, when this occurs, a limit cycle is, as predicted, generated at the boundary equilibrium bifurcation, and that the amplitude of the limit cycle scales linearly with the parameter, rather than quadratically as in the classical Hopf bifurcation.

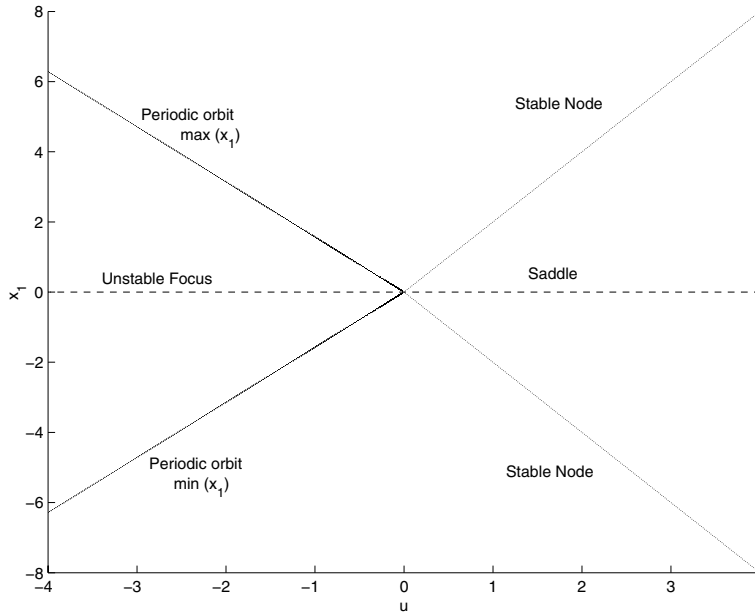


Fig. 6 Bifurcation diagram for the example in [75] (see (2.23) and (2.24)) showing the disappearance of a branch of limit cycles and an unstable focus and the appearance of two branches of stable nodes and a saddle at $\mu = 0$.

2.1.3. Some Nongeneric Phenomena. We close this section with a discussion of some other DIBs of equilibria studied in the literature which occur in nongeneric PWS continuous systems of the form (2.8), such as systems which are invariant under certain symmetries.

First, we review an example from [75], where a branch of stable periodic orbits and an unstable focus existing for $\mu < 0$ collide on the boundary Σ at the bifurcation point. For $\mu > 0$, the unstable focus becomes a saddle, the periodic orbit disappears, and two further stable equilibria appear (see Figure 6). Phase portraits corresponding to representative parameter values $\mu = -1, 0, 1$ have also been computed and are depicted in Figure 7. This transition, named *multiple crossing bifurcation* in [73, 75], has no counterpart in smooth systems.

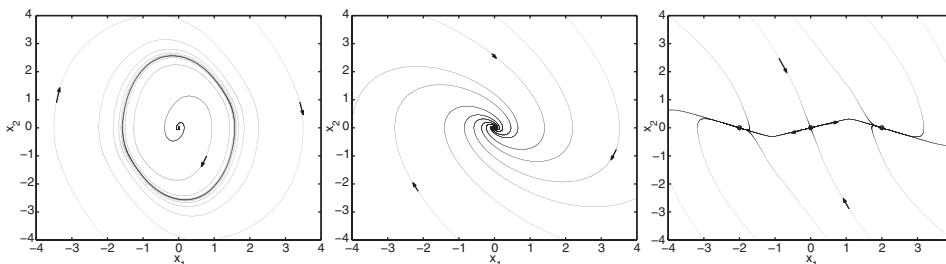


Fig. 7 Phase portraits for Figure 6 corresponding to (left) $\mu = -1$, (middle) $\mu = 0$, and (right) $\mu = 1$ (cf. [75, p. 160, Fig. 8.19]).

As a second case, we refer again to Example 2.2, the system (2.23). Depending on the value of the parameters, regular equilibria can collide with Σ giving rise to one of the local bifurcations discussed above. In addition to this, for some degenerate cases, nonsmooth *global* bifurcations are also possible involving intersections of stable and unstable manifolds with Σ . Indeed, it has been shown that global phenomena like single or double saddle connections (homoclinic or heteroclinic loops) can occur when parameters of the system are varied.

To illustrate the occurrence of such global nonsmooth phenomena, we briefly outline below some results presented in [53]. It can be proved for planar systems that a continuous piecewise linear vector field with one discontinuity surface Σ has at most one limit cycle; see the so-called Lum–Chua conjecture [78]. Moreover, if it exists, the limit cycle is either attracting or repelling. Also, under some additional conditions, existence of homoclinic loops can be proved. For example, the left panel of Figure 8 shows a bifurcation diagram with bifurcation parameter μ_1 , where a continuum of homoclinic loops (shaded region) is born at the bifurcation value. At this point, the global attractor at the origin changes its stability character. A phase portrait corresponding to $\mu = 1.75$ is shown in the right panel of Figure 8, where the homoclinic loops are clearly seen.

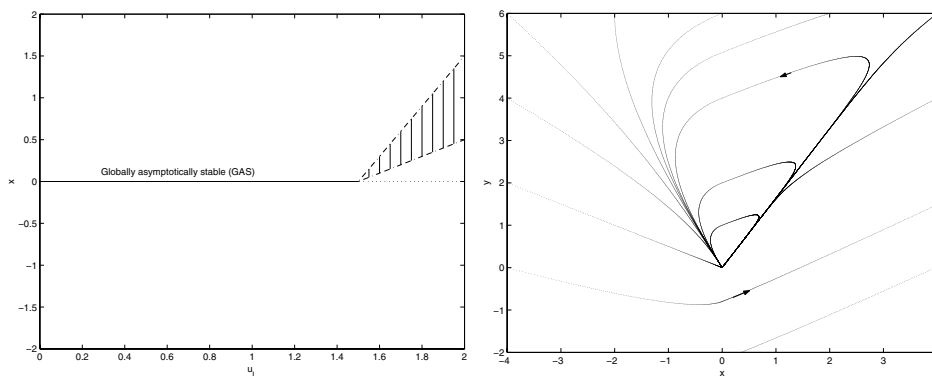


Fig. 8 A bifurcation diagram showing the occurrence of a continuum of homoclinic orbits (left) and a phase portrait corresponding to a parameter value with a continuum of homoclinic orbits (right).

2.2. DIBs of Limit Cycles. Having looked at the bifurcations of the equilibria of PWS systems, we now turn to a study of the bifurcations of the limit cycles of the same system. In this study we first look at the changes in the behavior of the system associated with the case of a limit cycle that undergoes a so-called grazing bifurcation.

DEFINITION 2.8. A grazing bifurcation is said to occur at a parameter value $\mu = 0$ of a PWS system (1.1)

$$\dot{x} = f(x, \mu), \quad x \in \mathbb{R}^n, \quad \mu \in \mathbb{R},$$

depending smoothly on a parameter μ , if there is a T -periodic orbit $x(t) = p(t)$ that has a point of tangency with a discontinuity set Σ_{ij} . Moreover, we suppose that, close to the tangency point, the flow is unfolded in a generic way with respect to μ .

We will show that in the neighborhood of a grazing bifurcation we may expect to see the creation of many new periodic orbits, with the additional possibility of chaotic behavior associated with a period-adding cascade. In section 2.3, we then study the case of a limit cycle passing through a point where two boundaries cross. In the case of grazing, we shall start with some preliminary discussion which introduces the main technique of analysis that we shall use when dealing with bifurcations of limit cycles and of the (Poincaré) maps associated with them.

2.2.1. Discontinuity Mappings. Suppose there is a grazing bifurcation as defined above at parameter value $\mu = 0$. Without loss of generality (with a translation of phase space and time if necessary), we assume that grazing occurs at a point $x = 0 = p(0)$ and with respect to a locally unique discontinuity boundary Σ that is independent of μ . Moreover, we suppose that $p(t)$ is a hyperbolic limit cycle and is hence isolated (we shall not consider the Hamiltonian case here).

As with smooth bifurcations, we also need a nondegeneracy hypothesis, that the parameter μ really does unfold the bifurcation. An important such condition is that if, for $\mu < 0$, there is a periodic orbit existing wholly in S_1 which grazes Σ when $\mu = 0$, then for $\mu > 0$ the orbit, if considered to be a solution of the differential equation $\dot{x} = F_1(x, \mu)$ alone, would persist (for small values of μ), but would necessarily intersect Σ transversally. In this rather dull case, a periodic orbit of the full system $\dot{x} = f(x, \mu)$ exists for $\mu > 0$ which is close to the original but which penetrates Σ . We shall see this is only one possibility from a rich set of different dynamical scenarios.

To make progress we now introduce a set of maps associated with the flow. A study of these maps will allow us to classify the various forms of behavior that we will encounter at the bifurcation point. Suppose that we have a surface $\Pi \subset S_1$ which is transverse to the periodic orbit $p(t)$ and intersects it at the point x_p . The Poincaré map $P(z) : \Pi \rightarrow \Pi$ is given by computing the flow of the dynamical system $\dot{x} = f(x, \mu)$ forward in time, starting at $x = z$, and determining the first intersection of this flow with Π . Provided that z is close to x_p this map is well defined and continuous, with $P(x_0) = x_0$. The local behavior of P for z close to x_0 is what will concern us. Essentially, three different scenarios occur for a general periodic solution $p(t)$. First, $p(t)$ may not intersect Σ and lies entirely within S_1 . In this case we have simply that

$$P(z) = x_p + A(z - x_p) + \mathcal{O}(|z - x_p|^2),$$

where A is the linear operator associated with the linearization of the flow of F_1 about $p(t)$. Second, $p(t)$ may intersect Σ at a point x with a *high normal velocity*, so that $|H_x(x)F(x)|$ is not small, where H_x is the normal to Σ . In this case it can be shown [1, 81, 75] that there is another linear operator B such that

$$P(z) = x_p + B(z - x_p) + \mathcal{O}(|z - x_p|^2).$$

Here, B is a linear correction to the operator A to take account of the flow through the region S_2 . The correcting matrix is called the *saltation matrix*. The case that interests us most is that which arises when $|H_x(x)F(x)|$ is close to, or equal to, zero, so that $p(t)$ has a grazing intersection with Σ when $z = x_p$. In this case, the flow spends a small time in S_2 and this leads to a locally nonlinear expression for P . We will now show that, in this case, there are linear operators D, E and a vector β such that, to leading order,

$$P(z) = x_p + D(z - x_p) + E|z - x_p|^\gamma \beta,$$

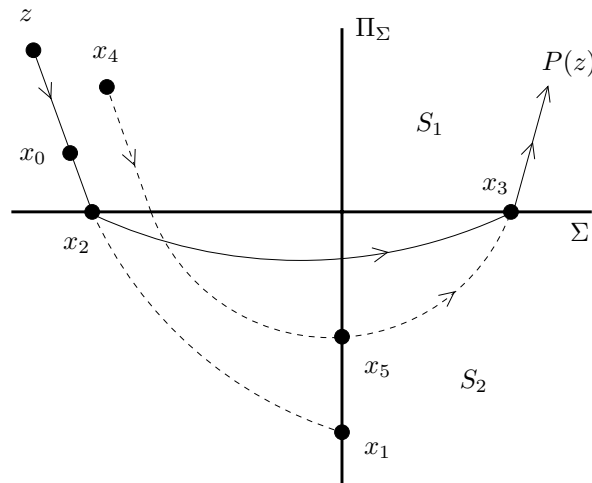


Fig. 9 A comparison between the two local maps ZDM and PDM in the neighborhood of a grazing orbit, grazing Σ at the origin. In this picture, the solid lines represent true trajectories, and the dotted lines represent trajectories continued into the part of S_1 lying on the S_2 side of Σ . The map $x_0 \rightarrow x_4$ is the ZDM and the map $x_1 \rightarrow x_5$ is the PDM.

where the value of γ depends upon the smoothness of the vector field. Indeed, γ can take the values of $1/2$ or $3/2$.

To derive this result, we now introduce the key concept of the (local) *discontinuity mapping* (DM) introduced by Nordmark [82, 84, 27]. This map (taken in the case of interest near to a grazing point) is the correction to the flow map in the region S_1 alone that must be applied to a trajectory to take account of the passage through region S_2 on the far side of the discontinuity set Σ . This DM is defined for all trajectories in a neighborhood of the grazing one, and has no reference to grazing trajectories being part of a periodic orbit. By definition, the DM will be the identity for non- Σ -crossing trajectories.

There are two useful ways of constructing such a map. For the first, suppose that we start a flow $q(t)$ from a point z close to a grazing trajectory $p(t)$ starting from x_p , which we assume intersects Σ at the point $x = 0$. The flow $q(t)$ will initially lie in S_1 and will intersect Σ at a point x_2 close to the origin. It will then continue in S_2 and will intersect Σ again at a point x_3 . Subsequently the flow will (at least locally) be in S_1 again and will evolve forwards to the point $P(z)$ in Π . We can further decompose this flow by considering it to be a flow (in S_1) from z to an arbitrary point x_0 close to the origin, with x_0 then mapped to x_3 . This is illustrated in Figure 9. Now, suppose that the flow from x_0 to x_3 takes a time δ . We can solve the system $\dot{x} = F_1$ for a time $-\delta$ starting at the point x_3 to give a point x_4 . This gives the *zero time discontinuity map* (ZDM) from x_0 to x_4 , which takes *zero time*. The entire flow from z to $P(z)$ is then a combination of two flows in S_1 (from $\phi_1 : z \rightarrow x_0$ and $\phi_2 : x_4 \rightarrow P(z)$) so that the *global Poincaré map* is given by

$$P = \phi_2 \circ \text{ZDM} \circ \phi_1.$$

The purpose of this construction is that, for x_0 small, the form of ZDM can be determined very precisely (and we proceed to do this in the next subsection), while

the maps ϕ_1 and ϕ_2 can be determined by simply looking at the flow in S_1 and have all the smoothness properties associated with such flows.

Alternatively, referring again to Figure 9, we can consider the surface $\Pi \equiv \Pi_\Sigma$ to lie normal to Σ and to pass through the origin. Locally, one side of this will lie in S_1 and the other in S_2 . Using this we may construct an alternative local DM, the *Poincaré discontinuity map* (PDM). The construction of this is a little less intuitive than that of the ZDM, but the PDM is often an easier map to work with from the point of view of analyzing the structure of bifurcations. If we consider the earlier scenario, then the trajectory which intersects Σ at the point x_2 can be continued in S_1 . If so, it will intersect Π_Σ at a point x_1 as illustrated. Similarly, the trajectory starting from the point x_3 may be continued backwards in time to intersect Π_Σ at a point x_5 . This gives a well-defined PDM from $x_1 \rightarrow x_5$. The *global* Poincaré map from Π_Σ to itself is then the usual Poincaré map associated with the orbit $p(t)$ considered to lie wholly in S_1 combined with the PDM.

The difference in concept between the ZDM and the PDM comes about when one considers how to embed them into a more global picture containing the dynamics around the periodic orbit. Using either, we can then derive a local “normal form” map for the grazing bifurcation, which, in the same sense as a normal form for smooth bifurcations of limit cycles, will capture all dynamics that remains in a neighborhood of the critical trajectory for nearby trajectories. (We will meet both maps again in section 4 when we look at impact oscillators.)

2.2.2. DMs for Grazing Bifurcations. Before stating the results in the form of theorems (which are derived explicitly in [27, 37, 86]), we need to consider the geometry near the grazing point.

In particular, if we have as before that $\Sigma = \{x : H(x) = 0\}$, then *grazing* occurs at $x = 0, t = 0$ if the following conditions are satisfied for $i = 1, 2$:

$$(2.25) \quad \left. \frac{dH(x(t))}{dt} \right|_{t=0} = H^0_x F_i^0 = 0, \quad \left. \frac{d^2 H(x(t))}{dt^2} \right|_{t=0} = (H^0_x F_i^0)_x F_i^0 > 0,$$

where a superscript “0” denotes quantities evaluated at $x = 0$. That superscript is dropped in what follows. The first condition states that the vector field is tangent to Σ there. The second condition ensures that the curvature of the trajectories in the direction normal to Σ is of the same sign in S_1 and S_2 . Without loss of generality, we assume this sign to be positive so that grazing occurs from the side S_1 . We are now in a position to state normal form results for grazing bifurcations, by constructing DMs within these local coordinates. The proofs can be obtained either by Taylor expansion of the flows corresponding to vector fields F_1 and F_2 in a neighborhood of the grazing point, using the conditions (2.25) explicitly, or by using Lie derivatives [62, 87]. The key observation behind all of the proofs is that the time spent flowing on the S_2 side of Σ scales like the square root of the penetration. If we introduce an extra scalar variable y for this square root, then we find a regular Taylor series in y and the initial condition x . This leads to DMs whose leading-order terms scale like some power y , which is $O(\sqrt{x})$. The precise form of this scaling depends upon the overall smoothness of the vector field.

THEOREM 2.9 (the ZDM for a vector field with a uniform discontinuity [86]). *Given the above assumptions and the assumed form of discontinuity (2.6) for $m \geq 2$, let $y(x) = \sqrt{-H_{\min}(x)}$, where $H_{\min}(x)$ is the minimum value of $H(x)$ attained along*

a trajectory of flow ϕ_1 ; then the ZDM is given by

$$(2.26) \quad x \mapsto \begin{cases} x & \text{if } H_{\min}(x) \geq 0, \\ x + e(x, y)y^{2m-1} & \text{if } H_{\min}(x) \leq 0, \end{cases}$$

where e is a sufficiently smooth function of its arguments within \mathcal{D} whose lowest-order term is given by

$$e(0, 0) = 2(-1)^{m+1}I(m)J(0)\sqrt{\frac{2}{(H_x F_1)_x F_1(0)}}$$

with

$$I(m) = \int_0^1 (1 - \xi^2)^{m-1} d\xi, \quad I(2) = \frac{2}{3}, \quad I(3) = \frac{8}{15}, \quad I(4) = \frac{16}{35}, \dots$$

The smoothness of e depends on the smoothness of F_1 , F_2 , and H , and if they are all analytic, then e is analytic.

If we do not assume that the vector field has a uniform discontinuity, then we have the following much more cumbersome expressions for the ZDM, which include the case of degree of smoothness 1. This expression must also include a condition that avoids sliding taking place.

THEOREM 2.10 (the ZDM at a general grazing bifurcation [37]). *Given the above assumptions but not (2.6), the local ZDM describing trajectories in a neighborhood of the grazing trajectory has generically (i) a square-root singularity at the grazing point if $F_1^0 \neq F_2^0$ and a nonsliding condition such as (2.7) holds; (ii) a 3/2-type singularity at the grazing point in the case where $F_1^0 = F_2^0$, while $\frac{\partial F_1^0}{\partial x} \neq \frac{\partial F_2^0}{\partial x}$ or $\frac{\partial^2 F_1^0}{\partial x^2} \neq \frac{\partial^2 F_2^0}{\partial x^2}$.*

Specific formulae for these maps are given for the two cases as follows, where a subscript x denotes partial differentiation and all quantities are evaluated at $x = 0$ (the superscript 0 being omitted).

(i) *If the vector field is discontinuous at grazing, we have*

$$(2.27) \quad x \mapsto \begin{cases} x & \text{if } H_{\min}(x) > 0, \\ 2\sqrt{\frac{-2H_{\min}(x)}{(H_x F_1)_x F_1}}v + O(x) & \text{if } H_{\min}(x) < 0, \end{cases}$$

where

$$(2.28) \quad v = \frac{(H_x F_2)_x F_1}{(H_x F_2)_x F_2}(F_2 - F_1),$$

$$(2.29) \quad H_{\min}(x) = H_x x + O(x^2).$$

(ii) *If the vector field is continuous, i.e., $F_1 = F_2 := F$, but has a discontinuous first or second derivative,*

$$(2.30) \quad x \mapsto \begin{cases} x & \text{if } H_{\min}(x) > 0, \\ x + 2\sqrt{\frac{-2H_{\min}(x)}{(H_x F_1)_x F}}(v_1 + v_2 + v_3) + O(x^2) & \text{if } H_{\min}(x) < 0, \end{cases}$$

Table 1 Relationship between the singularity of the system at the grazing point and the type of singularity in the corresponding local map.

Degree	Jump in	Map discontinuity	
		Uniform case	Nonuniform
0	x	Square root (section 4)	
1	F	-	Square root
2	F_x	(3/2)-type	(3/2)-type
3	F_{xx}	(5/2)-type	(3/2)-type

where $v_1, v_2, v_3 \in \mathbb{R}^n$ are given by

$$(2.31) \quad v_1 = - \left\{ - \frac{((H_x F_2)_x (F_1 - \frac{2}{3} F_2))_x F}{(H_x F_2)_x F} (F_2 - F_1)_x F + \left(F_{1x} F_2 - \frac{1}{3} F_{1x} F_1 - \frac{2}{3} F_{2x} F_2 \right)_x F \right\} \frac{H_x x}{(H_x F_1)_x F},$$

$$(2.32) \quad v_2 = (F_2 - F_1)_x x,$$

$$(2.33) \quad v_3 = -(F_2 - F_1)_x F \frac{(H_x F_2)_x x}{(H_x F_2)_x F},$$

$$(2.34) \quad H_{\min}(x) = H_x x + O(x^2).$$

Remarks.

1. Note the pattern implied by the nonuniform discontinuity results, in Theorem 2.10. If the flow map is discontinuous across Σ (impacting case) or we have a degree of smoothness 1 with a no-sliding condition as in (2.7), then we see a local square-root singularity in the DM. If, instead, there is a jump in first or second derivative, then the DM has a 3/2-law singularity; see Table 1.
2. In contrast, the uniform discontinuity result in Theorem 2.9 gives the more straightforward property that discontinuity of the n th derivative implies a map with an $O(n + 1/2)$ discontinuity to lowest order. In particular, this asserts that the $O(3/2)$ correction term of (2.30), which does not vanish if $F_{1x} = F_{2x}$ but $F_{1xx} \neq F_{2xx}$, must rely on the fact that the disagreement between the two Hessians does not occur with a factor $H(x)^2$ in the Taylor expansion of $F_1 - F_2$ at $x = 0$. We leave it as a (nontrivial!) exercise for the reader to show how the two formulae (2.30) and (2.26) agree in the case of uniform discontinuity.
3. In all cases, the ZDM can be seen to reduce to the identity map at each order when the two vector fields F_1 and F_2 are identical.
4. In the general, nonuniform case, equivalent expressions for the PDM applied at some local Poincaré section that contains the grazing point are given in [37].

Example 2.1 continued (the bilinear oscillator). Let us return to the bilinear oscillator example given by (2.2), (2.3), and (2.4), with a grazing on a limit cycle occurring at the time $t = t^*$. We refer the reader to [36] for more details and also numerical corroboration. First we will consider problems for which either the damping coefficient ζ_i or the stiffness coefficient k_i change across the switching manifold, while the forcing remains the same. In this case, we set $\hat{\beta}_1 = \hat{\beta}_2 = \hat{\beta}$ in (2.3) and, using the expressions in Theorem 2.10, we get the following expression for the lowest-order

approximation to the ZDM for $x_1 < 0$:

$$(2.35) \quad x \mapsto x + \begin{pmatrix} \frac{4}{3}(\zeta_2 - \zeta_1)\gamma_1^3 \\ \left[\frac{8}{3}(\zeta_1^2 - \zeta_1\zeta_2) + \frac{1}{3}(k_1^2 - k_2^2) \right] \hat{\beta}\gamma_1^3 + 2(k_1^2 - k_2^2)x_1\gamma_1 \\ 0 \end{pmatrix},$$

where $\gamma_1 = \sqrt{2\frac{|x_1|}{\hat{\beta}}}$. This gives an $|x|^{3/2}$ -correction to the leading-order behavior of the usual Poincaré map.

Consider next the case where $\beta_1 = \beta_2 := \hat{\beta}$ and, in addition, $\zeta_1 = \zeta_2 = \zeta$. Here we can apply the uniform discontinuity result (2.26) with $m = 1$. Applying (2.26), we find that $H_{\min}(x) = x_{1\min}$, which is equal to x_1 to lowest order. Hence to leading order for $x_1 < 0$ we get

$$x \mapsto x + \frac{2}{3}(k_2^2 - k_1^2)\sqrt{\frac{2}{\hat{\beta}}}\left(0, |x_1|^{\frac{3}{2}}, 0\right)^T.$$

Finally, we consider the local dynamics of the bilinear oscillator when the forcing amplitude varies across the switching manifold, i.e., $\hat{\beta}_1 \neq \hat{\beta}_2$ while $k_1 = k_2 = k$, $\zeta_1 = \zeta_2 = \zeta$ in (2.3). In this case, the bilinear oscillator is characterized by a discontinuous vector field at the grazing point and the formula for the ZDM yields to lowest order

$$(2.36) \quad x \mapsto \left(0, 2\frac{\hat{\beta}_1}{\hat{\beta}_2}(\hat{\beta}_2 - \hat{\beta}_1), \sqrt{2\frac{|x_1|}{\hat{\beta}_1}} \cdot 0\right)^T \quad \text{for } x_1 < 0.$$

This is a square-root map provided $\hat{\beta}_1 \neq 0$ and $\hat{\beta}_2 \neq 0$. Such maps will be discussed further in section 4 as they arise naturally in the study of impacting systems. In short, the extreme stretching of phase space resulting from the square-root behavior has a profound effect on the observed dynamics and leads to the creation of many new periodic (and chaotic) orbits.

2.2.3. The Dynamics Given by the Resulting Poincaré Maps. The above analysis derives a complete normal form for the Poincaré maps associated with limit cycles at grazing. However, so far we have said almost nothing about the dynamics of the iterations of these maps as a parameter in the underlying system is varied. We shall return to a treatment of maps with a square-root singularity in section 4. So let us conclude this section with a few remarks and an example that illustrate what can happen in maps with a 3/2-law singularity.

The simplest statement to make is that the 3/2-map is C^1 at the grazing point, so there can be no corresponding local bifurcation of fixed points of the map (assuming as we do that the orbit $p(t)$ is hyperbolic). Thus this DIB does not imply bifurcation in the classical sense. However, the slope of the map has a square-root singularity, so there can be a rapid (but continuous) change in the Floquet multipliers of the periodic orbit at the grazing point. This can lead to a nearby local bifurcation. The next example illustrates, through an application, that such a local bifurcation caused indirectly by the grazing can occur remarkably close to the grazing point itself.

Example 2.3 (a stick-slip oscillator). Friction oscillators give a natural application of the ideas of this section. In [25] a simple model was introduced aimed at explaining experimentally observed stick-slip motion using more realistic laws than

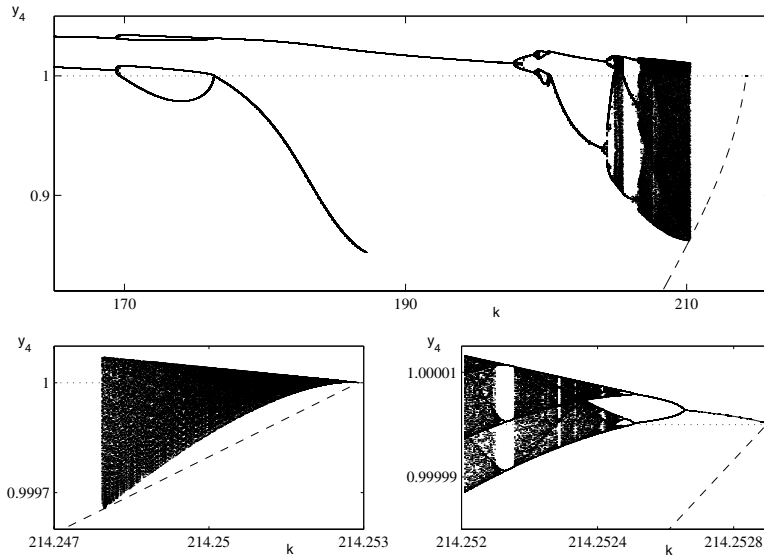


Fig. 10 (After [27].) Successive enlargements of a computed bifurcation diagram for $d = 0.1$, depicting local maxima of y_4 . The dotted line corresponds to the discontinuity set Σ and the dashed line to a branch of unstable limit cycles born in a subcritical Hopf bifurcation.

simple coulomb friction. This model was analyzed in more detail in [27] and is given by

$$(2.37) \quad \dot{y}_1 = y_2,$$

$$(2.38) \quad \dot{y}_2 = -1 + \left[1 - \gamma U |1 - y_4| y_2 + \beta U^2 (1 - y_4)^2 \sqrt{K}(y_1) \right] e^{y_1 - d},$$

$$(2.39) \quad \dot{y}_3 = y_4,$$

$$(2.40) \quad \dot{y}_4 = -s y_3 + \frac{\sqrt{g\sigma}}{U} e^{-d} \left[\mu (y_5 e^{-y_1} - 1) + \alpha U^2 S(y_1, y_4) \right],$$

$$(2.41) \quad \dot{y}_5 = \frac{1}{\tau} [(1 - y_4) - |1 - y_4| y_5],$$

where

$$K(y_1) = 1 - \frac{y_1 - d}{\Delta}, \quad S(y_1, y_4) = (1 - y_4) |1 - y_4| K(y_1) e^{-y_1} - 1 + \frac{d}{\Delta}.$$

Here the variable y_1 is a vertical and y_3 a horizontal degree of freedom of a mass being pulled across a horizontal surface by a spring whose other end moves at constant speed U . The extra coordinate $y_5 \in [-1, 1]$ is an internal variable measuring the shear deformation between the surface and the mass. The main discontinuity to feature in the dynamics is the set $\Sigma = \{y_4 = 1\}$ and this corresponds to motion with zero relative velocity between the mass and the surface. Motion with $y_4 < 1$ corresponds to the mass being dragged across the surface.

Figure 10 shows a bifurcation diagram where the bifurcation parameter is s , a rescaling of the spring stiffness (the ordinate k depicted in the plot) for the fixed value of the equilibrium surface separation $d = 0.1$. For the values of the other parameters used, the interested reader is referred to [27]. Note that for $k = 214.2528$, an unstable limit cycle grazes Σ . This causes the onset, upon decreasing k , of so-called

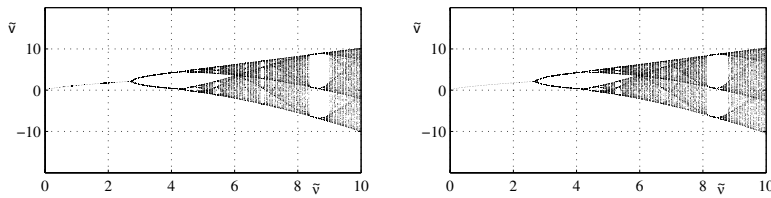


Fig. 11 (After [27].) Comparison between the numerical simulations (left panel) and the discontinuity mapping (right panel) local to the grazing bifurcation at $k = 214.2528$. Here \tilde{v} is a rescaling of y_4 and \tilde{v} is a rescaling of $-k$ (cf. Figure 10).

stick-slip motion that makes repeated tiny penetrations into the region with $y_4 > 1$. This motion can be quite involved and features chaotic dynamics and *period-adding bifurcations* (as one would expect in the case of normal form maps with a square-root dependency [82, 21]).

The onset of this rich dynamics observed upon decreasing k through the grazing value can be explained by the theory treated here. Specifically, an involved computation in [27] computes the normal form (2.30) in Theorem 2.10 (this was actually the first ever such computation in the case of smoothness degree 2). We omit the details here, but merely reproduce in Figure 11 the results of the iteration of the corresponding map composed with the flow map over a whole period. Note, over this small scale, the close agreement between the mapping and the simulations

Now, this example serves to illustrate a key point about grazing bifurcations where the degree of smoothness is 2 or more. A local analysis of the normal form shows that it is continuous at the grazing point and has a $3/2$ -type discontinuity. At the grazing point, there should be a well-defined tangent to the branch of fixed points. One might think that this would rule out any complex dynamics emerging from such DIBs. Yet, in the dynamics depicted in Figure 11, while there is no discontinuous jump in the slope, it is found that there is a fold at a \tilde{v} -value within 10^{-3} of the grazing point. Returning to the physical coordinates, this implies a fold for k within 10^{-7} of the grazing point (see Figure 10)! So even if no instantaneous change in stability occurs, grazing in piecewise-continuous systems can cause a rapid change in the curvature of a bifurcation branch giving rise to many nearby classical bifurcations. Moreover, when viewed in the large, the dynamics of the normal form may help explain some more global features of the dynamics such as period-adding cascades.

2.3. Bifurcations of Limit Cycles 2: Boundary-Intersection Crossing. Consider now a situation where two discontinuity boundaries Σ_1 and Σ_2 cross transversally: see Figure 12(a). It is clear that it would be of codimension-one for a periodic orbit to pass through the $(n - 2)$ -dimensional intersection C between these two boundaries. We call this situation a *boundary-intersection crossing*. The special case in Figure 12(b) has previously been called a *corner-collision bifurcation* [35]. We shall consider only the case where the vector field is discontinuous across each of Σ_1 and Σ_2 and shall show that to lowest order this leads to a piecewise-linear normal form for the global Poincaré map. The case where the vector field is continuous can be similarly shown to lead to a DM with a jump of quadratic order.

We consider first the general case depicted in Figure 12(a) and a set of local coordinates such that the point of intersection of the periodic orbit with $C = \Sigma_1 \cap \Sigma_2$ occurs at $x = 0$. The boundaries Σ_1 and Σ_2 are given by the zero sets of two smooth

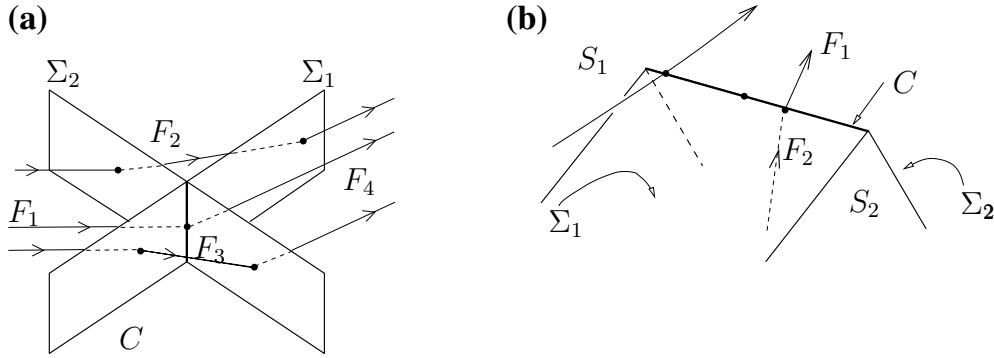


Fig. 12 (a) A boundary-intersection crossing trajectory that intersects the crossing manifold C between two discontinuity surfaces Σ_1 and Σ_2 , and two nearby trajectories. Here it is assumed that a different smooth vector field F_i applies in each of the four local phase space regions. (b) The special case where only two different vector fields, F_1 and F_2 , apply, and the crossing manifold might better be described as the corner in a single discontinuity surface made up of two smooth pieces Σ_1 and Σ_2 . Two distinct kinds of corner-intersecting trajectories are depicted: so-called external and internal corner collisions [35].

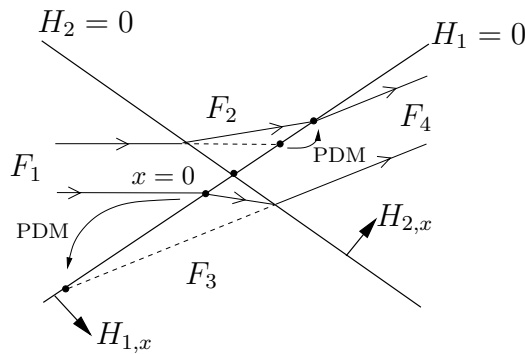


Fig. 13 A planar representation of the construction of the local PDM in a neighborhood of a boundary-crossing intersecting trajectory. Here it is assumed that the Poincaré section is $\Sigma_1 : \{H_1 = 0\}$.

functions $H_1(x)$ and $H_2(x)$, respectively, which, as in the previous section, we take for simplicity to be linear, $\Sigma_1 = \{H_1 = 0\}$ and $\Sigma_2 = \{H_2 = 0\}$, and the sense of their normal vectors is as depicted in Figure 13.

Now, it will transpire that the linear approximation to the flow and to the boundaries is sufficient to determine the leading-order expression for the DM in a neighborhood of $(x, \mu) = (0, 0)$. Thus $F_i(x, \mu)$ is replaced by $F_i(0, \mu)$ and we suppose for simplicity that the local situation near $x = 0$ is unchanged by the variation of μ , so $F_i(x, \mu) \approx F_i(0, 0) := F_i$. Let a final subscript indicate a component in the normal direction $H_{j,x}$, so that $F_{ij} = H_{j,x}F_i(0)$ and $x_j = H_{j,x}x$ for $j = 1, 2$.

We make the further assumption that there is no sliding or grazing in the neighborhood of $x = 0$, so that all four vector fields cross both Σ_1 and Σ_2 transversely and in the same sense. That is,

$$(2.42) \quad F_{ij} > 0 \quad \text{for } i = 1, \dots, 4, \quad j = 1, 2.$$

For simplicity, it is easier to work with a Poincaré section that lies in one of the boundaries. Without loss of generality we take the section $\Pi := \{H_1 = 0\}$ as in Figure 13. Then, constructing the local PDM as in the figure, we arrive after some algebra at the following theorem.

THEOREM 2.11 (local PDM at boundary-crossing point intersection [35, 38]). *Under the above assumptions, the local PDM based on the Poincaré section Σ_1 is given by*

$$(2.43) \quad x \mapsto \begin{cases} x + \frac{x_2}{F_{12}} \left(F_2 \frac{F_{11}}{F_{21}} - F_1 \right) + O(|x|^2) & \text{if } x_2 > 0, \\ x + \frac{x_2}{F_{32}} \left(F_4 \frac{F_{31}}{F_{41}} - F_3 \right) + O(|x|^2) & \text{if } x_2 < 0. \end{cases}$$

Here the correction is made to a trajectory which it is assumed evolves according to vector field F_1 before hitting Σ_1 and then vector field F_4 afterwards.

It is significant that to lowest order (2.43) is a piecewise-linear map, such that each of the maps for $x_2 > 0$ and $x_2 < 0$ is a rank-one update of the identity. This is precisely the form of map studied by Feigin [46, 47, 48, 49, 39] and, in one and two dimensions, by the Maryland group [88, 7], who first used the name *border-collision* bifurcations (of maps). The reader is referred to these works for a detailed description of the dynamics that may ensue under parameter variation. Among other possibilities it is possible for a sharp fold-like bifurcation to occur, a nonsmooth period-doubling, or a sudden jump to chaotic motion. The chaotic motion has the character of being *robust* [10], that is, containing no periodic windows.

Now suppose that the trajectory $p(t)$ that passes through the boundary-crossing point at $x = 0$, $\mu = 0$ is part of a periodic orbit. Then the above DM can be composed with the linear to lowest-order Poincaré map P_Π around the critical boundary-crossing intersecting periodic orbit. The following examples illustrate the construction of the ensuing piecewise-linear maps. Both correspond to the special case in Figure 12(b).

Example 2.4 (an explicitly calculable model). We consider first an example where a hyperbolic limit cycle grazes a corner in an autonomous, PWS vector field that is solvable in closed form. Specifically we take a system

$$(2.44) \quad \begin{aligned} \dot{x} &= \gamma, \\ \dot{y} &= \delta, \end{aligned} \quad \text{for } x > 0, y > 0, y < x \tan \beta \quad (\text{region } S_2),$$

$$(2.45) \quad \begin{aligned} \dot{r} &= \varepsilon r(a - r), \\ \dot{\theta} &= 1, \end{aligned} \quad \text{otherwise (region } S_1).$$

Here

$$x + 1 = r \cos \theta, \quad y = r \sin \theta,$$

and $\gamma, \delta, \beta, \varepsilon$, and a are real constants satisfying the constraints

$$(2.46) \quad 0 < \beta < \pi/2, \quad \delta > \gamma \tan \beta.$$

See Figure 14(a). Consider the system (2.45). For $a > 0$ there is a limit cycle which is stable if $\varepsilon > 0$. At $a = 1$ this limit cycle collides with the boundary of region S_2 in an external corner collision bifurcation. Under this construction we have

$$H_{2,x} = y \cos \beta (-x \sin \beta, \cos \beta).$$

The constraints (2.46) ensure that no sliding occurs along $\Sigma_{1,2}$.

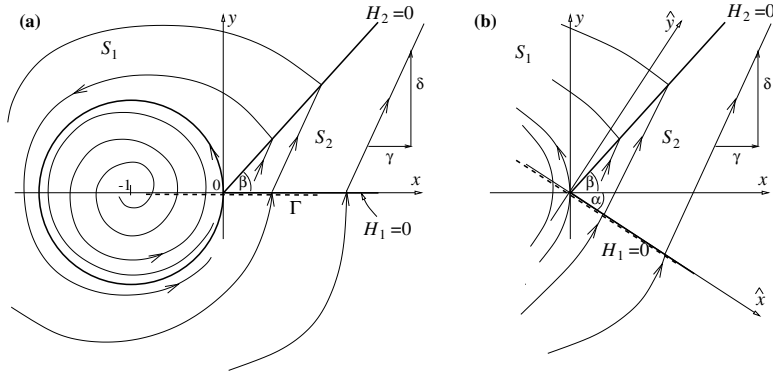


Fig. 14 (a) Sketch of the phase portrait of (2.44), (2.45) with $a = 1$. (b) An adaptation of the system.

Since the systems in regions S_1 and S_2 are solvable in closed form one can explicitly construct the Poincaré map $x \mapsto \Pi x$ associated with the Poincaré section $\{y = 0, x > -1\}$. After a short calculation, we obtain an explicit expression for this map when $x > 0$,

$$(2.47) \quad x \mapsto \frac{a\hat{r} \exp[\varepsilon a(2\pi - \hat{\theta})]}{\hat{r} \exp[\varepsilon a(2\pi - \hat{\theta})] + a - \hat{r}},$$

where

$$(2.48) \quad \hat{t} = \frac{x \tan \beta}{\delta - \gamma \tan \beta}, \quad \hat{r} \cos \hat{\theta} = x + \gamma \hat{t} + 1, \quad \hat{r} \sin \hat{\theta} = \delta \hat{t}.$$

This exact map may be compared to the global PDM calculated using the above theory, for which one easily obtains

$$(2.49) \quad x \mapsto \begin{cases} \exp(-2\varepsilon\pi)x + (1 - \exp(-2\varepsilon\pi))(a - 1) & \text{if } x < 0, \\ \frac{\delta \exp(-2\varepsilon\pi)}{\delta - \gamma \tan \beta} x + (1 - \exp(-2\varepsilon\pi))(a - 1) & \text{if } x > 0. \end{cases}$$

The benefit of this example is that it allows for the direct comparison between the “normal form” map (2.48) valid close to the corner collision and the explicit map; see [35] for details.

Example 2.5 (application: DC-DC Buck converter). We now study a certain piecewise-linear circuit used widely in power electronics for adjusting a given DC voltage to a lower value. The DC-DC buck converter under ramp voltage-mode control is used as an example exhibiting nonsmooth bifurcations. Figure 15 shows the block diagram of the buck converter. A nonsmooth, T -periodic control signal $V_r(t)$, given by

$$(2.50) \quad V_r(t) = \gamma + \eta(t \bmod T), \quad \gamma, \eta, T > 0,$$

is compared with the voltage $V(t)$ in the capacitor. If $V > V_r$, then the switch S_1 opens and the switch S_2 conducts, while if $V < V_r$, then the switch S_1 is closed, S_2 does not conduct, and the battery feeds the load.

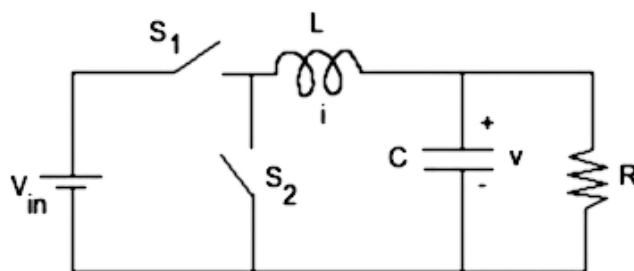


Fig. 15 Block diagram of the buck converter, where $V_{in} = E$.

Complex nonsmooth dynamics have been found in a number of similar configurations of power converters; see [51, 119, 122] and the references therein. Here we shall take the widely used form of converter studied in [31, 34], whose model equations are written in terms of a current $I(t)$ and voltage $V(t)$:

$$(2.51) \quad \dot{V} = -\frac{1}{RC}V + \frac{I}{C},$$

$$(2.52) \quad \dot{I} = -\frac{V}{L} + \begin{cases} 0, & V \geq V_r(t), \\ E/L, & V < V_r(t). \end{cases}$$

C , E , L , and R are positive constants representing a capacitance, battery voltage, inductance, and resistance, respectively, and V_r is a piecewise-linear but discontinuous “ramp” signal (2.50). For this system we have $\Sigma := \{V = V_r(t)\}$, which has corners whenever $t = 0 \bmod T$.

For the details of the electrical circuit represented by the model (2.51), (2.52) and for some of the rich features of its dynamics, see [51, 40, 34]. These features include periodic orbits and strange attractors that are characterized by trajectories that are close to both corner collision (at $t = 0 \bmod T$) and sliding (with $V(t) = V_r(t)$ for $(m-1)T < t < mT$ for some m). The parameter values taken were those used in the experiments of [31], which in SI units are

$$(2.53) \quad \begin{aligned} R &= 22\Omega, \quad C = 4.7\mu F, \quad L = 20mH, \quad T = 400\mu s, \\ \gamma &= 11.75238V, \quad \eta = 1309.524Vs^{-1}, \end{aligned}$$

with the bifurcation parameter $E \in (15, 60)$ being the input voltage.

In [35] an analytical explanation was offered for the phenomenon that was merely observed numerically in [34], namely, a periodic orbit crossing a boundary intersection causes a fold (actually a sharp corner) in the bifurcation diagram of a branch of periodic orbits. Specifically, a sequence of such folds was found for certain 3T- and 5T-periodic orbits as part of a bigger picture of a spiraling bifurcation diagram; see also [51, 40].

Figure 16 shows numerically computed 5T-periodic orbits that, in their fourth depicted T -interval, undergo a collision with the upper corner of the function $V_r(t)$ at

$$t = t_0 = 0 \bmod T, \quad V = \gamma + \eta T.$$

Moreover, we will consider the possibility of both internal and external collisions with this corner.

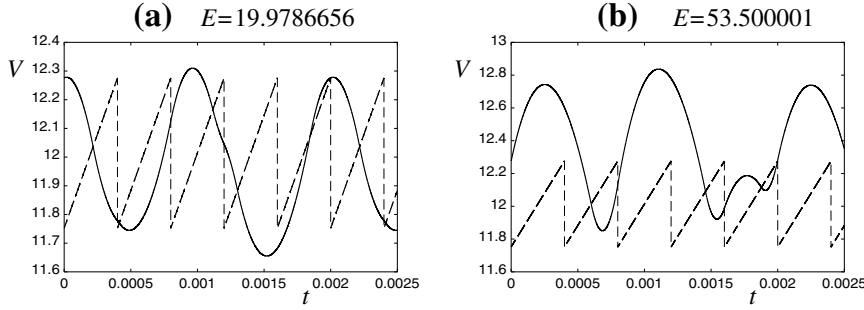


Fig. 16 Periodic orbits of the DC-DC buck converter with period $5T$ undergoing (a) an external and (b) an internal collision with the corner.

As a first step, we define local coordinates by

$$(2.54) \quad x = V - (\gamma + \eta T), \quad y = I - I_0, \quad z = t - t_0,$$

and rewrite (2.51), (2.52) in autonomous form to give the system

$$\begin{aligned} \dot{x} &= -a_1 + b_1 x - c_1 y, \\ \dot{y} &= -a_2 - c_2 y + d\Theta(\sigma(z) - x), \\ \dot{z} &= 1, \end{aligned}$$

in which

$$a_1 = \frac{\gamma + \eta T - RI_0}{RC}, \quad b_1 = \frac{1}{C}, \quad c_1 = \frac{1}{RC}, \quad a_2 = \frac{\gamma + \eta T}{L}, \quad c_2 = \frac{1}{L}, \quad d = \frac{E}{L},$$

Θ is the Heaviside step function, and

$$\sigma(z) = \eta[(z \bmod T) - T].$$

For this system we have

$$\Sigma_1 := \{H_1 = 0\} = \{x = \sigma(t)\}, \quad \Sigma_2 := \{H_2 = 0\} = \{z = 0\}, \quad C = \{x = 0, z = 0\}.$$

The boundary-intersection crossing event occurs at $x = y = z = 0$. The conditions of the preceding theory are met there with

$$F_1^0 = (-a_1, -a_2, 1), \quad F_2^0 = (-a_1, -a_2 + d, 1)$$

(observe that F is discontinuous only in the x -direction, and so the jump in derivatives of solutions is not seen in graphs of y against t as in Figure 16).

Using (2.43), specifically for an *external grazing*, the local DM for trajectories which cross the boundary-intersection point using the $\{z = 0\}$ Poincaré section takes the form

$$(2.55) \quad P_{\text{ZDM}} : \begin{pmatrix} x \\ y \end{pmatrix} \mapsto \begin{pmatrix} x \\ y + k_1(E)x \end{pmatrix} + \text{h.o.t.},$$

where

$$(2.56) \quad k_1(E) = -d\eta a_1 + \eta = -\frac{E RC}{L(\gamma + \eta T - RI_0 + \eta RC)}.$$

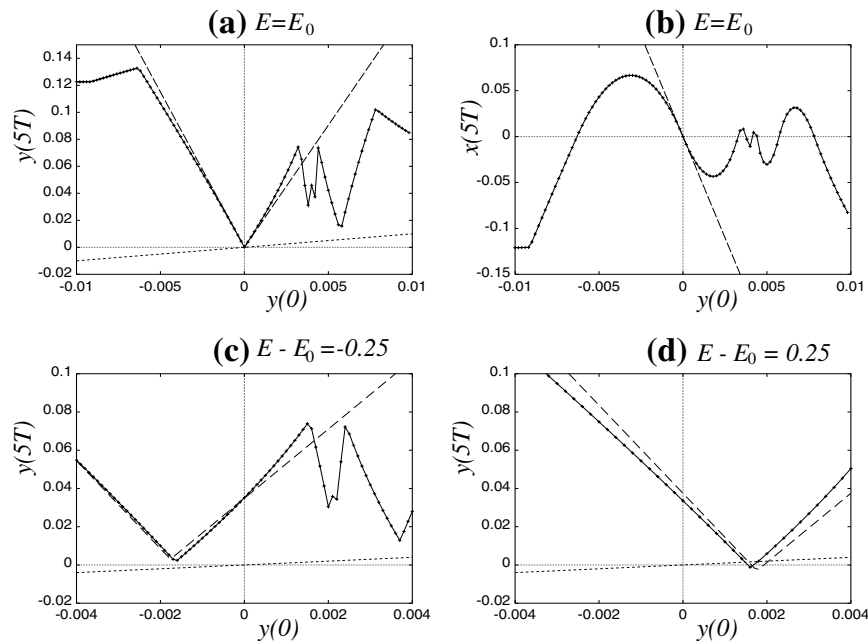


Fig. 17 The Poincaré map for a $5T$ -periodic orbit at $E_0 = 19.9786656$, which has an external collision with the boundary-intersection point, computed numerically (solid line with crosses) and via the analysis above (dashed line). A one-dimensional slice of the map is taken considering the effect of varying only the initial current $y(0)$. (a) and (b) depict the final current and voltage, respectively, for $E = E_0$; (c) and (d) show the effect on the final current of variation of the bifurcation parameter E . In the final current versus initial current figures, the 45° line is depicted as dotted; viewing the graphs as approximations of one-dimensional maps, intersections with this line are indicative of nearby fixed points of the two-dimensional map.

To compute the full Poincaré map, we must compose the local map P_{ZDM} with a global map which is found simply by taking the Jacobian derivative of the flow around the periodic orbit at $E = E_0$, ignoring the effects of the corner.

The results for the $5T$ -periodic orbit at $E = E_0 = 19.9786656$ are depicted in Figure 16, for which it was found, by examining the numerically computed trajectory, that $k_1(E_0) = -0.934$. The map (2.55) can be compared with a purely numerical evaluation of trajectories in a neighborhood of the corner-colliding one. We illustrate in Figure 17 a one-dimensional approximation to this two-dimensional map, by only displaying the effect of changes in initial current y . This is purely for illustrative convenience (similar results were found with other combinations of $x(0)$ and $y(0)$ varying as initial conditions), but we note from the numerical Jacobian that initial variations of current y have a much bigger effect (by a factor of about 10) than variations of voltage x .

The results in Figures 17(a) and (b) show good quantitative and qualitative agreement between the local theory and the numerical calculations at $E = E_0$. They also illustrate the extent of the region of validity for the local analysis; for $-0.006 < y(0) < -0.0035$ at $E = E_0$, the local map is qualitatively correct, but outside of this region the numerical map shows extra corners. This is due to other boundary-intersection crossing events taking place at $t = nT$ for some $n \leq 5$. Note

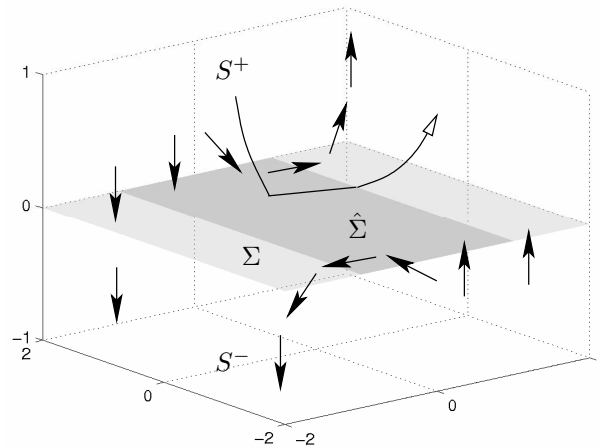


Fig. 18 Phase space topology of a system with discontinuous vector fields.

from panel (b) in particular that there is no corner in the x -component of the numerically computed map—this component of the map is smooth—which is in complete agreement with the analytical result (2.55) (there is no change in the x -component in the DM).

Panels (c) and (d) in Figure 17 show the effect of variation of E , with the existence of a fixed point on such a graph of $y(5T)$ against $y(0)$ being indicative only of a fixed point of the full two-dimensional map. Here again there is good agreement between theory and numerics on how the map is perturbed as E varies and on the fact that two fixed points (corresponding to unstable periodic orbits of the ODEs) are created at $E = E_0$ and coexist for $E > E_0$.

3. Filippov PWS Systems with Sliding. We now consider a more general system of the form (1.1) with a single well-defined switching manifold Σ . As mentioned in the introduction, a particular feature of such Filippov-type systems is the possibility of evolution of the system within its discontinuity set Σ . A subset of Σ where such an evolution is possible is termed the *sliding region* or *sliding subset*. Therefore, the sliding subset represents a region $\hat{\Sigma}$ within the switching manifold Σ , where trajectories hitting the manifold are not allowed to switch to another vector field as they are pushed back toward the manifold itself. Thus, there exists the possibility of a motion within Σ which is termed *sliding motion*. An example of a three-dimensional phase space with a sliding region, say $\hat{\Sigma}$, is schematically depicted in Figure 18. Two formalisms exist in the literature for deriving the equations for flows governing the dynamics within the sliding region. These are *Utkin’s equivalent control method* [110] and *Filippov’s convex method* [50], which are algebraically equivalent; see also [75].

In Filippov’s method, for example, one defines the sliding vector field as a convex combination of the two vector fields

$$F_s = (1 - \alpha)F_1 + \alpha F_2$$

with $0 \leq \alpha \leq 1$, where

$$\alpha = \frac{H_x F_1}{H_x (F_1 - F_2)}.$$

The control $\alpha = 0$ means that the flow is governed by F_1 alone, which must by definition be tangent to Σ there. Similarly, $\alpha = 1$ represents a tangency of flow F_2 with Σ . Hence, we can define the sliding region as

$$\hat{\Sigma} := \{x \in \Sigma : 0 \leq \alpha(x) \leq 1\}$$

and the boundaries of the sliding region as

$$\partial\hat{\Sigma}^+ := \{x \in \Sigma : \alpha(x) = 1\} \quad \text{and} \quad \partial\hat{\Sigma}^- := \{x \in \Sigma : \alpha(x) = 0\},$$

where one of the vector fields is tangent to Σ .

In section 3.1, we will discuss the most significant types of DIBs of equilibria using a planar Filippov system as a representative example. Nonsmooth transitions of equilibria in this class of systems have been little studied in the literature. An overview of local phenomena in planar Filippov systems was presented in [70]. A nongeneric class of Filippov systems was studied in [69]. It was shown that a class of transitions, termed *generalized Hopf bifurcations* in [69], can be observed in such systems when a family of limit cycles is generated, under parameter variations, as a focus located on the switching surface is perturbed. The transition to sliding cycles (a cycle with a segment of sliding motion) in planar Filippov systems is studied in [57]. Also, global phenomena can occur with heteroclinic connections to equilibrium points [70]. An interesting set of examples in applications is given by certain models of the DC-DC converters considered in the last section. We will study in some detail a model of a buck converter, an adaption of Example 2.5 above [91].

In section 3.3 we focus our attention on *sliding bifurcations* of limit cycles. We depict four possible cases of this type of DIB which are a distinct feature of Filippov-type systems. Their heuristic description is followed by the presentation of the normal forms capturing the essence of sliding bifurcations. Finally, an example where one of these bifurcations leads to the sudden onset of chaos is discussed.

3.1. Equilibrium Bifurcations. We consider Filippov systems of the form

$$(3.1) \quad \dot{x} = \begin{cases} F_1(x, \mu) & \text{if } H(x, \mu) > 0, \\ F_2(x, \mu) & \text{if } H(x, \mu) < 0, \end{cases}$$

where $F_1 \neq F_2$ on $H = 0$. It is possible to identify different types of equilibria in a Filippov system. We give the following definitions.

DEFINITION 3.1. *We say that a point $x \in D$ is a regular equilibrium of (3.1) if*

$$(3.2) \quad \begin{aligned} F_1(x, \mu) &= 0, \\ \lambda_1 &:= H(x, \mu) > 0 \end{aligned}$$

or

$$\begin{aligned} F_2(x, \mu) &= 0, \\ \lambda_2 &:= H(x, \mu) < 0. \end{aligned}$$

DEFINITION 3.2. *We say that a point \tilde{x} is a pseudoequilibrium if it is an equilibrium of the sliding flow, i.e.,*

$$(3.3) \quad \begin{aligned} F_1(\tilde{x}, \mu) + \tilde{\lambda}(F_2 - F_1) &= 0, \\ H(\tilde{x}, \mu) &= 0, \\ 0 < \tilde{\lambda} < 1. \end{aligned}$$

DEFINITION 3.3. A point \hat{x} is termed a boundary equilibrium of (3.1) if

$$\begin{aligned} F_1(\hat{x}, \mu) &= 0, \\ H(\hat{x}, \mu) &= 0 \end{aligned}$$

or

$$\begin{aligned} F_2(\hat{x}, \mu) &= 0, \\ H(\hat{x}, \mu) &= 0. \end{aligned}$$

Note that a boundary equilibrium is always located on the boundary of the sliding region defined by where $H_x F_1(x) \rightarrow 0$ or $H_x F_2(x) \rightarrow 0$.

Similar to what was shown in section 2.1 for nonsmooth continuous systems, in Filippov systems a boundary equilibrium can appear for some value of the system parameter μ . We shall seek to unfold the bifurcation scenarios that can occur when μ is perturbed away from the origin, i.e., the possible branches of solutions originating from a boundary equilibrium. Specifically, we give the following definition.

DEFINITION 3.4. A boundary equilibrium bifurcation occurs at $x = x^*$, $\mu = \mu^*$ if

- $F_i(x^*, \mu^*) = 0$, $i = 1$ or 2 ,
- $H(x^*, \mu^*) = 0$, and
- $F_{jx}(x^*, \mu^*)$ is invertible (or equivalently $\det(F_{jx}) \neq 0$) for $j = 1$ and 2 .

3.2. Well-posedness.

3.2.1. Overview of the Possible Cases. Without loss of generality, we assume that $F_1(0, 0) = 0, H(0, 0) = 0$, i.e., $x = 0$ is a boundary equilibrium when $\mu = 0$. We shall now seek to find conditions to distinguish between the simplest possible unfoldings of a boundary equilibrium as μ is perturbed away from the origin. We will show that scenarios similar to those presented in section 2.1 for nonsmooth continuous systems are possible. Namely, we can observe *persistence* where a branch of regular equilibria can turn into a branch of pseudoequilibria or a *nonsmooth fold* where a branch of regular equilibria can disappear after colliding with a branch of pseudoequilibria. We will not investigate here the case of Filippov systems without sliding. In that case, two branches of regular equilibria can exist and be involved in the bifurcation.

3.2.2. Persistence and Nonsmooth Folds. Let x be a regular equilibrium of (3.1) and \tilde{x} a pseudoequilibrium. Then, linearizing (3.2) and (3.3) about the boundary equilibrium point at the origin, we have

$$(3.4) \quad \begin{aligned} Ax + B\mu &= 0, \\ Cx + D\mu &= \lambda_1 > 0 \end{aligned}$$

and

$$(3.5) \quad \begin{aligned} A\tilde{x} + B\mu + E\tilde{\lambda} &= 0, \\ C\tilde{x} + D\mu &= 0, \\ \tilde{\lambda} &> 0, \end{aligned}$$

where $A = F_{1x}, B = F_{1\mu}, C = H_x, D = H_\mu$, and $E = F_2 - F_1$ are all evaluated at $x = 0, \mu = 0$.

Now, from Definition 3.4 and (3.4) we have $x = -A^{-1}B\mu$ and

$$(3.6) \quad \lambda_1 = (D - CA^{-1}B)\mu.$$

Moreover, from (3.6), $\tilde{x} = -A^{-1}B\mu - A^{-1}E\tilde{\lambda}$. Hence, we find

$$(3.7) \quad \tilde{\lambda} = \frac{(D - CA^{-1}B)\mu}{CA^{-1}E}$$

or, equivalently,

$$(3.8) \quad \tilde{\lambda} = \frac{\lambda_1}{CA^{-1}E}.$$

In order for x and \tilde{x} to exist for the same value of μ , both λ_1 and $\tilde{\lambda}$ must share the same sign, while they will exist for opposite values of μ if λ_1 and $\tilde{\lambda}$ have opposite signs. Therefore, using (3.8), we can state the following theorem.

THEOREM 3.5 (equilibrium points branching from a boundary equilibrium). *For the systems of interest, assuming*

$$(3.9) \quad \det(A) \neq 0,$$

$$(3.10) \quad D - CA^{-1}B \neq 0,$$

$$(3.11) \quad CA^{-1}E \neq 0,$$

- *persistence is observed at the boundary equilibrium bifurcation point if*

$$(3.12) \quad CA^{-1}E < 0;$$

- *a nonsmooth fold is observed instead if*

$$(3.13) \quad CA^{-1}E > 0.$$

Note that the conditions found here are different, as expected, from those presented in section 2.1 for nonsmooth continuous systems and are valid for any n -dimensional Filippov system of the given type.

3.2.3. Planar Filippov Systems. A comprehensive analysis of possible bifurcations in Filippov systems was given by Kuznetsov, Rinaldi, and Gragnani in [70]. In reviewing this material, we will consider in this section only DIBs which involve sliding on the discontinuity boundary. In fact, the appearance or disappearance of a sliding segment is already a DIB. Following [70], we term a point T on the switching manifold a *tangent point* if the vectors $F_i(T)$, $i = 1, 2$, are nonzero but at least one of them is tangent to Σ . We can distinguish between two cases, namely, the *visible* and *invisible* tangent points (see Figure 19).

To meet all of the generic one-parameter DIBs involving the discontinuity boundary Σ we use the following criterion: for a given parameter value μ , we consider the sliding set $\hat{\Sigma}$ and find all the pseudoequilibria and tangent points in it. These points are finite in number but can collide as μ varies, leading to local codimension-one bifurcations. Another local codimension-one DIB can occur when a standard hyperbolic equilibrium in S_1 or S_2 collides with Σ , i.e., a boundary equilibrium bifurcation. There are no other local codimension-one DIBs. Global codimension-one DIBs involving sliding are discussed in [70].

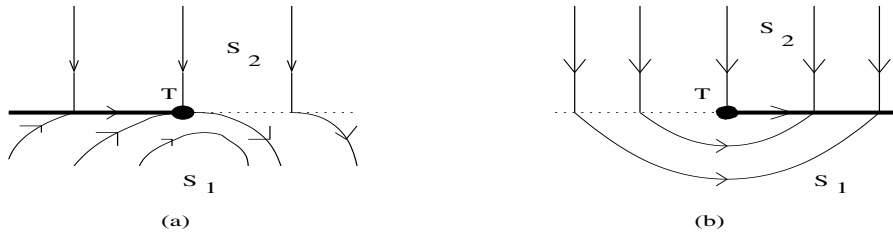


Fig. 19 Visible (a) and invisible (b) tangent points.

3.2.4. Collisions of Equilibria with the Boundary. We can distinguish three main cases:

- *Boundary focus.* There are five generic critical cases (see Figure 20(b)). In each of them there is a visible tangent point for $\mu < 0$ and an invisible tangent point for $\mu > 0$. The cases are distinguished by the relative position of the focus zero-isoclines and the behavior of the orbit departing from the visible tangent point into S_1 , as well as by the direction of the motion in S_2 . If we assume that the colliding focus is unstable and has counter clockwise rotation nearby, we can distinguish all five cases in Figure 20. Cases (1), (2), and (5) are nonsmooth fold bifurcations, while (3) and (4) correspond to persistence.
- *Boundary node.* Depending on the direction of motion in S_2 , there are two generic critical cases, which are shown in Figure 21. Case (1) is a persistence bifurcation while case (2) corresponds to a fold.
- *Boundary saddle.* When the colliding equilibrium is a saddle, there are three generic cases determined by the slope of the saddle zero-isoclines, as can be seen in Figure 22. In all cases, there is an invisible tangent point for $\mu < 0$ and a visible tangent point for $\mu > 0$. These points delimit the sliding segments on the discontinuity boundary. Cases (1) and (2) are folds, while case (3) corresponds to persistence.

Note that when μ varies, two pseudoequilibria can collide and disappear via a standard saddle-node bifurcation on the sliding set $\hat{\Sigma}$, which in this case we will call a pseudo-saddle-node bifurcation. Figure 23 illustrates this case for a stable sliding segment.

Global phenomena such as those depicted in Figures 24 and 25 are also possible and were studied in [70]. For example, a pseudoequilibrium $\tilde{x}(\mu)$ can have a sliding orbit that starts from and returns back to it for $\mu = 0$. This is possible if $\tilde{x}(0)$ is either a pseudo-saddle-node or a pseudosaddle (see Figure 24(1), (2)). Moreover, a standard saddle x_μ can have a homoclinic orbit containing a sliding segment at $\mu = 0$ (see Figure 24(3)).

3.2.5. Nongeneric Situations. Other phenomena concerning equilibria in Filippov systems have been reported in some nongeneric cases. For example, it has been observed that a branch of limit cycles can appear after a focus changes its stability on the boundary.

In a nongeneric case, where the focus is always in the origin, Küpper and Moritz [69] studied parameter-dependent Filippov dynamical systems of the form

$$\begin{pmatrix} \dot{x}(t) \\ \dot{y}(t) \end{pmatrix} = \begin{cases} K^+(x(t), y(t), \lambda) & \text{if } x(t) > 0, \\ K^-(x(t), y(t), \lambda) & \text{if } x(t) < 0, \end{cases}$$

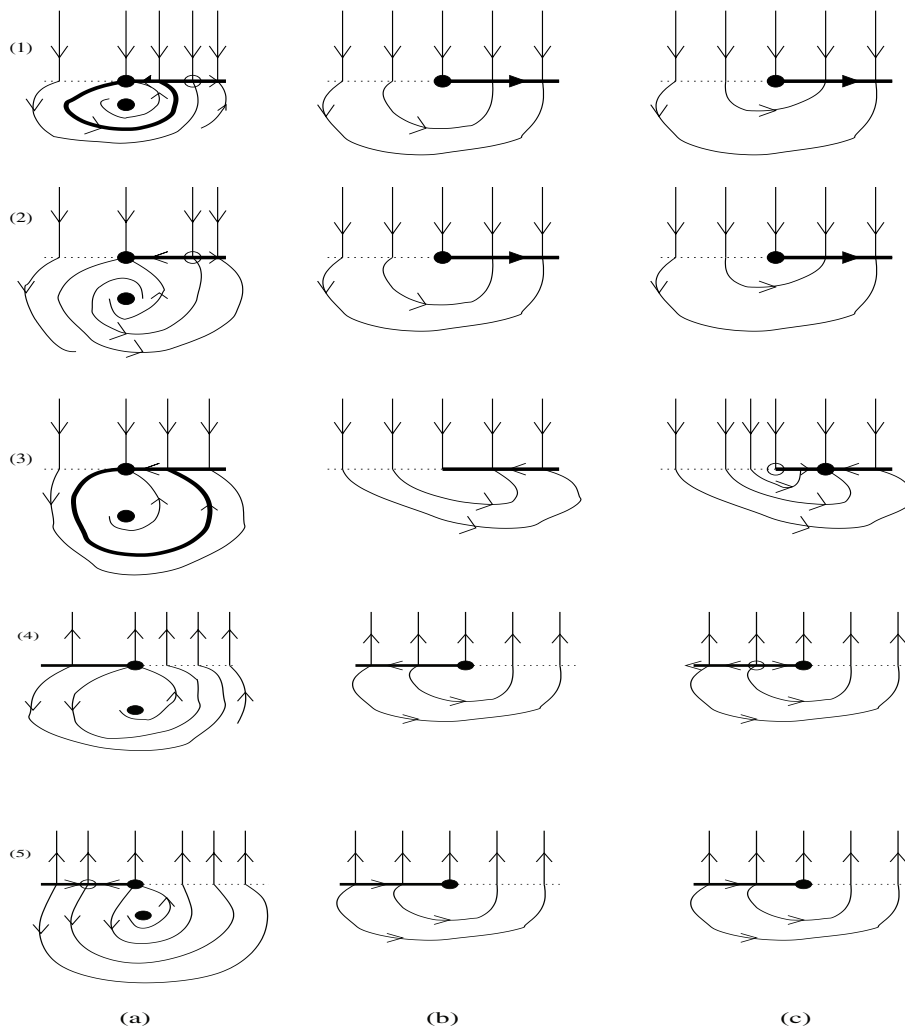


Fig. 20 *Boundary focus bifurcations. (a) $\mu < 0$, (b) $\mu = 0$, (c) $\mu > 0$. (1), (2), and (5) are nonsmooth folds, while (3) and (4) correspond to persistence (see [70]).*

where the right-hand sides $K^+, K^- : \mathbb{R}^2 \times I \mapsto \mathbb{R}^2$ for some interval I containing 0 are given by

$$K^+(x, y, \lambda) = A_\alpha^+(\lambda) \begin{pmatrix} x \\ y \end{pmatrix} + \begin{pmatrix} g_1^+(x, y, \lambda) \\ g_2^+(x, y, \lambda) \end{pmatrix}$$

and

$$K^-(x, y, \lambda) = A_\alpha^-(\lambda) \begin{pmatrix} x \\ y \end{pmatrix} + \begin{pmatrix} g_1^-(x, y, \lambda) \\ g_2^-(x, y, \lambda) \end{pmatrix}.$$

The parameter-dependent matrices $A_\alpha^+(\lambda)$ and $A_\alpha^-(\lambda)$ are assumed to be of the standard form used in the treatment of Hopf bifurcation in smooth systems, i.e.,

$$A_\alpha^+(\lambda) = \begin{pmatrix} \lambda & w^+(\lambda) \\ -w^+(\lambda) & \lambda \end{pmatrix}$$

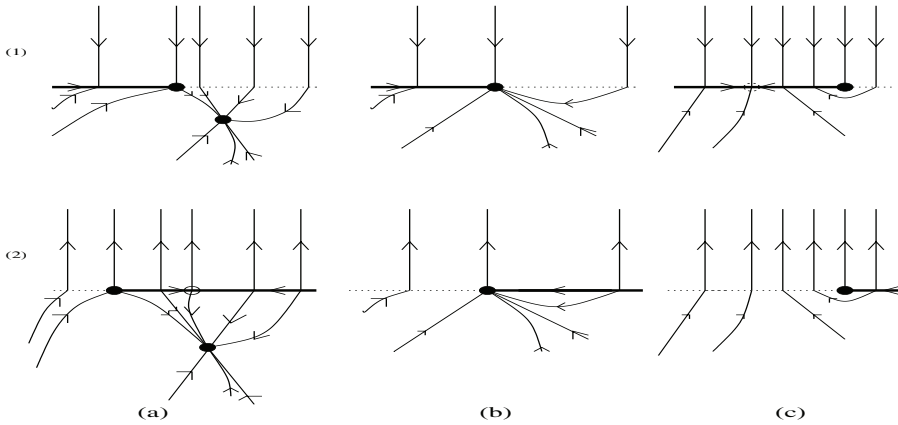


Fig. 21 *Boundary node bifurcations. (a) $\mu < 0$, (b) $\mu = 0$, (c) $\mu > 0$. (1) is a persistence while (2) corresponds to a nonsmooth fold (see [70]).*

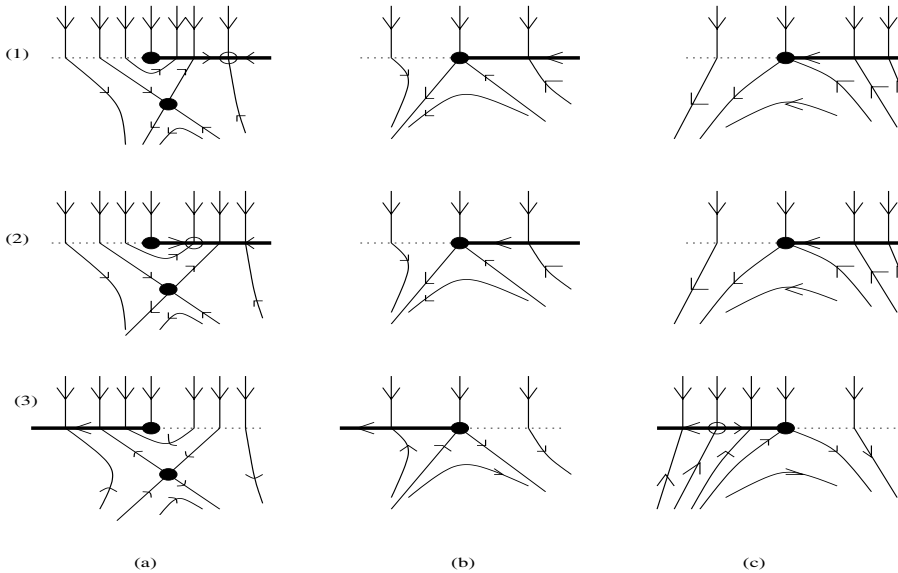


Fig. 22 *Boundary saddle bifurcations. (a) $\mu < 0$, (b) $\mu = 0$, (c) $\mu > 0$. (1) and (2) are nonsmooth folds while (3) corresponds to persistence (see [70]).*

and

$$A_{\alpha}^{-}(\lambda) = \begin{pmatrix} \alpha\lambda & w^{-}(\lambda) \\ -w^{-}(\lambda) & \alpha\lambda \end{pmatrix},$$

where $\alpha = 1$ or $\alpha = -1$. Then, as shown in [69], it is possible to give conditions for a continuous isolated branch of periodic orbits to bifurcate from the boundary equilibrium at the origin.

Another special case is described in Zou and Küpper [124], where the existence of periodic orbits bifurcating from a corner-like manifold in a planar Filippov dynamical system is discussed. There, the creation of a branch of cycles is determined by

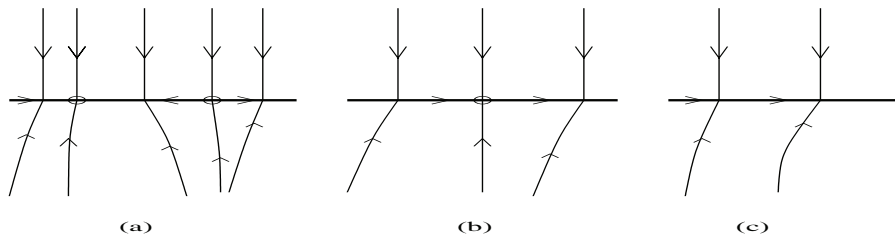


Fig. 23 Pseudo-saddle-node bifurcation. (a) $\mu < 0$, (b) $\mu = 0$, (c) $\mu > 0$.

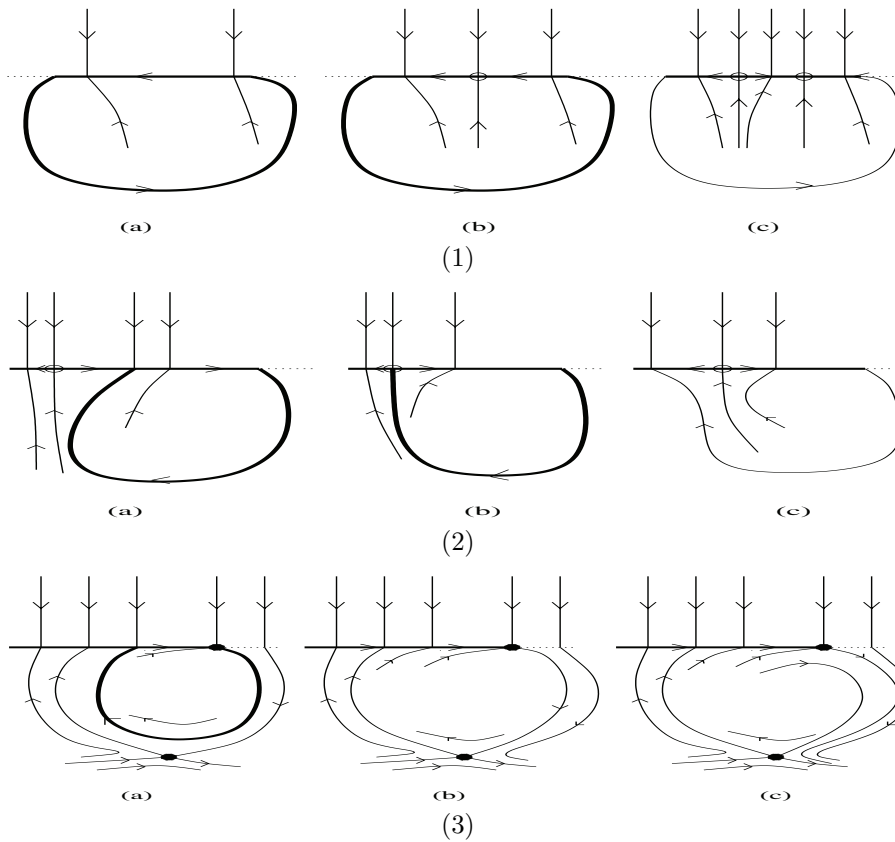


Fig. 24 Global phenomena: (1) Sliding homoclinic orbit to a pseudo-saddle-node; (2) sliding homoclinic orbit to a pseudo-saddle; (3) sliding homoclinic orbit to a saddle. (a) $\mu < 0$, (b) $\mu = 0$, (c) $\mu > 0$.

interactions between the geometrical structure of the corner and the eigenstructure of each smooth subsystem.

Still another nongeneric Filippov system (with symmetry) modeling a relay system is studied in [57]. Specifically, a piecewise-linear system is considered of the form

$$\dot{u} = Au + \operatorname{sgn}(w^T u)v,$$

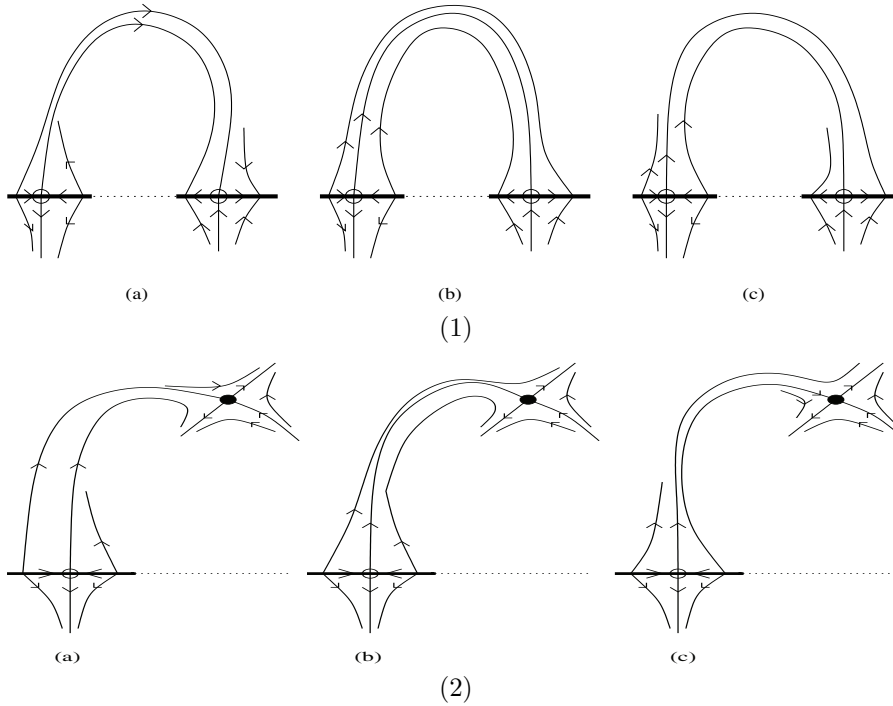


Fig. 25 Global phenomena: (1) Heteroclinic connection between two pseudo-saddles; (2) heteroclinic connection between a pseudo-saddle and a saddle. (a) $\mu < 0$, (b) $\mu = 0$, (c) $\mu > 0$.

where A is a 2×2 real matrix and u, v, w are two-dimensional real vectors. The theory of point transformation is applied to obtain conditions for the existence and stability of periodic solutions without sliding motion. The case where A has complex eigenvalues with a nonzero real part is studied completely. It is further shown that if A has real or purely imaginary eigenvalues, then the system has no periodic solutions with sliding motion. Further results are given concerning branches of periodic solutions both with and without sliding motions.

Return to Example 2.5. In fact, Example 2.5 is a Filippov system which at parameter values other than those used in the previous section can have equilibrium solutions where the voltage is equal to the reference signal V_r . In [24] a DC-DC Boost converter was shown to exhibit several DIBs associated with equilibria in the sliding surface. Here we review the related study of a DC-DC buck converter in [91]. The equations of motion are again (2.51), (2.52) but in this case we assume mixed voltage and a current control, so that the reference signal (2.50) is

$$V_r = V_{low} - ZI(t),$$

where Z is an impedance constant. The differential equations which drive the system are

$$\begin{pmatrix} \dot{V} \\ \dot{I} \end{pmatrix} = \begin{pmatrix} -1/(RC) & 1/C \\ -1/L & 0 \end{pmatrix} \begin{pmatrix} V \\ I \end{pmatrix} + \begin{pmatrix} 0 \\ E/L \end{pmatrix} u,$$

where $u = 0$ if $V_{con} := V(t) + ZI(t) > V_{low}$ and $u = 1$, otherwise.

Thus we have two linear topologies in continuous conduction mode. We will not consider discontinuous conduction mode here since we will assume that we have bidirectional switches, which allow negative currents. If we fix a set of initial conditions $V_0 = V(t_0)$ and $I_0 = I(t_0)$, since the systems of differential equations are linear, we will be able to compute exactly the solution of each one.

Let us write

$$(3.14) \quad k = \frac{1}{2RC}, \quad w = \sqrt{\frac{1}{LC} - k^2},$$

and suppose that

$$(3.15) \quad \frac{1}{LC} - k^2 > 0,$$

which is the usual case since oscillatory solutions are desired. We also define the real matrix

$$A = \begin{pmatrix} -k/w & 1/(Cw) \\ -1/(Lw) & k/w \end{pmatrix}.$$

Then we have the following solutions for the two systems below:

- System 1: $V_{con} > V$

$$\begin{pmatrix} V(t) \\ I(t) \end{pmatrix} = e^{-k(t-t_0)} [\text{Id} \cos w(t-t_0) + A \sin w(t-t_0)] \begin{pmatrix} V_0 \\ I_0 \end{pmatrix};$$

- System 2: $V_{con} < V$

$$\begin{pmatrix} V(t) \\ I(t) \end{pmatrix} = \begin{pmatrix} E \\ E/R \end{pmatrix} + e^{-k(t-t_0)} [\text{Id} \cos w(t-t_0) + A \sin w(t-t_0)] \begin{pmatrix} V_0 - E \\ I_0 - E/R \end{pmatrix},$$

where Id is the identity matrix. It follows that, between two commutation consecutive ramp intersection times, we know exactly the state variables of the system. Essentially, they are a combination of exponential and sinusoidal functions.

In each linear topology we can compute the equilibrium points and their stability. The equilibrium point when $u = 0$ is $P_0 := (0, 0)$, and when $u = 1$, $P_1 := (E, E/R)$. It is easy to check that the equilibrium points are spiral sinks with eigenvalues $-k + iw$, but we should not forget that the system switches topologies depending on the switching condition

$$V(t) + ZI(t) = V_{low}$$

and thus, in the nonlinear switched system, it can happen that none, one, or two of the equilibrium points are active.

One of the equilibrium points is always at the origin, and the other moves as parameter E is varied. Phase-space diagrams for the two cases are plotted in Figure 26. The line corresponding to the switching condition is also plotted in the figure, and some representative orbits are also shown. The fixed parameters are $R = 22\Omega$, $C = 47\mu F$, $L = 0.02H$, $V_{low} = 5V$, and $Z = -10$ and E is varied between 7.9 and 9.5 as a bifurcation parameter to obtain the different configurations.

For $E = 7.9$, there exists only a stable focus at $(E, E/R)$ (see left panel of Figure 26). For $E = 8.0012$, a standard saddle-node bifurcation of cycles occurs and

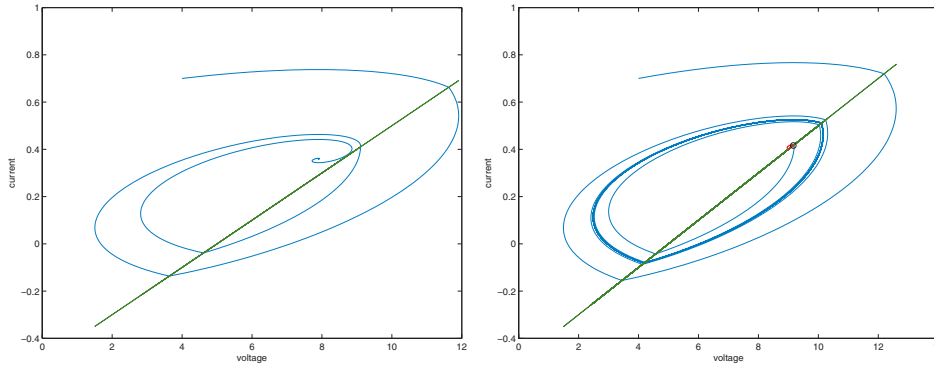


Fig. 26 (Left, $E = 7.9V$) a phase-space diagram showing the only attractor is a stable focus at $(E, E/R)$. (Right, $E = 9.167V$) a phase-space diagram showing the stable limit cycle that occurs.

a stable limit cycle and an unstable limit cycle are created. The unstable limit cycle is inside the stable one, and the stable focus is inside the unstable cycle, which delimits its basin of attraction. As parameter E is continuously increased the amplitude of the unstable limit cycle gets smaller and smaller, and finally it disappears in a DIB, when the stable focus collides with the cycle at

$$E = \frac{V_{low}}{1 + Z/R}$$

(see right panel of Figure 26). The stability of the focus changes and an unstable equilibrium point remains on the switching manifold as E_{in} is further increased.

3.3. Sliding Bifurcations of Limit Cycles. Sliding bifurcations are defined here as interactions between limit cycles of the system and the sliding region $\hat{\Sigma}$. According to the results presented in [43, 65, 66] and in more detail in [49], we can identify four possible cases of interactions between the system flow and the sliding section. These can be generalized to the case of n -dimensional PWS dynamical systems of the form (3.1). A three-dimensional schematic representation is given in Figure 27, where we assume the phase-space topology introduced in section 2.1 and depict only segments of trajectories (denoted in the figure by “1,” “2,” and “3”) that interact with the sliding region. In order for a DIB to occur as a parameter is varied, we suppose that these depicted trajectories represent parts of a limit cycle for three different parameter values.

Figure 27(a) depicts the scenario we term a *crossing-sliding bifurcation*. Here, under parameter variation, a part of the system trajectory transversally crosses the boundary of the sliding strip at the bifurcation point (trajectory labeled “2” in Figure 27(a)). Further variations of the parameter cause the trajectory to enter the sliding region $\hat{\Sigma}$, leading to the onset of sliding motion. Note that the sliding trajectory then moves locally toward the boundary of $\hat{\Sigma}$. Since at the boundary $F_s = F_1$ or F_2 (without loss of generality we henceforth assume $F_s = F_1$ there, i.e., we are on $\partial\hat{\Sigma}^-$), the trajectory leaves the switching manifold tangentially.

In the case presented in Figure 27(b), a section of trajectory lying in region S^+ grazes the boundary of the sliding region from above. Again, this causes the formation of a section of sliding motion which locally tends to leave $\hat{\Sigma}$. We term this a *grazing-*

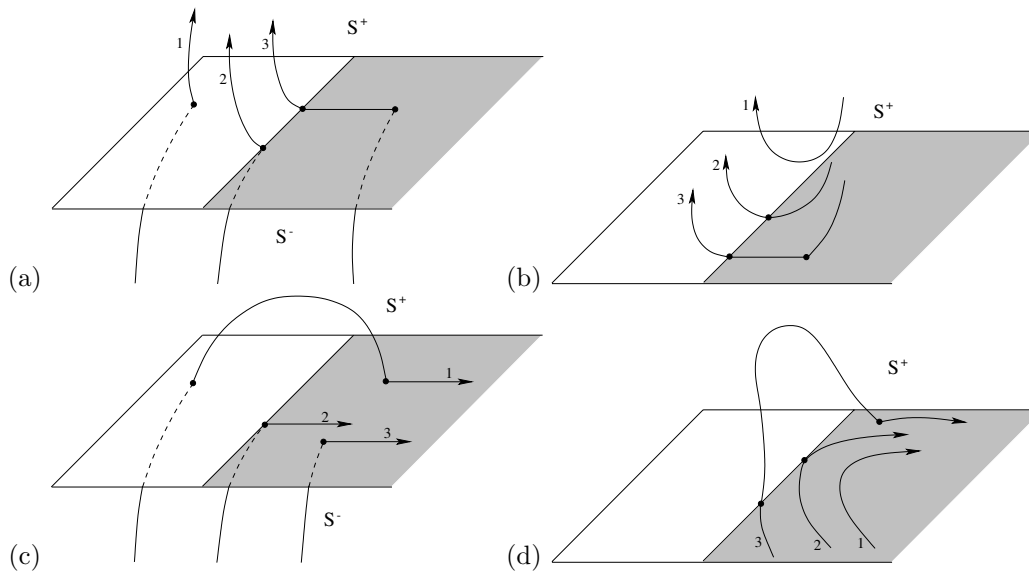


Fig. 27 The four possible bifurcation scenarios involving collision of a segment of the trajectory with the boundary of the sliding region $\partial\hat{\Sigma}^-$.

sliding bifurcation. We note that this DIB is the natural generalization of grazing bifurcations (see section 2.2) to dynamical systems with sliding.

A different bifurcation event, which we shall call a *switching-sliding bifurcation*, is depicted in Figure 27(c). This scenario is similar to the crossing-sliding bifurcation shown in Figure 27(a). We see a section of the trajectory transversally crossing the boundary of the sliding region. Now, though, the trajectory stays locally within the sliding region instead of leaving the switching manifold Σ .

The fourth and last case is the *adding-sliding bifurcation*, shown in Figure 27(d). It differs from the scenarios presented above since the segment of the trajectory which undergoes the bifurcation lies entirely within the sliding region $\hat{\Sigma}$. Thus, as parameters are varied, a sliding section of the system trajectory tangentially (*grazes*) hits the boundary of the sliding region. Further variation of the parameter causes the formation of an additional segment of trajectory lying above the switching manifold, i.e., in region S^+ .

3.3.1. DMs for Sliding Bifurcations. To capture the dynamics of sliding bifurcations one can obtain normal-form mappings using the concept of the ZDM (see section 2.2). We will not give details of the construction of the DMs but only present final results; a detailed derivation can be found in [44, 87]. It is assumed that we have uniform discontinuity (see Definition 2.1) across the switching manifold Σ . Since Σ is a well-defined surface, at the bifurcation point x^* we have $H(x^*) = 0$ and $H_x(x^*) \neq 0$. The additional condition

$$(3.16) \quad H_x(F_2 - F_1) > 0,$$

which we assume to hold across $\hat{\Sigma}$, ensures that the sliding region is simultaneously attracting from both regions S_1 and S_2 . Under these assumptions we shall introduce conditions which need to be satisfied at every sliding bifurcation. These are presented in Table 2.

Table 2 Analytical conditions determining a particular sliding bifurcation scenario.

Bifurcations	Defining conditions
Crossing-sliding	$H_x F_1 = 0, (H_x F_1)_x F_1 > 0$
Grazing-sliding	$H_x F_1 = 0, (H_x F_1)_x F_1 > 0$
Switching-sliding	$H_x F_1 = 0, (H_x F_1)_x F_1 < 0$
Adding-sliding	$H_x F_1 = 0, (H_x F_1)_x F_1 = 0, ((H_x F_1)_x F_1)_x F_1 < 0$

THEOREM 3.6. *Given the above assumptions and that condition (3.16) holds, then, under the appropriate additional conditions summarized in Table 2, we have the following ZDMs:*

- crossing-sliding

$$(3.17) \quad x \mapsto \begin{cases} x & \text{if } H_x F_1(x) \leq 0, H(x) = 0, \\ x + \mathbf{v} + O(x^3) & \text{if } H_x F_1(x) > 0, H(x) = 0; \end{cases}$$

- grazing-sliding

$$(3.18) \quad x \mapsto \begin{cases} x & \text{if } H_{\min}(x) \geq 0, \\ x + \mathbf{u} + O(x^{3/2}) & \text{if } H_{\min}(x) < 0; \end{cases}$$

- switching-sliding

$$(3.19) \quad x \mapsto \begin{cases} x & \text{if } H_x F_1(x) \leq 0, H(x) = 0, \\ x + \mathbf{w} + O(x^4) & \text{if } H_x F_1(x) > 0, H(x) = 0; \end{cases}$$

- adding-sliding

$$(3.20) \quad x \mapsto \begin{cases} x & \text{if } v_{\min} \geq 0, \\ x + \mathbf{z} + O(x^{5/2}) & \text{if } v_{\min} < 0, \end{cases}$$

where

$$(3.21) \quad H_{\min}(x) = H_x x + O(x^2), \quad v_{\min}(x) = H_x F_1(x) + O(x^2),$$

$$(3.22) \quad \mathbf{v} = \frac{1}{2} \frac{((H_x F_1)_x x)^2}{(H_x F_d)((H_x F_1)_x F_1)} F_d,$$

$$(3.23) \quad \mathbf{u} = -\frac{H_x x}{H_x F_d} F_d,$$

$$(3.24) \quad \mathbf{w} = \frac{2}{3} \frac{((H_x F_1)_x x)^3}{(H_x F_d)^2 ((H_x F_1)_x F_1)^2} [(H_x F_d)(F_{1x} F_d - F_{dx} F_1) - (H_x(F_{1x} F_d - F_{dx} F_1)) F_d],$$

$$(3.25) \quad \mathbf{z} = -\frac{9}{2} \frac{((H_x F_1)_x x)^2}{(H_x F_d)^2 ((H_x F_1)_x F_1)_x F_1} [(H_x F_d)(F_{1x} F_d - F_{dx} F_1) - (H_x(F_{1x} F_d - F_{dx} F_1)) F_d],$$

and $F_d = F_2 - F_1$.

The proof of the above theorem can be found in [44].

As shown in the examples in section 2.2.2, the appropriate composition of the ZDM with a smooth (Poincaré) map gives rise to a map whose dynamics describes the behavior of a limit cycle which undergoes the particular DIB. We can state that, generically, the type of discontinuity found in the ZDM will characterize the full Poincaré map. Thus, the leading-order discontinuity of the (local) ZDM can be used to make general statements on the system's dynamics following any sliding bifurcation.

Let us briefly discuss consequences following from the character of each ZDM.

3.3.2. Dynamical Consequences of the Character of the ZDMs. The ZDM characterizing the crossing-sliding bifurcation scenario causes discontinuity in the second derivative terms ($\mathbf{v} = \mathcal{O}(x^2)$). Thus, the Poincaré mapping describing the bifurcating orbit will be continuous with continuous first derivative, but there will be a second derivative discontinuity across the boundary of the sliding region. The mapping will be singular with a one-dimensional null space on the sliding side of the discontinuity; this is because sliding introduces a reduction of system dimension by 1. The eigenvalues of the Jacobian matrix of the Poincaré map describing the bifurcating cycle vary continuously across the discontinuity. Thus, a hyperbolic cycle undergoing the crossing-sliding bifurcations will preserve its stability properties and period, although codimension-two DIBs can be expected in the case that the bifurcating cycle is nonhyperbolic [67].

The second case of sliding bifurcations considered here is the grazing-sliding scenario. The correction which needs to be made to account for the sliding flow in this case influences terms at the linear order, $\mathbf{u} = \mathcal{O}(x)$. Thus, for such a mapping we cannot conclude that the periodic orbit will persist under parameter variations that would cause it to acquire a sliding portion. If the orbit survives the bifurcation, we can expect a jump in eigenvalues as the periodic orbit goes through a tangency with the boundary of the sliding set. The jump in eigenvalues is nicely illustrated by the fact that a sliding periodic orbit must have at least one eigenvalue zero, whereas there is no such restriction for an orbit which does not contain any sliding segments. The presence of the higher-order term in the ZDM (the $\mathcal{O}(3/2)$ -term) will cause the eigenvalues to have a square-root singularity with respect to parameter variation as the bifurcation is approached from the sliding side. It is worth mentioning here that in the case of grazing bifurcations in systems with degree of smoothness 1 that do not slide, the normal form map is characterized by a square-root singularity (see section 2.2). Grazing in the presence of sliding changes the nature of DIBs and gives rise to a normal form that is piecewise linear to leading order.

To classify the possible bifurcation scenarios we can use the classification strategies for border-collision bifurcations in maps [7, 8, 39, 88, 89]. Note, however, that sliding motion introduces a loss in the rank of the map on one side of the discontinuity, which requires special treatment. See [92, 64], where a classification strategy for bifurcations arising due to grazing-sliding in three-dimensional Filippov-type flows is introduced.

The third case, namely, switching-sliding, leads to a normal form which has continuous derivatives up to order 2 ($\mathbf{w} = \mathcal{O}(x^3)$). Hence, as for crossing-sliding, a hyperbolic trajectory will persist under parameter variation since the mapping has continuous first parameter derivatives, but the second parameter derivative is discontinuous. Similarly, in the fourth case, adding-sliding bifurcations, the ZDM has continuous first derivative and therefore a hyperbolic periodic orbit will persist under parameter variation. However, the first parameter derivative of the eigenvalues will undergo a jump across the bifurcation point.

Example 3.1 (a simple dry-friction oscillator). In what follows, we present an example of a dry-friction oscillator model which serves as an illustration of how the ZDMs can be used to explain and also predict a particular bifurcation scenario arising in Filippov systems. More details can be found in [64].

Friction oscillators are of Filippov type when the friction characteristic is modeled by some set-valued function [99, 98, 55]. A characteristic feature of the dynamics of systems with friction is so-called stick-slip motion. As shown in [101], the stick phase of an oscillatory motion corresponds to sliding. Therefore, different transitions from slip motion to more complex stick-slip oscillations, often present in friction oscillators, correspond to sliding bifurcations. Examination of slip to stick-slip transitions found in [99, 98, 56, 55] reveals that at least three of the four aforementioned cases of sliding bifurcations have been observed there, namely, crossing-sliding, switching-sliding, and grazing-sliding. In fact, all four sliding bifurcation scenarios have been reported to have been exhibited in a simple model of the friction oscillator (see [49] for details).

Here we focus on a more intricate stick-slip transition which leads to the sudden onset of chaotic stick-slip behavior. Following [118, 73], the dry-friction oscillator under investigation can be expressed in dimensionless form as

$$(3.26) \quad \ddot{y} + y = f(1 - \dot{y}) + F \cos(\nu t),$$

where

$$(3.27) \quad f(1 - \dot{y}) = \alpha_0 \operatorname{sgn}(1 - \dot{y}) - \alpha_1(1 - \dot{y}) + \alpha_2(1 - \dot{y})^3$$

is a kinematic friction characteristic and $1 - \dot{y}$ corresponds to the relative velocity between the driving belt and moving block. In the case when $\dot{y} = 1$, the relative velocity is 0 and the kinematic friction is set-valued, i.e., $-\alpha_0 < f(1 - \dot{y}) < \alpha_0$. The coefficients of the kinematic friction characteristic are positive constants, which in our example shall take the values

$$\alpha_0 = \alpha_1 = 1.5, \quad \alpha_2 = 0.45, \quad \text{while} \quad F = 0.1$$

is the amplitude of forcing. As a bifurcation parameter, we take ν , the normalized angular velocity, and let $T = 2\pi/\nu$ represent the forcing period. We focus, in particular, on the bifurcation scenario for $\nu \approx 1.7078$ that gives rise to the sudden emergence of chaotic stick-slip motion. As shown in Figure 28(a), at the bifurcation point a $4T$ -periodic orbit grazes the switching manifold $\Sigma = \{\dot{y} = 1\}$ at the boundary of the sliding region (denoted in the figure by a short vertical line). The observed scenario corresponds to a grazing-sliding bifurcation, as the bifurcating orbit grazes from below the boundary of the region where stick motion can take place. This can be more clearly seen in Figure 28(b).

To study the dynamics ensuing due to this bifurcation we can proceed as in section 2.2 for grazing bifurcations. That is, we need to obtain a global Poincaré mapping which describes the behavior of the bifurcating cycle. Such a mapping is obtained by a composition of the ZDM to lowest order for the grazing-sliding bifurcation with an affine transformation such as (3.28), which captures the dynamics of the nonsliding hyperbolic cycle. Here we have a forced dynamical system with bifurcating orbit of period $4T$, i.e., four times the period of the external forcing term; the natural Poincaré map is a $4T$ -stroboscopic mapping, say, P_{4T} , which we assume to be affine and well represented by its linear terms; i.e.,

$$(3.28) \quad P_{4T} : x_{n+1} = Ax_n + B\nu = \begin{pmatrix} a_{11} & a_{12} \\ a_{21} & a_{22} \end{pmatrix} x_n + \begin{pmatrix} b_1 \\ b_2 \end{pmatrix} \nu,$$

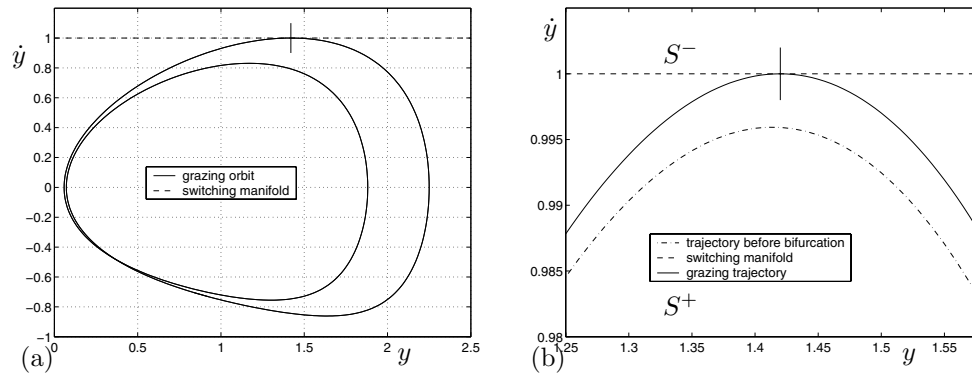


Fig. 28 (a) Orbit of (3.26) of period $4T$ ($8\pi/\nu$) undergoing grazing-sliding bifurcation for $\nu = 1.7077997$. (b) Enlargement of the region where grazing-sliding occurs; the dash-dotted segment corresponds to the periodic orbit for $\nu = 1.7082$ that clearly does not reach the switching manifold.

where x_n is the two-dimensional state vector, corresponding in our case to position and velocity of the dry-friction oscillator, obtained by sampling the system states at time instants that are multiples of $4T$. Note that the map is smooth away from the bifurcation point, i.e., when the orbit does not contain any segments of sliding (stick) motion. Smoothness is lost under parameter variation as the orbit grazes and then enters the sliding region.

To capture the influence of the grazing-sliding event we then need to compose (3.28) with the normal-form map for grazing-sliding given by (3.18) with correction term (3.23). Thus, the final map obtained from a composition of (3.28) with the ZDM takes the form

$$(3.29) \quad x_{n+1} = \begin{cases} \begin{pmatrix} a_{11} & a_{12} \\ a_{21} & a_{22} \end{pmatrix} x_n + \begin{pmatrix} b_1 \\ b_2 \end{pmatrix} \nu & \text{if } x_{2n} < 0, \\ \begin{pmatrix} a_{11} & 0 \\ a_{21} & 0 \end{pmatrix} x_n + \begin{pmatrix} b_1 \\ b_2 \end{pmatrix} \nu & \text{if } x_{2n} > 0. \end{cases}$$

A detailed derivation leading to the mapping (3.29) was presented in [45]. Following [45], we introduce numerical values of the matrix coefficients: $a_{11} = -1.85$, $a_{12} = 4.396$, $a_{21} = -1.14$, $a_{22} = 2.704$, $b_1 = 4.498$, and $b_2 = -1.755$. Bifurcations that can be observed in (3.29) under the variation of the bifurcation parameter ν correspond to bifurcations in the friction oscillator. Note that map (3.29) is noninvertible in one of its regions of definition. Noninvertibility can be heuristically understood from the fact that *sliding motion* introduces a loss of 1 in system dimension, which appears in the map as a loss of rank. Under appropriate coordinate transformation (3.29) can be written as

$$(3.30) \quad x_{n+1} = \begin{cases} \begin{pmatrix} \delta_1 & 1 \\ \tau_1 & 0 \end{pmatrix} x_n + \begin{pmatrix} 1 \\ 0 \end{pmatrix} \mu & \text{if } x_{1n} < 0, \\ \begin{pmatrix} \tau_2 & 1 \\ 0 & 0 \end{pmatrix} x_n + \begin{pmatrix} b_1 \\ b_2 \end{pmatrix} \nu & \text{if } x_{1n} > 0, \end{cases}$$

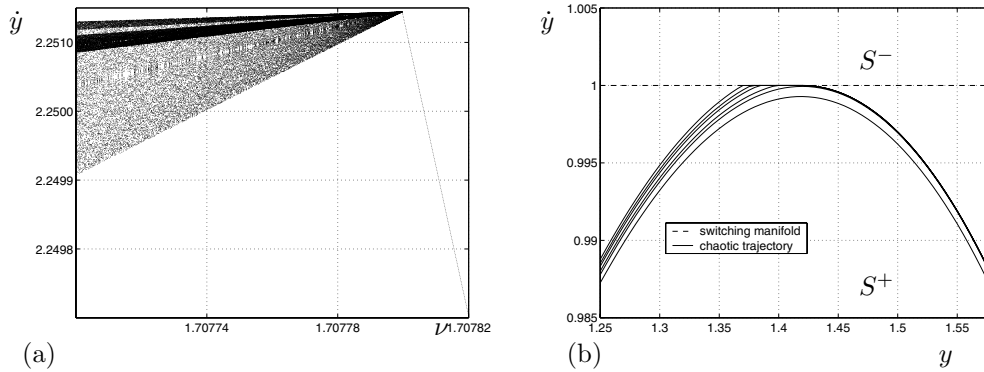


Fig. 29 (a) A bifurcation diagram obtained from the numerical integration of the system under consideration, and (b) a part of a trajectory in the neighborhood of the switching manifold.

where δ_1, τ_1, τ_2 are the determinant and traces of the matrices on either side of the discontinuity. The map (3.30) is a canonical normal form for grazing-sliding bifurcations in three-dimensional Filippov-type flows. Here we have that $\tau_1 = 0.854, \delta_1 = 0.009,$ and $\tau_2 = -1.85,$ which according to the criterion developed in [64] implies sudden onset of chaos under variation of μ . The bifurcation diagram computed from numerical integration of the system is depicted in Figure 29(a). Note that the chaos is *robust* in the sense introduced in [10], that is, it has no embedded periodic windows. A part of the chaotic trajectory born in the bifurcation is shown in Figure 29(b).

It is worth mentioning that if we add an extra vertical degree of freedom to the system and the normal contact force varies with time, then the system is no longer a Filippov inclusion and it is possible to encounter a Painlevé paradox (see section 1.1, [12], and [74]).

4. Impacting Systems.

Example 4.1 (motivating example: a driven linear impact oscillator). Suppose a one-degree-of-freedom linear, damped, harmonically driven oscillator described by the point $u(t)$ is constrained to move in the region $u > 0$. We will consider the situation that if the oscillator impacts the constraint at $u(t) = 0$ with nonzero velocity, an instantaneous rebound will take place. We assume the outgoing velocity following the impact to be proportional to the incoming velocity.

The study of the surprisingly complex dynamics of such simple impact oscillators goes back at least to the work of Peterka [93, 94]; see, e.g., [6, 49] for reviews. There was a resurgence of interest in such systems in the 1980s [103, 102, 108, 117, 116], which inspired much of the work on DMs in the 1990s, e.g., [82, 16, 63], on which this review is based. See also the more recent work [20] that explains the geometry of such systems (e.g., the complex shapes that occur in Figure 3) and the work on control of impacting systems [13, 54, 79, 30, 26, 28].

Let us suppose that the nonimpact dynamics of the system can be written as

$$\ddot{u} + 2\zeta\dot{u} + \omega_0^2 u = \cos(t),$$

where $u > 0$ and the instantaneous impact law is given by

$$\dot{u}^+ = -r\dot{u}^-, \quad 0 \leq r \leq 1,$$

at $u = 0$. Using the state variables

$$\begin{aligned}x_1 &= u, \\x_2 &= \dot{u}, \\x_3 &= t,\end{aligned}$$

the impact system can be described by

$$(4.1) \quad \dot{x} = F(x) = \begin{pmatrix} x_2 \\ -2\zeta x_2 - \omega_0^2 x_1 + \cos(x_3) \\ 1 \end{pmatrix} \text{ when } H(x) \equiv x_1 > 0$$

and

$$(4.2) \quad x^+ = R(x^-) = \begin{pmatrix} x_1^- \\ -r x_2^- \\ x_3^- \end{pmatrix} \text{ when } H(x) = 0.$$

Equation (4.2) can also be written as

$$(4.3) \quad x^+ = x^- + W(x^-)H_x F(x^-) = x^- + \begin{pmatrix} 0 \\ -(1+r) \\ 0 \end{pmatrix} x_2^-.$$

In the next section we will study impact systems described by the three functions F , W , and H . The chosen form of the impact law covers systems with multiple impacting rigid bodies, when no friction is assumed in the impact. When friction is present, the assumption of low incoming velocity $H_x F$ leading to a small change of state in (4.3) does not necessarily hold (see, for example, the Painlevé paradox studied in [74]).

Apart from motion with $H > 0$ interrupted by isolated impacts, there are some special types of motion in these systems. In the linear oscillator, if we start at the point

$$x = \begin{pmatrix} 0 \\ 0 \\ 3\pi/2 \end{pmatrix},$$

which is at the boundary with zero velocity, we find that we cannot leave the boundary through the vector field, as the acceleration $(H_x F)_x F = \cos(3\pi/2)$ is negative. The impact law will just return us to the same state, so we have to assume that *sticking* motion takes place along the boundary until the acceleration becomes positive again at $x_3 = 0 \bmod 2\pi$, which can be thought of as higher-order sliding, i.e., motion along a codimension-two surface. Further, if the coefficient of restitution satisfies $0 < r < 1$, then starting at the point

$$x = \begin{pmatrix} 0 \\ \text{small} \\ 3\pi/2 \end{pmatrix}$$

will lead to a rapid series of impacts accumulating in finite time (like a ping-pong ball coming to rest), which we call *chattering*; see [16, 114, 115]. After the chattering has completed, sliding motion will follow until the acceleration becomes positive again.

Note that by chattering we refer here to the accumulation of an infinite sequence of impacts in finite time. Such an accumulation of events is also referred to as *Zeno behavior* in the hybrid control literature [120].

For mechanical systems with contact involving friction, equilibrium positions are often not isolated; consider, for example, a block resting on a flat table. Here we will present results in a more abstract and general setting, albeit one that precludes impact with friction.

Simplifying (1.1) and (1.2) we will consider systems of the form

$$(4.4) \quad \dot{x} = F(x) \quad \text{if } H(x) > 0,$$

with impact at the surface Σ defined by the smooth scalar function $H(x) = 0$, where the impact law takes the specific form

$$(4.5) \quad x^+ = R(x^-) = x^- + W(x^-)H_x F(x^-),$$

where $R : \Sigma \rightarrow \Sigma$ is smooth and $\Sigma = \{x \mid H(x) = 0\}$, so W is a smooth vector field that maps Σ to itself. For convenience, we will also define the velocity $v(x)$ and acceleration $a(x)$ (of the vector field F relative to H) as

$$(4.6) \quad v(x) = H_x F(x),$$

$$(4.7) \quad a(x) = (H_x F)_x F(x).$$

Note in the above that $x \in \mathbb{R}^n$ represents the full state vector of the system. In particular, for application to mechanical systems, this includes both position and velocity. The form of the impact law we consider is motivated by applications to such systems. In particular, for a single-degree-of-freedom system with displacement u , one might have $x = (u, v)$ and the discontinuity defined by $u = \sigma$ for some constant σ . Then $H(x) = u$ and the reset law R is none other than a coefficient of restitution law with $W = -(1+r)e_v$, where e_v is a unit vector in the v direction and r is Newton's coefficient of restitution.

Other approaches sometimes used in the literature involve formulations in terms of Lagrangian mechanics, e.g., [12]. Here one typically writes

$$M(q)\ddot{q} + f(q, \dot{q}) = \nabla h(q)\lambda,$$

where M is a positive definite mass matrix, f is a force term, and $h(q)$ is a constraint subject to the so-called complementarity condition

$$0 \leq \lambda \perp h(q) \geq 0.$$

To this one adds the restitution law in the form

$$h_q(q)^T \dot{q}^+ = -r h_q(q)^T \dot{q}^- \quad \text{when } H(q) = 0 \quad \text{and } h_q(q)^T \dot{q}^- < 0.$$

We leave it as an exercise to the reader to show that such a formulation of impact mechanics can be written in the form (4.4), (4.5).

Note that these systems also have the possibility of *sliding* motion, through points satisfying

$$(4.8) \quad H(x) = 0,$$

$$(4.9) \quad v(x) = 0,$$

where the impact mapping is the identity. The mechanism for maintaining sliding motion is the same as for low velocity impacts, so the sliding vector field should be

$$(4.10) \quad \dot{x} = F_s(x) = F(x) - \lambda(x)W(x),$$

where $\lambda > 0$ is chosen to keep $H = 0$, $v = 0$. This is possible for the typical mechanical impacting system since, at these points, we must have $H_x W = 0$ as the impact mapping should map points in the impact surface back to the impact surface, and thus W must be parallel to the impact surface for small impact velocities. It is notable that it is possible to define a complementarity system from (4.5) and (4.10) together with a complementarity relation between $\lambda(x)$ and $H(x)$. Further, defining

$$(4.11) \quad b(x) = (H_x F)_x W(x),$$

we have for the typical system that $b \leq -1$ at these points, since a negative incoming velocity should produce a positive outgoing velocity. The requirement that the acceleration also vanishes for the sliding flow, i.e., that $a(x)$ defined by (4.7) with F replaced by F_s is zero for the sliding flow (4.10), leads to the condition that

$$\lambda(x) = a(x)/b(x).$$

Now since $\lambda(x) > 0$ we find this equivalent to $a(x) < 0$, so the acceleration is directed toward the boundary. We can interpret λ physically as a measure of the contact force provided by the boundary. Thus the sliding set $\hat{\Sigma}$ is determined by

$$\begin{aligned} H(x) &= 0, \\ v(x) &= 0, \\ a(x) &< 0. \end{aligned}$$

4.1. Bifurcations of Boundary Equilibria. In addition to regular equilibrium points x^* with $F = 0$, $H > 0$, there is a possibility of pseudoequilibrium points x^* with $F_s = 0$, $H = 0$. The equations to solve are

$$\begin{aligned} F(x^*) &= 0, \\ H(x^*) &> 0 \end{aligned}$$

and

$$\begin{aligned} F(x^*) - \lambda^* W(x^*) &= 0, \\ H(x^*) &= 0, \\ \lambda^* &> 0, \end{aligned}$$

respectively. In the latter case, λ^* is most conveniently regarded as an independent variable.

Now assume that the system depends on a single parameter μ and that $x = \bar{x}$, $\mu = \bar{\mu}$ satisfy

$$\begin{aligned} F(\bar{x}, \bar{\mu}) &= 0, \\ H(\bar{x}, \bar{\mu}) &= 0. \end{aligned}$$

This point may be called a boundary equilibrium point. If the parameter μ is changed, regular and/or pseudoequilibrium points may branch off the boundary equilibrium. Assuming for simplicity $\bar{x} = \bar{\mu} = 0$ and linearizing, we find

$$\begin{aligned} Ax^* + M\mu^* &= 0, \\ Cx^* + N\mu^* &> 0 \end{aligned}$$

for a regular equilibrium and

$$\begin{aligned} Ax^* + M\mu^* + B\lambda^* &= 0, \\ Cx^* + N\mu^* &= 0, \\ \lambda^* &> 0 \end{aligned}$$

for a boundary equilibrium, where

$$\begin{aligned} A &= F_x(\bar{x}, \bar{\mu}), & M &= F_\mu(\bar{x}, \bar{\mu}), \\ C &= H_x(\bar{x}, \bar{\mu}), & N &= H_\mu(\bar{x}, \bar{\mu}), \\ B &= -W(\bar{x}, \bar{\mu}), & CB &= 0. \end{aligned}$$

If the linear systems are not degenerate, they will be representative of what happens locally in the full system. We find the following theorem.

THEOREM 4.1 (equilibrium points branching from a boundary equilibrium). *For systems in this class, assuming*

$$\begin{aligned} \det(A) &\neq 0, \\ e = N - CA^{-1}M &\neq 0, \\ s = CA^{-1}B &\neq 0, \end{aligned}$$

there exist a unique regular equilibrium point branching off from \bar{x} when $e(\mu^ - \bar{\mu})$ is small and positive, and a unique pseudoequilibrium point branching off from \bar{x} when $(e/s)(\mu^* - \bar{\mu})$ is small and positive. The derivative of the points with respect to the parameter exists and has a limit as $\mu^* \rightarrow \bar{\mu}$ from the side where the point exists.*

Note the similarity of this result to Theorem 3.5; the proof follows along similar lines. We note that if $s > 0$, the regular and pseudopoints are both present for one sign of $\mu^* - \bar{\mu}$ and none are present for the other sign. Thus one can say that the points annihilate each other as μ^* changes, in a *saddle-node-like* bifurcation. If $s < 0$, one equilibrium point is present for any small value of $\mu^* - \bar{\mu}$, and the regular equilibrium *persists* into a pseudopoint as μ^* changes.

The local stability of a regular equilibrium point in the limit $\mu^* \rightarrow \bar{\mu}$ is determined by the eigenvalues of the matrix A . The question of local stability of a pseudoequilibrium point can be split into attractivity of the sliding set and stability in the sliding vector field when restricted to the sliding set, respectively; see, e.g., [111].

A simple calculation shows that local attractivity of the sliding set is guaranteed if

$$-2 < b(\bar{x}) \leq -1$$

(essentially because expression $-(1+b)$ acts like a “coefficient of restitution”). If this is fulfilled, a small disturbance in initial condition will decay toward the sliding set through an infinite number of impacts in finite time (“chattering”).

The linearization of the sliding vector field (4.10) at $\bar{\mu}$ and near \bar{x} is simplified since $\lambda = F = 0$, $-W = B$, $b = -CAB$, and $a_x = CAA$ at $(\bar{x}, \bar{\mu})$. The result is

$$A_s = \left(I - \frac{BCA}{CAB} \right) A,$$

and we see that there is a 2×2 Jordan block corresponding to eigenvalue 0 with left eigenvector CA and left generalized eigenvector C . This of course corresponds to the invariance of the codimension-two sliding set. The rest of the eigenvalues of A_s correspond to dynamics within the sliding set, and if all have negative real part, the pseudoequilibrium is stable within the sliding set.

Example 4.2 (a simple two-dimensional system). Consider the system

$$(4.12) \quad \begin{aligned} F(x, \mu) &= \begin{pmatrix} x_2 \\ \mu - kx_1 + x_2 \end{pmatrix}, \\ H(x) &= x_1, \\ W &= -(1+r) \begin{pmatrix} 0 \\ 1 \end{pmatrix}, \end{aligned}$$

describing a one-degree-of-freedom mechanical system with position x_1 , velocity x_2 , a spring force with spring constant k , damping coefficient -1 , and an impact coefficient of restitution r . Note this is like an unforced, but negatively damped (energy inputting) version of Example 4.1. At $\bar{x} = 0$, $\bar{\mu} = 0$ we have a boundary equilibrium. We find that

$$\begin{aligned} v(x) &= x_2, \quad a(x) = \mu - kx_1 + x_2, \\ b(x) &= -(1+r), \quad F_s(x, \mu) = \begin{pmatrix} x_2 \\ 0 \end{pmatrix}, \\ A &= \begin{pmatrix} 0 & 1 \\ -k & 1 \end{pmatrix}, \quad M = \begin{pmatrix} 0 \\ 1 \end{pmatrix}, \\ C &= (1 \ 0), \quad N = 0, \\ B &= (1+r) \begin{pmatrix} 0 \\ 1 \end{pmatrix}, \quad e = 1/k, \\ s &= -(1+r)/k, \quad A_s = \begin{pmatrix} 0 & 1 \\ 0 & 0 \end{pmatrix}. \end{aligned}$$

This is consistent with the explicit solution for the regular equilibrium

$$\begin{aligned} x^* &= \begin{pmatrix} \mu^*/k \\ 0 \end{pmatrix}, \\ \mu^*/k &> 0 \end{aligned}$$

and the pseudoequilibrium

$$\begin{aligned} x^* &= \begin{pmatrix} 0 \\ 0 \end{pmatrix}, \\ \lambda^* &= -\mu^*/(1+r), \\ \mu^*/(1+r) &< 0. \end{aligned}$$

If $k = 1$, the regular equilibrium exists for $\mu > 0$ and the pseudoequilibrium for $\mu < 0$. If $k = -1$, neither exist for $\mu > 0$ and both exist for $\mu < 0$. The regular equilibrium

point is unstable (a saddle point if $k < 0$). The pseudoequilibrium point is stable if $0 \leq r < 1$ (owing to attractivity of the sliding set, A_s has no nontrivial eigenvalues).

Little is known about the existence of limit sets besides equilibrium points when perturbing a boundary equilibrium. The type of analysis required clearly has a strong resemblance to what would be needed in the corresponding cases for Filippov and nonsmooth continuous systems in sections 2.1 and 3.1, where planar systems are fully understood, but only relatively weak results apply in three and higher dimensions. Here we will merely give some examples where single-impact limit cycles exist for Example 4.2, system (4.12). In each case, the limit cycle will branch off the boundary equilibrium as μ passes through 0. In particular, we can show after some calculations that

- if $k = 1$, $0 \leq r < \exp(-\pi/\sqrt{3})$, and $\mu > 0$, a stable impacting limit cycle surrounds the regular unstable focus equilibrium point;
- if $k = 1$, $\exp(-\pi/\sqrt{3}) < r < 1$, and $\mu < 0$, an unstable impacting limit cycle surrounds the stable pseudoequilibrium point;
- if $k = -1$, $(3 - \sqrt{5})/2 < r < 1$, and $\mu < 0$, an unstable impacting limit cycle surrounds the stable pseudoequilibrium point, but not the regular saddle point.

Figure 30 shows one example of each of these situations.

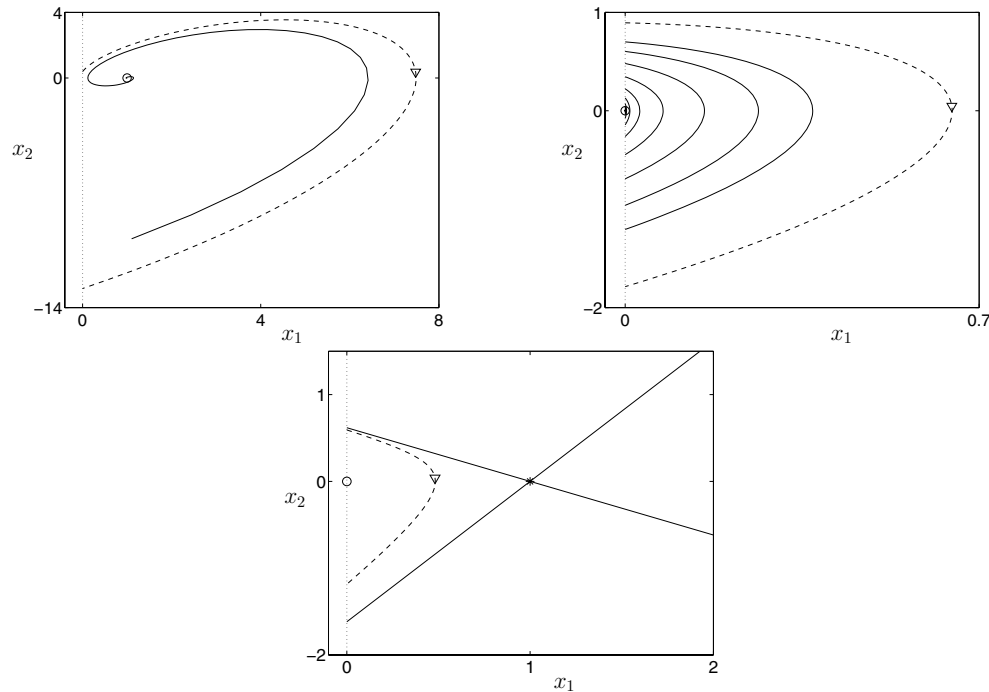


Fig. 30 *Limit cycles in boundary equilibrium bifurcations. Top left: $k = 1$, $r = 0.03$, $\mu = 1$. Impacting stable limit cycle (dashed) together with orbit (solid) starting near unstable focus (circle). Top right: $k = 1$, $r = 0.5$, $\mu = -1$. Impacting unstable limit cycle (dashed) together with chattering orbit (solid) converging to the stable pseudoequilibrium (circle). Bottom: $k = -1$, $r = 0.5$, $\mu = -1$. Impacting unstable limit cycle (dashed) together with stable pseudoequilibrium (circle), saddle point (star), and the nonimpacting parts of its stable and unstable manifolds.*

4.2. Grazing Bifurcations of Limit Cycles. Impacting systems have flows Ψ which consist of smooth flows ϕ satisfying $\dot{x} = F$ and applications of the impact map R . They may have limit cycles which are either entirely flows ϕ or are again a mix of ϕ and R . Our interest lies in any such limit cycle which evolves under parameter changes so that an additional (zero velocity) grazing impact occurs. Therefore, we will again consider systems that (at least locally) take the form given at the beginning of this section,

$$\dot{x} = F(x) \quad \text{if } H(x) > 0,$$

with impact at the surface defined by $H(x) = 0$, where the impact law takes the form

$$x^+ = R(x^-) = x^- + W(x^-)H_x F(x^-).$$

In such a system, there is the possibility of a periodic orbit that contains an isolated point of zero impact velocity $H_x F$. This is called a *grazing* impact. At such a point we can see a dramatic change in the behavior of the orbit. Nearby trajectories may have a low velocity impact close to the grazing impact point, or they may miss the impact surface; see Figure 31. Since nearby trajectories can undergo different events, it is suitable to encapsulate this into a DM acting on a neighborhood of the grazing point.

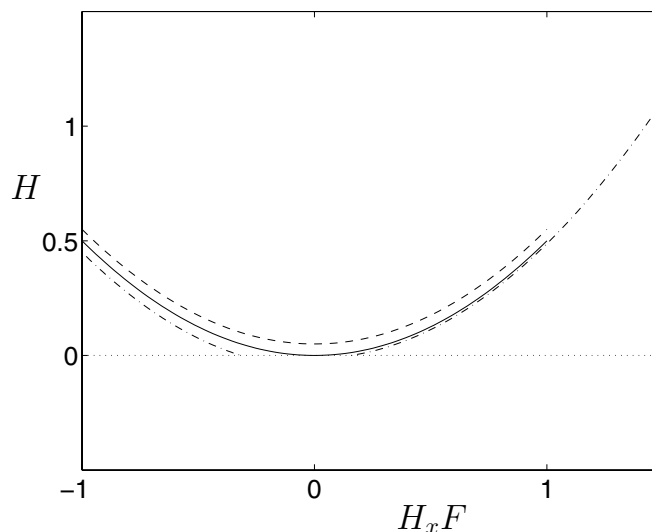


Fig. 31 A grazing trajectory (solid), an impacting trajectory (dot-dashed), and a missing trajectory (dashed), all simulated for the same length of time. Note the large shift in endpoint for the trajectory with a low velocity impact.

4.2.1. DMs for Grazing Impact. The derivation and form of the DM for grazing impact was first performed for single-degree-of-freedom impact oscillators in [82] and for more general systems in [52]. The results presented here have been adapted to the more general form of system specified by arbitrary F , W , and H .

Consider a grazing set $\Sigma_0 \subset \Sigma$, where

$$\begin{aligned} H(x) &= 0, \\ v \equiv H_x F(x) &= 0, \\ a \equiv (H_x F)_x F(x) &> a_0 > 0 \end{aligned}$$

for some a_0 . We assume that all functions are as smooth as necessary in a neighborhood of Σ_0 . Through each point of Σ_0 passes a grazing trajectory of the system that has a quadratic tangency to the impact surface. The form of the impact law ensures that grazing trajectories are well defined whether or not they are considered as impacting, and that incoming trajectories that are close stay close after passing through a neighborhood of Σ_0 . In a neighborhood of Σ_0 , we define a ZDM as the identity if the trajectory does not impact, and as the result of going through an impact and returning to time zero along the flow if the trajectory impacts (see Figure 32). Suppose that we start at a point x_0 close to Σ_0 . A trajectory starting from x_0 will typically impact Σ at a point x_2 close to x_0 at a time δ . We can (at least theoretically) continue this trajectory past x_2 until $H(x)$ takes its minimum value H_{\min} at the point x_1 . The point x_2 is mapped to x_3 by the impact. We can continue the flow ϕ backwards by a time $-\delta$ to reach another point x_4 . The map $x_0 \rightarrow x_4$ is the ZDM. We find now, if $x \equiv x_0$ and $\|v(x_0)\| \ll 1$ and $\|H(x_0)\| \ll 1$, then the following holds.

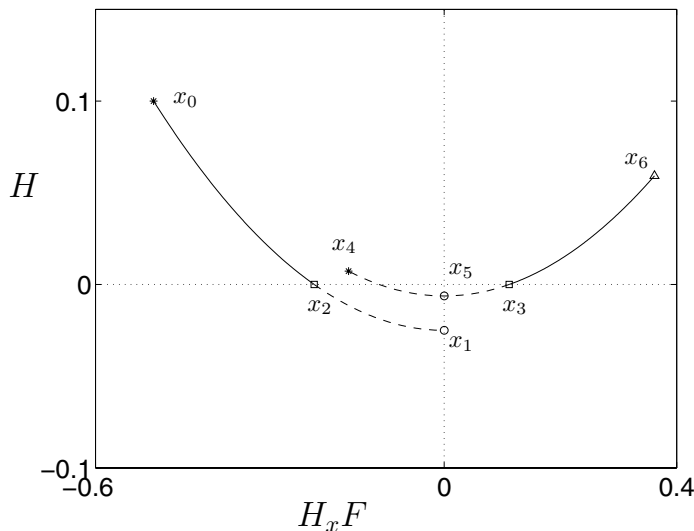


Fig. 32 DMs close to a grazing impact at the origin. A trajectory starts at x_0 , impacts at x_2 , is mapped to x_3 by the impact law, and continues to x_6 . The ZDM maps x_0 to x_4 . The PDM maps x_1 to x_5 .

THEOREM 4.2 (the ZDM for grazing impact; reformulation of result in [52]). *For systems in this class, there is a neighborhood of Σ_0 where the ZDM can be written*

$$(4.13) \quad ZDM(x) = x + \begin{cases} 0 & \text{if } H_{\min}(x, v) \geq 0, \\ \beta(x, y, v)y & \text{if } H_{\min}(x, v) < 0, \end{cases}$$

where

$$\begin{aligned}
 \beta(x, y, v) &= -W(x)\sqrt{2a(x)} + r_2(x, y, v), \\
 r_2(x, y, v) &\rightarrow 0 \quad \text{if } y, v \rightarrow 0, \\
 y(x, v) &= \sqrt{-H_{\min}(x, v)}, \\
 (4.14) \quad H_{\min}(x, v) &= H(x) - v^2 \left(\frac{1}{2a(x)} + r_1(x, v) \right), \\
 r_1(x, v) &\rightarrow 0 \quad \text{if } v \rightarrow 0, \\
 v(x) &= H_x F(x), \\
 a(x) &= v_x F(x),
 \end{aligned}$$

and β and H_{\min} are smooth in their arguments.

Note that the set Σ_0 is determined by the facts that H and $H_x F$ are zero and that the auxiliary variables v and y are independent variables measuring the closeness of x to Σ_0 . Note also that y is not smooth when $H_{\min} = 0$. Thus the full ZDM is not smooth at points where $H_{\min} = 0$. The lowest-order approximation is

$$\begin{aligned}
 \beta(x, y, v) &\approx -W(x)\sqrt{2a(x)}, \\
 H_{\min}(x, v) &\approx H(x).
 \end{aligned}$$

By choosing an incoming and a (possibly different) outgoing surface that are both transversal to the flow and contain Σ_0 , we can derive PDMs for grazing impact. A convenient surface to use is $H_x F = 0$, which satisfies all requirements. For this choice, also illustrated in Figure 32, the PDM maps x_1 to x_5 . Setting now $x = x_1$ and $\|H(x_1)\| \ll 1$ we have:

THEOREM 4.3 (a PDM for grazing impact [35, 38]). *For systems in this class, there is a neighborhood of Σ_0 where the PDM from an incoming to an outgoing $H_x F = 0$ surface can be written*

$$(4.15) \quad PDM(x) = x + \begin{cases} 0 & \text{if } H(x) \geq 0, \\ \beta(x, y)y & \text{if } H(x) < 0, \end{cases}$$

where

$$\begin{aligned}
 \beta(x, y) &= -\sqrt{2a(x)} \left(W(x) - \frac{b(x)}{a(x)} F(x) \right) + r_2(x, y), \\
 r_2(x, y) &\rightarrow 0 \quad \text{if } y \rightarrow 0, \\
 (4.16) \quad y(x) &= \sqrt{-H(x)}, \\
 a(x) &= (H_x F)_x F(x), \\
 b(x) &= (H_x F)_x W(x),
 \end{aligned}$$

and β is smooth in its arguments.

Note that H attains its minimum in the Poincaré surface, so no calculation of the minimum value is needed. Note also that if F and W are parallel, the lowest-order term of β drops out. Observe that the PDM and the ZDM are both $I + \mathcal{O}(|\sqrt{H}|)$, where I is the identity.

4.2.2. Poincaré Mappings for the Full System.

The PDM

$$D(x) = x + \begin{cases} 0 & \text{if } H(x) \geq 0, \\ \beta(x, y)y & \text{if } H(x) < 0, \end{cases}$$

where

$$y(x) = \sqrt{-H(x)},$$

can now be composed with a mapping $P(x)$ from the outgoing surface to the incoming, where any low velocity impacts at the beginning or toward the end are disregarded, and it is assumed that no low velocity impacts are taking place elsewhere. In this case, the mapping P is smooth, and the full mapping from the outgoing surface back to itself is $D \circ P$ and contains all dynamics.

Note again that this mapping is not the usual Poincaré mapping derived from the same section, as the low velocity impact is always taken into account at the end of the mapping, whereas in the usual Poincaré mapping, low velocity impacts could come either at the beginning or at the end. Usual Poincaré mappings are best taken at a section away from Σ_0 . On the other hand, the mapping $D \circ P$ is related to any Poincaré mapping through a smooth coordinate transformation, using a section away from Σ_0 , and so it is equivalent when it comes to analyzing the dynamics.

Example 4.3 (an explicitly calculable model). We now consider an example where we can compute all mappings explicitly. Let x_1 and x_2 be position and velocity, and let x_3 be a variable defined modulo 4 that keeps track of the driving phase. We write the state variables collectively as

$$x = \begin{pmatrix} x_1 \\ x_2 \\ x_3 \end{pmatrix}.$$

The three-dimensional ODE system for $x_1 > 0$ will be taken to have different forms depending on the values of x_3 . For $x_1 > 0, 0 < x_3 < 2$ (region S_1) we use

$$\dot{x} = \begin{pmatrix} \dot{x}_{2p} - (2d/w)(x_2 - x_{2p}) - (1/w^2)(x_1 - x_{1p}) \\ x_2 \\ 1 \end{pmatrix},$$

where the particular solution x_p is

$$\begin{pmatrix} x_{1p} \\ x_{2p} \end{pmatrix} (x_3) = \begin{pmatrix} 1/2 + \mu + x_3 - x_3^2/2 \\ 1 - x_3 \end{pmatrix}.$$

For $x_1 > 0, 2 < x_3 < 4$ (region S_2) we use

$$\dot{x} = \begin{pmatrix} x_2 \\ 1 \\ 1 \end{pmatrix}.$$

As $\dot{x}_3 = 1$ there is no possibility of sliding along the boundary between regions S_1 and S_2 . At $x_1 = 0$ an impact with coefficient of restitution r takes place: $x_2^+ = -rx_2^-$.

In S_1 the system is controlled toward the particular solution x_p using the positive control parameters d and w , and the position of the particular solution is determined by the parameter μ . In this region, the particular solution represents those initial conditions that lead to constant negative acceleration equal to -1 . In region S_2 , the acceleration is constant and equal to 1.

When $\mu > 0$, the system admits a nonimpacting periodic solution

$$\begin{pmatrix} x_1 \\ x_2 \end{pmatrix} = x_p = \begin{pmatrix} 1/2 + \mu + x_3 - x_3^2/2 \\ 1 - x_3 \end{pmatrix}$$

in S_1 and

$$\begin{pmatrix} x_1 \\ x_2 \end{pmatrix} = \begin{pmatrix} 1/2 + \mu - (x_3 - 2) + (x_3 - 2)^2/2 \\ -1 + (x_3 - 2) \end{pmatrix}$$

in S_2 . The minimal x_1 value of this orbit is μ at $x_3 = 3$. When $\mu = 0$ we have a periodic orbit with a grazing impact at

$$x^* = \begin{pmatrix} 0 \\ 0 \\ 3 \end{pmatrix}.$$

The grazing orbit is shown in Figure 33.

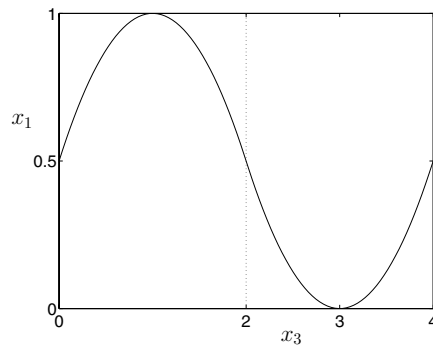


Fig. 33 Grazing periodic orbit of Example 4.3.

For this system we can explicitly write down mappings for trajectories close to the grazing one. The flow mapping for region S_1 is, assuming no impacts and $0 \leq x_3, x_3 + t \leq 2$,

$$\Phi_1(x, t) = \begin{pmatrix} A_1(t) \left[\begin{pmatrix} x_1 \\ x_2 \end{pmatrix} - \begin{pmatrix} x_1 \\ x_2 \end{pmatrix}_p(x_3) \right] + \begin{pmatrix} x_1 \\ x_2 \end{pmatrix}_p(x_3 + t) \end{pmatrix},$$

where

$$A_1(t) = e^{B_1 t},$$

$$B_1 = \begin{pmatrix} 0 & 1 \\ -(2d/w) & -(1/w^2) \end{pmatrix}.$$

In region S_2 , there is at most one impact. Assuming no impacts and $2 \leq x_3, x_3 + t \leq 4$, the flow mapping is

$$\Phi_2(x, t) = \begin{pmatrix} x_1 + x_2 t + t^2/2 \\ x_2 + t \\ x_3 + t \end{pmatrix}.$$

For initial conditions with $x_3 < 3$ near the grazing periodic orbit, there is a low velocity impact near $x_3 = 3$ precisely if

$$H_{\min}(x) = x_1 - x_2^2/2$$

is negative. If we take an impact into account whenever $H_{\min}(x) < 0$ (regardless of whether the impact takes place inside or outside the time interval studied), we arrive at the mapping

$$(4.17) \quad \Phi'_2(x, t) = \Phi_2(x, t) + \begin{cases} 0 & \text{if } H_{\min}(x) \geq 0, \\ \sqrt{2}(1+r) \begin{pmatrix} \sqrt{2}y + x_2 + t \\ 1 \\ 0 \end{pmatrix} y & \text{if } H_{\min}(x) < 0, \end{cases}$$

where $y = \sqrt{-H_{\min}(x)}$. Setting $t = 0$ in (4.17) gives us the ZDM

$$D(x) = x + \begin{cases} 0 & \text{if } H_{\min}(x) \geq 0, \\ \beta(x, y)y & \text{if } H_{\min}(x) < 0, \end{cases}$$

where

$$\beta(x, y) = \sqrt{2}(1+r) \begin{pmatrix} \sqrt{2}y + x_2 \\ 1 \\ 0 \end{pmatrix}.$$

These results for H_{\min} and β are in agreement with the equations (4.13)–(4.14) of the grazing ZDM for a system with impact, if the expression for $v = x_2$ is introduced.

Knowing these mappings we can easily build other mappings. For example, a Poincaré mapping from the surface $x_3 = 0$ back to itself is $\Phi_2(\cdot, 1) \circ D \circ \Phi_2(\cdot, 1) \circ \Phi_1(\cdot, 2)$ near the grazing periodic orbit. An equivalent mapping is $D \circ \Phi_2(\cdot, 1) \circ \Phi_1(\cdot, 2) \circ \Phi_2(\cdot, 1)$, which is essentially the Poincaré mapping at $x_3 = 3$ except for the fact that the impact is always taken into account last. Using only

$$z = \begin{pmatrix} x_1 \\ x_2 \end{pmatrix}$$

as the variables, the mapping can be written $D \circ P$, where

$$P(z) = Az + M\mu,$$

where

$$A = \begin{pmatrix} 1 & 1 \\ 0 & 1 \end{pmatrix} A_1(2) \begin{pmatrix} 1 & 1 \\ 0 & 1 \end{pmatrix},$$

$$M = \begin{pmatrix} 1 \\ 0 \end{pmatrix} - \begin{pmatrix} 1 & 1 \\ 0 & 1 \end{pmatrix} A_1(2) \begin{pmatrix} 1 \\ 0 \end{pmatrix},$$

and

$$D(z) = z + \begin{cases} 0 & \text{if } h(z) \geq 0, \\ b(z, y)y & \text{if } h(z) < 0, \end{cases}$$

where

$$b(z, y) = \sqrt{2}(1+r) \begin{pmatrix} \sqrt{2}y + x_2 \\ 1 \end{pmatrix},$$

$$h(z) = x_1 - x_2^2/2.$$

4.2.3. Unfolding a Grazing Periodic Orbit. The dynamical behavior near (in state and parameter space) a grazing orbit can be quite rich, with the grazing orbit at the limit point of an infinite series of other smooth bifurcations and DIBs. Various aspects of the behavior have been studied in [82, 21, 17, 84, 52, 85]. It has been shown that up to an infinite number of different periodic orbits can branch off the grazing orbit as a parameter is varied, and also that a chaotic attractor may exist. Here we will present some results that are valid in any finite number of space dimensions.

4.2.4. Existence of Low Period Periodic Orbits. Assume that the system depends on single parameter μ , and that $x = \bar{x}$, $\mu = \bar{\mu}$ satisfies

$$\begin{aligned} P(\bar{x}, \bar{\mu}) &= \bar{x}, \\ H(\bar{x}, \bar{\mu}) &= 0. \end{aligned}$$

This means that \bar{x} lies on a grazing periodic orbit. If the parameter μ is changed, nonimpacting and/or impacting periodic orbits (fixed or periodic points for the mapping) may branch off the grazing orbit. Finding all of these is a difficult task, given that the Poincaré mapping has different expressions depending on the sign of H at each iterate, but if one decides to look for a specific period and a specific pattern of signs of H for each iterate, one can formulate a smooth system of equations to solve, whose solutions are subject to the condition that they must agree with the assumed pattern [85]. In the following, when an iterate is referred to as being “impacting” or not, we mean the presence or absence of a low velocity impact near the grazing point. There may well be other impacts along the trajectory.

Thus, the conditions for a nonimpacting period-one point are

$$\begin{aligned} P(x^*, \mu^*) &= x^*, \\ H(x^*, \mu^*) &> 0, \end{aligned}$$

and the conditions for a single-impact period-one point are

$$\begin{aligned} P(x^*, \mu^*) + \beta(P(x^*, \mu^*), y^*, \mu^*)y^* &= x^*, \\ H(P(x^*, \mu^*), \mu^*) + y^2 &= 0, \\ y^* &> 0. \end{aligned}$$

Assuming for simplicity $\bar{x} = \bar{\mu} = 0$ and linearizing, we find

$$\begin{aligned} Ax^* + M\mu^* &= x^*, \\ Cx^* + N\mu^* &> 0 \end{aligned}$$

for the nonimpacting period-one point and

$$\begin{aligned} Ax^* + M\mu^* + By^* &= x^*, \\ CAx^* + (CM + N)\mu^* &= 0, \\ y^* &> 0 \end{aligned}$$

for the single-impact period-one point, where

$$\begin{aligned} A &= P_x(\bar{x}, \bar{\mu}), \\ M &= P_\mu(\bar{x}, \bar{\mu}), \\ C &= H_x(\bar{x}, \bar{\mu}), \\ N &= H_\mu(\bar{x}, \bar{\mu}), \\ B &= \beta(\bar{x}, 0, \bar{\mu}), \\ CB &= 0. \end{aligned}$$

If the linear systems are not degenerate, they will be representative of what happens locally in the full system. Introducing the notation

$$s(\lambda, n) = CA^n(\lambda I - A^n)^{-1}B,$$

we find the following theorem by solving the linear systems.

THEOREM 4.4 (period-one orbits branching from a grazing orbit [85]). *For systems in this class, assuming*

$$\begin{aligned} \det(I - A) &\neq 0, \\ e = N + C(I - A)^{-1}M &\neq 0, \\ s(1, 1) = CA(I - A)^{-1}B &\neq 0, \end{aligned}$$

there exists a unique nonimpacting period-one point branching off from \bar{x} when $e(\mu^ - \bar{\mu})$ is small and positive, and a unique single-impact period-one point branching off from \bar{x} when $(e/s(1, 1))(\mu^* - \bar{\mu})$ is small and negative. The derivative of the points with respect to the parameter exists and has a limit as $\mu^* \rightarrow \bar{\mu}$ from the side where the point exists.*

We note that if $s(1, 1) < 0$, the nonimpacting and single-impact points are both present for one sign of $\mu^* - \bar{\mu}$ and none are present for the other sign. Thus one can say that the points annihilate each other as μ^* changes, much like in a saddle-node bifurcation for smooth systems. If $s(1, 1) > 0$, one equilibrium point is present for any small value of $\mu^* - \bar{\mu}$, and the nonimpacting is transformed into a single-impact point as μ^* changes. Note the similarity of this result to Theorem 4.1 for equilibria.

Concerning orbits of period-two, a nonimpacting orbit branching off the grazing orbit will in general (if A does not have an eigenvalue -1) be just the nonimpacting period-one orbit traversed twice, and likewise for a double-impact orbit, so the interesting case is when a period-two point has a single impact. Then we find the equations

$$\begin{aligned} P(x_1^*, \mu^*) &= x_2^*, \\ P(x_2^*, \mu^*) + \beta(P(x_2^*, \mu^*), y^*, \mu^*)y^* &= x_1^*, \\ H(P(x_2^*, \mu^*), \mu^*) + y^2 &= 0, \\ H(x_2^*, \mu^*) &> 0, \\ y^* &> 0 \end{aligned}$$

(note that suffixes means iterate numbers here, not component numbers). Linearizing as before gives us the following.

THEOREM 4.5 (period-two orbits branching from a grazing orbit [85]). *For systems in this class, assuming*

$$\begin{aligned} \det(I - A) &\neq 0, \\ \det(I + A) &\neq 0, \\ e = N + C(I - A)^{-1}M &\neq 0, \\ s(-1, 1) = -CA(I + A)^{-1}B &< 0, \\ s(1, 2) = CA^2(I - A^2)^{-1}B = (s(1, 1) + s(-1, 1))/2 &\neq 0, \end{aligned}$$

there exists a unique single-impact period-two point branching off from \bar{x} when it holds that $(e/s(1, 2))(\mu^ - \bar{\mu})$ is small and negative. The derivative of the points with respect to the parameter exists and has a limit as $\mu^* \rightarrow \bar{\mu}$ from the side where the point exists.*

Note that $s(-1, 1)$ determines whether the orbit is possible, and $s(1, 2)$ determines on which side of the bifurcation parameter value the orbit exists. Note also that the relation among $s(1, 1)$, $s(-1, 1)$, and $s(1, 2)$ shows the impossibility of having a nonimpacting and a single-impact period-one orbit on one side of the bifurcation and a single-impact period-two orbit on the other side.

One can note that these results have a strong resemblance to the results for existence in continuous PWS mappings [39]. This is a strong hint that there are underlying topological properties that may be used to shed light on these results.

For higher periods the analytical solution of the linearized equation and conditions becomes more complicated, but there is of course no problem with solving the linearized equations numerically for a given system and then checking the linearized inequalities. In this way the existence of periodic orbits up to, say, period-ten can be quickly established for a given grazing bifurcation.

For two-dimensional mappings, the situation is known more completely; see [85].

Local Stability. The local stability of the nonimpacting orbit is determined by the eigenvalues of A . If all eigenvalues are within the unit circle, the orbit is stable. For the single-impact period-one orbit, if $CAB \neq 0$, the orbit must be unstable with an eigenvalue of leading order $-CAB/(2y)$ as the bifurcation point is approached. For the single-impact period-two orbit, if $CA^2B \neq 0$, the orbit must likewise be unstable with an eigenvalue of leading order $-CA^2B/(2y)$. In general, all impacting orbits that branch off the grazing orbit are violently unstable close to the bifurcation point unless there is some additional degeneracy. Away from the bifurcation point, the branches may well turn stable, of course (see, e.g., [85] for an example where this happens).

4.2.5. Attractors. Although all impacting periodic orbits are in general unstable close to the bifurcation point, there is nonetheless a possibility of finding an attractor branching off the grazing orbit. An attractor is guaranteed if we can show that the grazing orbit is asymptotically stable. The stability of the grazing orbit depends on whether repeated low velocity impacts can be avoided, as each such impact, through the square-root terms, tends to shift motion away from the grazing orbit by a (relatively) large amount. Repeated impacts are avoided if $CA^nB > 0$ for all $n > 0$. Thus we have the following.

THEOREM 4.6 (stability of a grazing orbit [52]). *For systems in this class, a grazing orbit is stable if A is stable (all eigenvalues within the unit circle) and $CA^nB > 0$ for all $n > 0$. If $CA^{n_1}B < 0$ for some $n_1 > 0$, the grazing orbit is unstable.*

For a two-dimensional mapping, the conditions for stability (and the existence of an attractor) are fulfilled if the eigenvalues of A are real and satisfy $0 < \lambda_2 < \lambda_1 < 1$

and $CAB > 0$. For N -dimensional mappings, if A has a single real positive stable eigenvalue λ_1 of largest modulus with right eigenvector ϕ and left eigenvector ϕ^* , and $(C\phi)(\phi^*B)/(\phi^*\phi) > 0$, then $CA^nB > 0$ for large enough n , so only a finite number of CA^nB need be checked.

Assuming we have a single positive stable eigenvalue λ_1 of largest modulus and a nonzero value of e , we will have one stable nonimpacting period-one orbit when $e(\mu - \bar{\mu}) > 0$. When $e(\mu - \bar{\mu}) < 0$, there is an attractor of size proportional to $\sqrt{-e(\mu - \bar{\mu})}$. The dynamics of this attractor depends mainly on the value of λ_1 ; see [84]:

- If $2/3 < \lambda_1 < 1$, there will be a chaotic attractor for all small negative $e(\mu - \bar{\mu})$.
- If $1/4 < \lambda_1 < 2/3$, there will be an alternating sequence of chaotic and stable periodic motion for small negative $e(\mu - \bar{\mu})$. Each chaotic or periodic band is mapped to the next if $\mu - \bar{\mu}$ is multiplied by a factor that has the asymptotic value λ_1^2 as $\mu - \bar{\mu} \rightarrow 0$. The period of the periodic motion is increased by 1 from one band to the next (“period-adding”). For λ_1 close to $2/3$ the periodic bands will be narrow, and for λ_1 close to $1/4$ the chaotic bands will be narrow.
- If $0 < \lambda_1 < 1/4$, the periodic bands start to overlap and there is no attracting chaotic motion for small negative $e(\mu - \bar{\mu})$. The same parameter scaling as before applies. For each parameter value, there is either a unique stable periodic orbit or two different stable orbits with periods differing by 1.

The chaotic attractor, when it exists, has a general structure consisting of segments in the positive A^nB directions for $0 \leq n \leq N$ (see Figure 35). The segments get thinner and their number increases as $\mu \rightarrow \bar{\mu}$.

Let us end this discussion on grazing in impacting systems with two examples that illustrate this period-adding and chaos.

Return to Example 4.3. In the example system, set $d = 0.7$, $w = 2$, and $r = 0.8$. This gives

$$\begin{aligned} A &= \begin{pmatrix} 0.4663 & 1.4337 \\ -0.2277 & -0.1713 \end{pmatrix}, \\ M &= \begin{pmatrix} 0.5337 \\ 0.2277 \end{pmatrix}, \\ B &= \begin{pmatrix} 0 \\ 2.5456 \end{pmatrix}, \\ C &= (1 \quad 0), \\ N &= 0. \end{aligned}$$

Checking orbits up to period-three, we find for small positive μ there is a nonimpacting period-one orbit and a single-impact period-three orbit, and for small negative μ there are single-impact unstable orbits of periods one and two, as well as a double impact orbit of period-three. Since $CA^3B < 0$, there is no continuous transition from the nonimpacting orbits into an attractor as μ decreases through 0. All impacting orbits are highly unstable close to the bifurcation point. In the left panel of Figure 34 we can see how the stable nonimpacting period-one orbit existing when $\mu = 0.4$ vanishes at $\mu = 0$. The single-impact orbit of period-three becomes stable in a saddle-node bifurcation near $\mu = 0.1$, but vanishes in another grazing bifurcation just below $\mu = 0$. The single-impact orbit of period-two becomes stable in a period-doubling bifurcation near $\mu = -0.3$ and is still stable at $\mu = -0.6$. There are several other bifurcations in this plot.

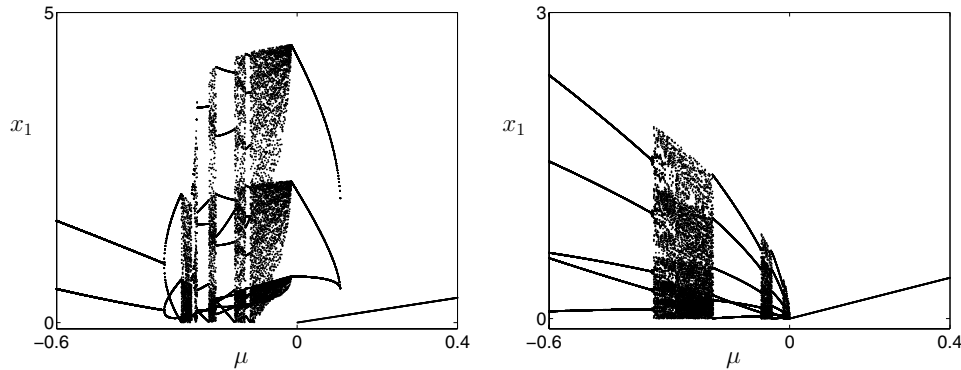


Fig. 34 Grazing bifurcations in Example 4.3. Left: $d = 0.7$, $w = 2$, $r = 0.8$ (discontinuous transition). Right: $d = 1.5$, $w = 5$, $r = 0.8$ (continuous transition).

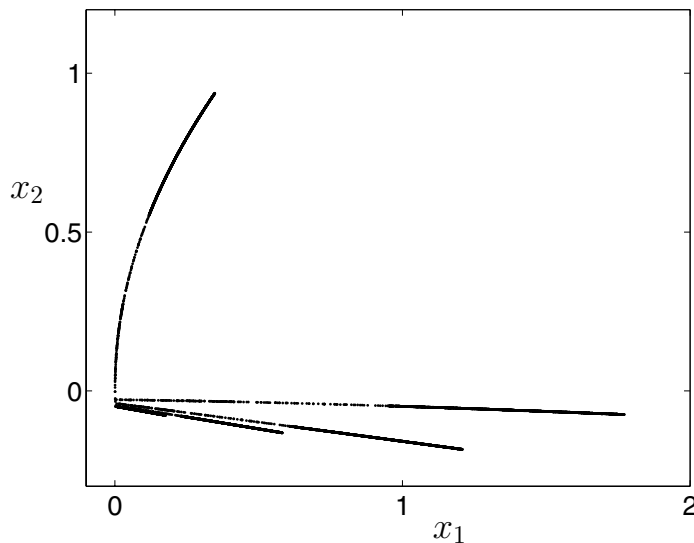


Fig. 35 Star-shaped chaotic attractor when $d = 1.5$, $w = 5$, $r = 0.8$, $\mu = -0.3$.

Now change the parameters to $d = 1.5$, $w = 5$, and $r = 0.8$. This gives

$$A = \begin{pmatrix} 0.7883 & 1.6660 \\ -0.0895 & -0.0175 \end{pmatrix},$$

$$M = \begin{pmatrix} 0.2117 \\ 0.0895 \end{pmatrix}.$$

The eigenvalues of A are 0.50 and 0.27 and thus we expect a continuous transition from a nonimpacting periodic orbit to an attractor. Since the largest eigenvalue is between $1/4$ and $2/3$, we expect periodic windows with increasing periods, with the size of the windows scaling by 0.50^2 near the bifurcation point. This is shown in the right panel of Figure 34. Periodic windows of periods 5, 6, and 7 can be distinguished, with the higher periodic windows being too narrow to be seen. When there is a chaotic attractor, it has a *fingered structure*, as shown in Figure 35.

Example 4.4 (an impacting pendulum). We now return to the problem considered in the introduction. In [97] a simple rigid-arm pendulum that strikes an impact surface is considered experimentally (see right panel of Figure 1). By horizontally shaking the supporting pivot of the pendulum a variety of dynamic behaviors can be observed including chaos. However, with the impact barrier located at static equilibrium the velocity of impact tends to be relatively high and thus grazing bifurcations of the fundamental period-one orbit do not typically occur. But, by inclining the angle $\hat{\theta}$ at which the pendulum mass strikes the barrier (see left panel of Figure 1), it is possible to observe a transition between nonimpacting and impacting dynamic behavior. Due to speed limitations of the forcing mechanism the assembly is inclined at an angle of Θ (out of plane, see middle panel of Figure 1) in order to change the effect of gravity, i.e., $g_e = \cos(\Theta)g$, and thus reduce the natural frequency of the system. For a more careful discussion of this system see [11, 104, 97]. The nondimensionalized equations of motion for the mechanism described above can be written

$$(4.18) \quad \dot{x} = \begin{pmatrix} \dot{x}_1 \\ \dot{x}_2 \\ \dot{x}_3 \end{pmatrix} = \begin{pmatrix} x_2 \\ \alpha \cos(x_1 + \hat{\theta}) \sin(x_3) - \frac{2\beta}{\eta} x_2 - \frac{1}{4\eta^2} \sin(x_1 + \hat{\theta}) \\ 1 \end{pmatrix},$$

where $(x_1, x_2, x_3)^T = (\theta - \hat{\theta}, \theta', \tau \bmod 2\pi)^T$ and

$$(4.19) \quad \eta = \frac{\omega}{\omega_0}, \quad \omega_0 = 2\sqrt{\frac{g_e}{L}}, \quad \tau = \omega t, \quad \alpha = \frac{A}{L}, \quad \beta = \frac{\kappa}{2\omega_0}.$$

Here ω_0 is the frequency of small amplitude motion of the impacting oscillator (when $\hat{\theta} = 0$), which is twice the natural frequency of the nonimpacting system. At impact, as $x_1 = 0$, we assume a simple restitution law of the form (4.5) is applied; thus

$$(4.20) \quad x^+ = x^- - \begin{pmatrix} 0 \\ 1+r \\ 0 \end{pmatrix} x_2^-,$$

where r is the coefficient of restitution. We assume further that x_{im} and τ_{im} are the point and time of grazing, respectively; i.e., $h(x(\tau_{im})) = h(x_{im}) = x_1 = 0$. Following (4.13) and (4.14) the lowest-order approximation of the ZDM for the present system can be written as

$$(4.21) \quad D(x) = \begin{cases} x + \begin{pmatrix} 0 \\ 1+r \\ 0 \end{pmatrix} \sqrt{-2x_1 a(x_{im})}, & h(x) \leq 0, \\ x, & h(x) > 0, \end{cases}$$

where we have used $y = \sqrt{-x_1}$, $a = x_2'$, and $x_{im} = (0, 0, \tau_{im})^T$. The complete Poincaré map Π around the grazing periodic orbit can then be written as

$$(4.22) \quad \Pi(x, T) = \Phi_2(x, T - \tau_{im}) \circ D(x) \circ \Phi_1(x, \tau_{im}),$$

where $T > 0$ is the period of the grazing periodic orbit and Φ_1 and Φ_2 are the flow functions before and after the grazing, respectively (cf. section 4.2.2). Estimation of the motion near grazing using the map (4.22) can be compared with experimental results and direct numerical simulations. In Figures 36(a) and (b) bifurcation diagrams close to grazing using direct numerical simulations and the full Poincaré map (4.22)

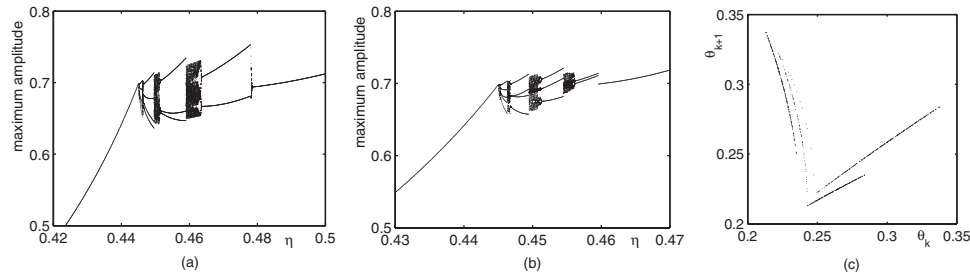


Fig. 36 Grazing transitions in the forced impacting pendulum under variation of η and using (a) direct numerical simulation, (b) the full Poincaré map including the ZDM. (c) A plot of the chaotic attractor of the impacting pendulum for $\eta = 0.4458$ near grazing using direct numerical simulation (cf. Figure 1). In all figures the angle of the impact barrier $\theta = 40^\circ$ and $r = 0.7675$.

are shown, respectively, where we vary η . At $\eta \approx 0.445$ there is a grazing transition from a nonimpacting state for $\eta < 0.445$ to a complex motion for $\eta > 0.445$. In this particular example the largest in magnitude eigenvalue is $|\lambda_{\max}| \approx 0.51$ for the grazing orbit and therefore, as expected (see section 4.2.5), a period-adding sequence is clearly visible. Figure 36(c) shows a finger-shaped plot of the chaotic attractor of the system close to the grazing bifurcation at $\eta = 0.7675$ using direct numerical simulation. The square-root term in the grazing normal form (4.21) clearly shows its presence as the almost vertical finger, and if the full Poincaré map is used very similar results are found (not depicted). If Figure 36(a) is compared with Figure 2(a), the η -value at which grazing occurs is almost the same. While there are also some differences in the details between the simulations and the experiment, there is clear experimental evidence for a period-adding sequence (upon decreasing η) interspersed with regions of chaos.

5. Discussion. While we have tried to be comprehensive in this review, there are many things that we have not addressed. For example (in no particular order), we have not dealt with more complex impact laws than (4.5), such as those required to explain the so-called Painlevé paradox [74]. We have also not treated systems with multiple impacts (but see, e.g., [58]). In the case of equilibrium bifurcation, general unfoldings in N dimensions remain unknown (sections 2.1 and 3.1). For sliding bifurcations of limit cycles we have not dealt with repelling sliding regions. Perhaps the biggest area that remains open is the unfolding of all the possible dynamics of the normal form we have derived. Set-valued Coulomb friction laws [111], chattering (the infinite accumulation of impacts), higher-order sliding (sliding along the intersection of two or more discontinuity surfaces) [19], and the possible existence of sets of equilibria in the sliding or sticking set have not been touched on here as often more precise mathematical tools such as differential inclusions are required.

Also, the review has (deliberately) limited its scope to codimension-one equilibrium and periodic orbit bifurcations. For some hints on how certain codimension-two DIBs can act as organizing centers, see [67]. There is also literature on global bifurcations in nonsmooth systems (an idea that was touched on in section 3.1); see also [70, 100, 105] for other examples. There is also literature on nonsmooth invariant tori bifurcations that we have not touched on here [29, 123].

Finally we mention infinite-dimensional systems generated by PDEs or delay equations; see, e.g., [72, 113]. In real continuous structures with impact, for example, many modes may be excited at impact and there may be a delay associated with the dissi-

pation of the shock wave (see, e.g., [58, 107, 121] for more realistic models of impact mechanisms).

Clearly we are just scratching the surface of a bifurcation theory for nonsmooth systems, yet it is the opinion of the authors that such a theory is pressing, since rattles, bangs, and switches are perhaps the most common (and grossest) form of nonlinearity found in applications.

REFERENCES

- [1] M. A. AIZERMAN AND F. R. GANTMAKHER, *On the stability of periodic motions*, J. Appl. Math. Mech., 22 (1958), pp. 1065–1078. Translated from Russian.
- [2] A. A. ANDRONOV, S. E. KHAIKIN, AND A. A. VITT, *Theory of Oscillators*, Pergamon Press, Oxford, 1965.
- [3] D. V. ANOSOV, *Stability of the equilibrium positions in relay systems*, Autom. Remote Control, 20 (1959), pp. 135–149.
- [4] D. K. ARROWSMITH AND C. M. PLACE, *An Introduction to Dynamical Systems*, Cambridge University Press, Cambridge, UK, 1990.
- [5] J. AUBIN AND A. CELLINA, *Differential Inclusion*, Springer-Verlag, Berlin, 1984.
- [6] V. I. BABITSKII, *Theory of Vibro-impact Systems. Approximate Methods*, Nauka, Moscow, 1978.
- [7] S. BANERJEE AND C. GREBOGI, *Border collision bifurcations in two-dimensional piecewise smooth maps*, Phys. Rev. E, 59 (1999), pp. 4052–4061.
- [8] S. BANERJEE AND C. GREBOGI, *Border collision bifurcations at the change of state-space dimension*, Chaos, 12 (2002), pp. 1054–1069.
- [9] S. BANERJEE AND G. VERGHESE, *Nonlinear Phenomena in Power Electronics*, IEEE Press, New York, 2001.
- [10] S. BANERJEE, J. A. YORKE, AND C. GREBOGI, *Robust chaos*, Phys. Rev. Lett., 80 (1998), pp. 3049–3052.
- [11] P. BAYLY AND L. VIRGIN, *An experimental study of an impacting pendulum*, J. Sound Vibration, 164 (1993), pp. 364–374.
- [12] B. BROGLIATO, *Nonsmooth Mechanics: Models, Dynamics and Control*, Springer-Verlag, London, 1999.
- [13] B. BROGLIATO, *Impacts in Mechanical Systems: Analysis and Modelling*, Lecture Notes in Phys. 551, Springer-Verlag, Berlin, Heidelberg, 2000.
- [14] B. BROGLIATO, *Some perspectives on the analysis and control of complementarity systems*, IEEE Trans. Automat. Control, 48 (2003), pp. 918–935.
- [15] B. BROGLIATO, A. TEN DAM, L. PAOLI, F. GENOT, AND M. ABADIE, *Numerical simulation of finite dimensional multibody nonsmooth mechanical systems*, ASME Appl. Mech. Rev., 55 (2002), pp. 107–150.
- [16] C. J. BUDD AND F. DUX, *Chattering and related behaviour in impact oscillators*, Phil. Trans. Roy. Soc. Lond. A, 347 (1994), pp. 365–389.
- [17] C. J. BUDD AND F. DUX, *Intermittency in impact oscillators close to resonance*, Nonlinearity, 7 (1994), pp. 1191–1224.
- [18] V. CARMONA, E. FREIRE, E. PONCE, AND F. TORRES, *On simplifying and classifying piecewise linear systems*, IEEE Trans. Circuits Systems I Fund. Theory Appl., 49 (2002), pp. 609–620.
- [19] P. CASINI AND F. VESTRONI, *Nonstandard bifurcations in oscillators with multiple discontinuity boundaries*, Nonlinear Dynam., 35 (2004), pp. 41–59.
- [20] D. CHILLINGWORTH, *Discontinuity geometry for an impact oscillator*, Dynam. Systems, 17 (2002), pp. 380–420.
- [21] W. CHIN, E. OTT, H. E. NUSSE, AND C. GREBOGI, *Grazing bifurcations in impact oscillators*, Phys. Rev. E, 50 (1994), pp. 4427–4444.
- [22] S. CHOW AND J. HALE, *Methods of Bifurcation Theory*, Grundlehren Math. Wiss. 251, Springer-Verlag, New York, 1982.
- [23] E. CODDINGTON AND N. LEVINSON, *Theory of Ordinary Differential Equations*, McGraw-Hill, New York, 1955.
- [24] F. CUNHA, D. PAGANO, AND U. MORENO, *Sliding bifurcations of equilibria in planar variable structure systems*, IEEE Trans. Circuits Systems I Fund. Theory Appl., 50 (2003), pp. 1129–1134.
- [25] H. DANKOWICZ, *On the modeling of dynamic friction phenomena*, ZAMM Z. Angew. Math. Mech., 79 (1999), pp. 399–409.

- [26] H. DANKOWICZ AND J. JERRELEND, *Control of near-grazing dynamics in impact oscillators*, Proc. Roy. Soc. London A, 461 (2005), pp. 3365–3380.
- [27] H. DANKOWICZ AND A. B. NORDMARK, *On the origin and bifurcations of stick-slip oscillations*, Phys. D, 136 (1999), pp. 280–302.
- [28] H. DANKOWICZ AND P. PIHOINEN, *Exploiting discontinuities for stabilization of recurrent motions*, Dynam. Systems, 17 (2002), pp. 317–342.
- [29] H. DANKOWICZ, P. PIHOINEN, AND A. NORDMARK, *Low-velocity impacts of quasiperiodic oscillations*, Chaos Solitons Fractals, 14 (2002), pp. 241–255.
- [30] H. DANKOWICZ AND X. ZHAO, *Local analysis of co-dimension-one and co-dimension-two grazing bifurcations in impact microactuators*, Phys. D, 2 (2005), pp. 238–257.
- [31] J. H. B. DEANE AND D. C. HAMILL, *Analysis, simulation and experimental study of chaos in the buck converter*, in Proceedings of the Power Electronics Specialists Conf. (PESC 1990), IEEE Press, New York, 1990, pp. 491–498.
- [32] K. DEIMLING, *Multivalued Differential Equations*, Walter De Gruyter, Berlin, 1992.
- [33] M. DI BERNARDO, *Normal forms of border collisions in high dimensional nonsmooth maps*, in ISACS 2003, IEEE International Symposium on Circuits and Systems, Vol. 3, IEEE Press, New York, 2003, pp. 76–79.
- [34] M. DI BERNARDO, C. J. BUDD, AND A. R. CHAMPNEYS, *Grazing, skipping and sliding: Analysis of the nonsmooth dynamics of the DC/DC buck converter*, Nonlinearity, 11 (1998), pp. 858–890.
- [35] M. DI BERNARDO, C. J. BUDD, AND A. R. CHAMPNEYS, *Corner collision implies border-collision bifurcation*, Phys. D, 154 (2001), pp. 171–194.
- [36] M. DI BERNARDO, C. J. BUDD, AND A. R. CHAMPNEYS, *Grazing and border-collision in piecewise smooth systems: A unified analytical framework*, Phys. Rev. Lett., 86 (2001), pp. 2553–2556.
- [37] M. DI BERNARDO, C. J. BUDD, AND A. R. CHAMPNEYS, *Grazing bifurcations in n-dimensional piecewise-smooth dynamical systems*, Phys. D, 160 (2001), pp. 222–254.
- [38] M. DI BERNARDO, C. J. BUDD, A. R. CHAMPNEYS, AND P. KOWALCZYK, *Piecewise Smooth Dynamical Systems: Theory and Applications*, Springer-Verlag, London, 2008.
- [39] M. DI BERNARDO, M. I. FEIGIN, S. J. HOGAN, AND M. E. HOMER, *Local analysis of C-bifurcations in n-dimensional piecewise smooth dynamical systems*, Chaos Solitons Fractals, 10 (1999), pp. 1881–1908.
- [40] M. DI BERNARDO, E. FOSSAS, G. OLIVAR, AND F. VASCA, *Secondary bifurcations and high periodic orbits in voltage controlled buck converter*, Internat. J. Bifurcations and Chaos, 7 (1997), pp. 2755–2771.
- [41] M. DI BERNARDO, F. GAROFALO, L. GLIELMO, AND F. VASCA, *Switchings, bifurcations and chaos in DC/DC converters*, IEEE Trans. Circuits Syst. I, 45 (1998), pp. 133–141.
- [42] M. DI BERNARDO, F. GAROFALO, L. IANELLI, AND F. VASCA, *Bifurcations in piecewise-smooth feedback systems*, Internat. J. Control, 75 (2002), pp. 1243–1259.
- [43] M. DI BERNARDO, K. H. JOHANSSON, AND F. VASCA, *Self-oscillations and sliding in relay feedback systems: Symmetry and bifurcations*, Internat. J. Bifurcations and Chaos, 11 (2001), pp. 1121–1140.
- [44] M. DI BERNARDO, P. KOWALCZYK, AND A. NORDMARK, *Bifurcations of dynamical systems with sliding: Derivation of normal-form mappings*, Phys. D, 170 (2002), pp. 175–205.
- [45] M. DI BERNARDO, P. KOWALCZYK, AND A. NORDMARK, *Sliding bifurcations: A novel mechanism for the sudden onset of chaos in dry-friction oscillators*, International J. Bifurcation and Chaos, 13 (2003), pp. 2935–2948.
- [46] M. I. FEIGIN, *Doubling of the oscillation period with C-bifurcations in piecewise continuous systems*, Phys. Met. Metallogr., 34 (1970), pp. 861–869.
- [47] M. I. FEIGIN, *On the generation of sets of subharmonic modes in a piecewise continuous system*, Phys. Met. Metallogr., 38 (1974), pp. 810–818.
- [48] M. I. FEIGIN, *On the structure of C-bifurcation boundaries of piecewise continuous systems*, Phys. Met. Metallogr., 42 (1978), pp. 820–829.
- [49] M. I. FEIGIN, *Forced Oscillations in Systems with Discontinuous Nonlinearities*, Nauka, Moscow, 1994 (in Russian).
- [50] A. F. FILIPPOV, *Differential Equations with Discontinuous Right-Hand Sides*, Kluwer Academic, Dordrecht, The Netherlands, 1988.
- [51] E. FOSSAS AND G. OLIVAR, *Study of chaos in the buck converter*, IEEE Trans. Circuits Systems I Fund. Theory Appl., 43 (1996), pp. 13–25.
- [52] M. H. FREDRIKSSON AND A. B. NORDMARK, *Bifurcations caused by grazing incidence in many degrees of freedom impact oscillators*, Proc. Royal Soc. Lond. A, 453 (1997), pp. 1261–1276.

- [53] E. FREIRE, E. PONCE, F. RODRIGO, AND F. TORRES, *Bifurcation sets of continuous piecewise linear systems with two zones*, Internat. J. Bifurcation and Chaos, 8 (1998), pp. 2073–2097.
- [54] S. GALEANI, L. MENINI, AND A. TORNAMBÈ, *A parametrization of exponentially stabilizing controllers for linear mechanical systems subject to non-smooth impacts*, IFAC Annual Reviews in Control, 28 (2004), pp. 13–21.
- [55] U. GALVANETTO, *Some discontinuous bifurcations in a two block stick-slip system*, J. Sound Vibration, 284 (2001), pp. 653–669.
- [56] U. GALVANETTO AND S. R. BISHOP, *Dynamics of a simple damped oscillator undergoing stick-slip vibrations*, Meccanica, 34 (2000), pp. 337–347.
- [57] F. GIANNAKOPOULOS AND K. PLIETE, *Planar systems of piecewise linear differential equations with a line discontinuity*, Nonlinearity, 14 (2001), pp. 1–22.
- [58] C. GLOCKER, *Set-valued Force Laws*, Lecture Notes in Appl. Mech. 1, Springer-Verlag, Berlin, Heidelberg, 2001.
- [59] J. GUCKENHEIMER AND P. HOLMES, *Nonlinear Oscillations, Dynamical Systems, and Bifurcations of Vector Fields*, Appl. Math. Sci. 42, Springer-Verlag, New York, 1983.
- [60] W. HEEMELS AND B. BROGLIATO, *The complementarity class of hybrid dynamical systems*, European J. Control, 9 (2003), pp. 311–319.
- [61] G. IOOSS AND D. JOSEPH, *Elementary stability and bifurcation theory*, Springer-Verlag, New York, 1980.
- [62] A. ISIDORI, *Nonlinear Control Systems*, Comm. Control Engrg. Ser., Springer-Verlag, London, 1995.
- [63] A. IVANOV, *Impact oscillations: Linear theory of stability and bifurcations*, J. Sound Vibration, 178 (1994), pp. 361–378.
- [64] P. KOWALCZYK, *Robust chaos and border-collision bifurcations in non-invertible piecewise linear maps*, Nonlinearity, 18 (2005), pp. 485–504.
- [65] P. KOWALCZYK AND M. DI BERNARDO, *Existence of stable asymmetric limit cycles and chaos in unforced symmetric relay feedback systems*, in Proceedings of European Control Conference, Porto, 2001, pp. 1999–2004.
- [66] P. KOWALCZYK AND M. DI BERNARDO, *On a novel class of bifurcations in hybrid dynamical systems: The case of relay feedback systems*, in Proceedings of Hybrid Systems: Computation and Control, Springer-Verlag, Berlin, 2001, pp. 361–374.
- [67] P. KOWALCZYK, M. DI BERNARDO, A. R. CHAMPNEYS, S. J. HOGAN, M. HOMER, Y. A. KUZNETSOV, A. B. NORDMARK, AND P. T. PIIRONEN, *Two-parameter nonsmooth bifurcations of limit cycle: Classification and open problems*, Internat. J. Bifurcation and Chaos, 16 (2006), pp. 601–629.
- [68] M. KUNZE, *Non-smooth Dynamical Systems*, Lecture Notes in Math. 1744, Springer-Verlag, Berlin, Heidelberg, 2000.
- [69] T. KÜPPER AND S. MORITZ, *General Hopf bifurcations for non-smooth planar systems*, Phil. Trans. Roy. Soc. Lond. A, 359 (2001), pp. 2483–2498.
- [70] Y. KUZNETSOV, S. RINALDI, AND A. GRAGNANI, *One-parameter bifurcations in planar Filippov systems*, Internat. J. Bifurcation and Chaos, 13 (2003), pp. 2157–2188.
- [71] Y. A. KUZNETSOV, *Elements of Applied Bifurcation Theory*, 2nd ed., Appl. Math. Sci. 112, Springer-Verlag, New York, 1998.
- [72] A. C. LAZER AND P. J. MCKENNA, *Large-amplitude periodic oscillations in suspension bridges: Some new connections with nonlinear analysis*, SIAM Rev., 32 (1990), pp. 537–578.
- [73] R. LEINE, *Bifurcations in Discontinuous Mechanical Systems of Filippov-Type*, Ph.D. thesis, Technische Universiteit Eindhoven, The Netherlands, 2000.
- [74] R. LEINE, B. BROGLIATO, AND H. NIJMEIJER, *Periodic motions and bifurcations induced by the Painlevé paradox*, Eur. J. Mech. A Solids, 21 (2002), pp. 869–896.
- [75] R. LEINE AND H. NIJMEIJER, *Dynamics and Bifurcations of Non-smooth Mechanical Systems*, Lect. Notes Appl. Comput. Mech. 18, Springer-Verlag, Berlin, Heidelberg, 2004.
- [76] R. LEINE AND D. VAN CAMPEN, *Discontinuous fold bifurcations in mechanical systems*, Arch. Appl. Mech., 72 (2002), pp. 138–146.
- [77] R. LEINE AND D. VAN CAMPEN, *Bifurcations in nonsmooth dynamical systems*, Eur. J. Mech. A Solids, 25 (2006), pp. 599–616.
- [78] R. LUM AND L. CHUA, *Generic properties of continuous piecewise-linear vector fields in \mathbb{R}^2* , IEEE Trans. Circuits Syst., 38 (1991), pp. 1043–1066.
- [79] L. MENINI AND A. TORNAMBÈ, *Dynamic position feedback stabilization of multi-degrees-of-freedom linear mechanical systems subject to non-smooth impacts*, IEEE Proc. Control Theory Appl., 148 (2001), pp. 147–155.

- [80] J. MOREAU, *Unilateral contact and dry friction in finite freedom dynamics*, in Non-smooth Mechanics and Application, J. Moreau and P. Panagiotopoulos, eds., CISM Courses and Lectures 302, Springer-Verlag, Wien, 1988, pp. 1–82.
- [81] P. MÜLLER, *Calculations of Lyapunov exponents for dynamical systems with discontinuities*, Chaos Solitons Fractals, 5 (1995), pp. 1671–1681.
- [82] A. NORDMARK, *Non-periodic motion caused by grazing incidence in impact oscillators*, J. Sound Vibration, 2 (1991), pp. 279–297.
- [83] A. NORDMARK, *Grazing Conditions and Chaos in Impacting Systems*, Ph.D. thesis, Royal Institute of Technology, Stockholm, Sweden, 1992.
- [84] A. NORDMARK, *Universal limit mapping in grazing bifurcations*, Phys. Rev. E, 55 (1997), pp. 266–270.
- [85] A. NORDMARK, *Existence of periodic orbits in grazing bifurcations of impacting mechanical oscillators*, Nonlinearity, 14 (2001), pp. 1517–1542.
- [86] A. NORDMARK, *Discontinuity mappings for vector fields with higher-order continuity*, Dynam. Systems, 17 (2002), pp. 359–376.
- [87] A. B. NORDMARK AND P. KOWALCZYK, *A codimension-two scenario of sliding solutions in grazing-sliding bifurcations*, Nonlinearity, 19 (2006), pp. 1–26.
- [88] H. NUSSE, E. OTT, AND J. YORKE, *Border collision bifurcations: An explanation for observed bifurcation phenomena*, Phys. Rev. E, 49 (1994), pp. 1073–1076.
- [89] L. E. NUSSE AND J. A. YORKE, *Border-collision bifurcations including “period two to period three” for piecewise smooth systems*, Phys. D, 57 (1992), pp. 39–57.
- [90] L. E. NUSSE AND J. A. YORKE, *Border-collision bifurcations for piece-wise smooth one-dimensional maps*, Internat. J. Bifurcation and Chaos, 5 (1995), pp. 189–207.
- [91] G. OLIVAR, M. DI BERNARDO, AND F. ANGULO, *Discontinuous bifurcations in DC-DC converters*, in Proceedings of IEEE International Conference on Industrial Technology ICIT, 2003, pp. 842–845.
- [92] S. PARUI AND S. BANERJEE, *Border collision bifurcations at the change of state-space dimension*, Chaos, 12 (2002), pp. 1054–1069.
- [93] F. PETERKA, *Part 1: Theoretical analysis of n-multiple (1/n)-impact solutions*, CSAV Acta Technica, 19 (1974), pp. 462–473.
- [94] F. PETERKA, *Results of analogue computer modelling of the motion. Part 2*, CSAV Acta Technica, 19 (1974), pp. 569–580.
- [95] F. PFEIFFER AND C. GLOCKER, *Multibody Dynamics with Unilateral Contacts*, John Wiley, New York, 1996.
- [96] P. PIROIINEN AND Y. KUZNETSOV, *An event-driven method to simulate Filippov systems with accurate computing of sliding motions*, ACM Trans. Math. Software, 34 (2008), article 13.
- [97] P. PIROIINEN, L. VIRGIN, AND A. CHAMPNEYS, *Chaos and period-adding: Experimental and numerical verification of the grazing bifurcation*, J. Nonlinear Sci., 14 (2004), pp. 383–404.
- [98] K. POPP, N. HINRICHS, AND M. OESTREICH, *Dynamical behaviour of friction oscillators with simultaneous self and external excitation*, Sādhanā, 20 (1995), pp. 627–654.
- [99] K. POPP AND P. SHELTER, *Stick-slip vibrations and chaos*, Philos. Trans. Roy. Soc. A, 332 (1990), pp. 89–105.
- [100] M. RABINDER, ED., *Chua’s Circuit: A Paradigm for Chaos*, World Sci Ser. Nonlinear Sci. Ser. B Spec. Theme Issues Proc, World Scientific, River Edge, NJ, 1993.
- [101] S. SHAW, *On the dynamic response of a system with dry friction*, J. Sound Vibration, 108 (1986), pp. 305–325.
- [102] S. W. SHAW AND P. J. HOLMES, *Periodically forced linear oscillator with impacts: Chaos and long-periodic motions*, Phys. Rev. Lett., 51 (1983), pp. 623–626.
- [103] S. W. SHAW AND P. J. HOLMES, *A periodically forced piecewise linear oscillator*, J. Sound Vibration, 90 (1983), pp. 129–144.
- [104] K. SLADE, L. VIRGIN, AND P. BAYLY, *Extracting information from interimpact intervals in a mechanical oscillator*, Phys. Rev. E, 56 (1997), pp. 3705–3708.
- [105] C. SPARROW, *Chaos in a three-dimensional single loop system with a piecewise linear feedback function*, J. Math. Anal. Appl., 83 (1981), pp. 275–291.
- [106] D. E. STEWART, *Rigid-body dynamics with friction and impact*, SIAM Rev., 42 (2000), pp. 3–39.
- [107] W. STRONGE, *Impact Mechanics*, Cambridge University Press, Cambridge, UK, 2000.
- [108] J. M. T. THOMPSON AND R. GHAFFARI, *Chaotic dynamics of an impact oscillator*, Phys. Rev. A, 27 (1983), pp. 1741–1743.
- [109] P. THOTA AND H. DANKOWICZ, *Continuous and discontinuous grazing bifurcations in impact oscillators*, Phys. D, 214 (2006), pp. 187–197.
- [110] V. I. UTKIN, *Sliding Modes in Control Optimization*, Springer-Verlag, New York, 1992.

- [111] N. VAN DE WOUV AND R. LEINE, *Attractivity of equilibrium sets of systems with dry friction*, *Nonlinear Dynam.*, 35 (2004), pp. 19–39.
- [112] A. J. VAN DER SCHAFT AND J. M. SCHUMACHER, *An Introduction to Hybrid Dynamical Systems*, Springer-Verlag, New York, 2000.
- [113] D. WAGG, G. KARPODINIS, AND S. R. BISHOP, *An experimental study of the impulse response of a vibro-impacting cantilever beam*, *J. Sound Vibration*, 228 (1999), pp. 242–264.
- [114] Y. WANG, *Dynamic modeling and stability analysis of mechanical systems with time-varying topologies*, *ASME J. Mech. Design*, 115 (1993), pp. 808–816.
- [115] Y. WANG, *Global analysis and simulation of mechanical systems with time-varying topologies*, *ASME J. Mech. Design*, 115 (1993), pp. 817–821.
- [116] G. S. WHISTON, *Global dynamics of a vibro-impacting linear oscillator*, *J. Sound Vibration*, 118 (1987), pp. 395–429.
- [117] G. S. WHISTON, *The vibro-impact response of a harmonically excited and preloaded one-dimensional linear oscillator*, *J. Sound Vibration*, 115 (1987), pp. 303–324.
- [118] Y. YOSHITAKE AND A. SUEOKA, *Forced self-excited vibration with dry friction*, in *Applied Nonlinear Dynamics and Chaos of Mechanical Systems with Discontinuities*, M. Wiercigroch and B. de Kraker, eds., World Scientific, River Edge, NJ, 2000, pp. 237–259.
- [119] G. YUAN, S. BANERJEE, E. OTT, AND J. A. YORKE, *Border-collision bifurcations in the buck converter*, *IEEE Trans. Circuits Systems I Fund. Theory Appl.*, 45 (1998), pp. 707–716.
- [120] J. ZHANG, K. JOHANSSON, J. LYGEROS, AND S. SASTRY, *Zeno hybrid system*, *Internat. J. Robust Nonlinear Control*, 11 (2001), pp. 435–451.
- [121] G. ZHOU AND S. REID, EDS., *Impact on Composites*, Woodhead Publishers, Cambridge, UK, 2000.
- [122] Z. ZHUSUBALIYEV AND E. MOSEKILDE, EDS., *Bifurcation and Chaos in Piecewise-Smooth Dynamical Systems*, World Scientific, Singapore, 2003.
- [123] Z. ZHUSUBALIYEV, E. SOUKHOTERIN, AND E. MOSEKILDE, *Border-collision bifurcations on a two-dimensional torus*, *Chaos Solitons Fractals*, 13 (2003), pp. 1889–1915.
- [124] Y. ZOU AND T. KÜPPER, *Generalized Hopf bifurcation emanated from a corner for piecewise smooth planar systems*, *Nonlinear Anal.*, 61 (2005), pp. 1–17.